SUBBARRIER FUSION OF THE OXYGEN ISOTOPES

Thesis by

Volker Pönisch

In Partial Fulfillment of the Requirements

for the Degree of

Doctor of Philosophy

California Institute of Technology

Pasadena, California

1986

(Submitted May 19, 1986)

ACKNOWLEDGMENTS

Steven E. Koonin was my academic advisor for this work. It was a privilege and great pleasure to learn physics from him and work with him. Helpful discussions with C. A. Barnes, K. Langanke, J. Thomas, A. Winther, and S.-C. Wu are also gratefully acknowledged. Financial support for my studies and this work was provided by Caltech and the National Science Foundation.

To Carol

ABSTRACT

The subbarrier fusion process is studied for systems involving oxygen isotopes. A one-channel incoming wave boundary condition (IWBC) calculation gives an excellent fit to fusion cross section data for $^{16}O+^{16}O$. An IWBC coupled channels calculation for $^{17}O+^{16}O$ that includes inelastic excitations as well as one-neutron transfer with formfactors calculated in a consistent single-particle framework reproduces the subbarrier enhancement down to four fifths the barrier height, but not below that. The calculation does not invoke the adiabatic approximation, which would create non-unitarity in the coupled channels equations. The measured subbarrier fusion cross section for $^{18}O+^{16}O$ is well reproduced by an IWBC coupled channels calculation with two-neutron transfer, but the calculation disagrees with the above-barrier data.

TABLE OF CONTENTS

LIST OF FIGURES

CHAPTER I

Outline

Nuclear subbarrier fusion is an example of quantum tunnelling of a system through a potential barrier with a height larger than the available kinetic energy. This process was recognized early in the development of quantum mechanics as one of the features distinguishing it from classical mechanics and, as such, has been studied for a long time. However, new developments in condensed matter[1] and nuclear physics[2] have aroused new interest in this old phenomenon, and the tunnelling of systems more complex than can be described by a simple Schrödinger equation with one degree of freedom has extended the original problem.

Our focus is exclusively on the problem of nuclear fusion reactions below (and slightly above) the Coulomb barrier. Here, the outstanding feature is a tremendous underprediction (often some orders of magnitude) of some heavy ion fusion cross sections by simple theory. In Chapter II, we will give an overview over the subbarrier "puzzle". We emphasize and review the proof of the inadequacy of the simple one-dimensional model, independent of what parametrization for the nuclear potential is chosen, as well as a plausibility argument on how extra degrees of freedom enhance the subbarrier cross section. However, we believe that the only way to achieve a satisfactory solution of the nuclear subbarrier fusion puzzle is to study different simple systems in great detail, attempting to extract as much different information from experiment as possible (elastic, inelastic, and angular distribu-

tions, spin observables, etc.) and making detailed, complete theoretical models, whose implications can be studied numerically, that reproduce all these features in a consistent way.

In Chapters III through V, we present such a theoretical study for the reactions involving oxygen isotopes. At first, we argue why we think this to be an especially worthwhile system to study. The calculations for $^{16}O+^{16}O$ have been done before in very similar fashion, but we want to show them for completeness. Chapter IV deals with $^{17}O+^{16}O$ and contains most of our original work. We present a unified calculation of the fusion, elastic and inelastic cross sections and obtain good agreement with experiment. $^{18}O+^{16}O$ is treated in Chapter V, where a much simpler model leads to satisfactory results for the fusion cross section. In the concluding sixth chapter, we summarize our results.

All numerical computations for this work were done on a VAX-750 of the W. K. Kellogg Radiation Laboratory. This thesis was typeset in D. E. Knuth's "TEX," and the graphs were prepared with the graphics package "Topdrawer" from the Stanford Linear Accelerator Center.

CHAPTER II

II.1 Fusion above and below the Coulomb barrier

In the simplest description of nuclear collisions, the target and projectile are treated as structureless particles interacting through a potential $V(r)$ that depends only on the distance r between the centers of the two nuclei. V is the sum of the attractive, short-range strong interaction V_S and the long-range electric repulsion V_C. V_C determines V at large r, but at intermediate distances, V_S dominates V_C. V thus has the typical barrier shape illustrated in Fig.1.

Fusion can be defined by the transmission probability $T_l(E)$ of the partial scattering wave with angular momentum $\hbar l$ and center-of-mass energy E, so that the fusion cross section σ_f is:

$$\sigma_f(E) = \frac{\pi\hbar^2}{2mE}\sum_{l=0}^{\infty}(2l+1)T_l(E) \quad . \tag{II.1}$$

m is the reduced mass of the two nuclei. (We will actually derive (II.1) in the next chapter.) We will now consider the limiting cases of energies well above and below the barrier top.

Glas and Mosel[3,4] investigated the above-barrier fusion; we give a simplified version of their model: Classically, a particle will pass over a potential barrier if and only if its energy is larger than the barrier height. If we assume the location R_B of the barrier top in the combined s-wave plus centrifugal potential to be independent of l, then the barrier height V_{Bl} of this potential is $V_B + \hbar^2 l(l+1)/(2mR_B^2)$, where V_B is the s-wave barrier height (the maximum of V). Classically, the $T_l(E)$ in (II.1)

are 1, if $E > V_{Bl}$, and 0 otherwise. Therefore, (II.1) becomes

$$\sigma_f(E) = \frac{\pi\hbar^2}{2mE}\sum_{l=0}^{l_m}(2l+1) \quad , \tag{II.2}$$

where l_m is the largest integer smaller than the real number y given by $y(y+1) = [2m(E-V_B)R_B^2/\hbar^2]$. l_m is large for large E, so that $l_m \approx y$ and $\sum_0^{l_m}(2l+1)$ $\approx l_m(l_m+1)$. Thus,

$$\sigma_f(E) \approx \pi R_B^2\left(1-\frac{V_B}{E}\right) \quad . \tag{II.3}$$

For very large energies, l_m becomes too large and (II.2) has to be modified because the compound nucleus can only be created with l less than some critical value l_c. A critical radius R_c and barrier height $V_c < V_B$ can be defined so that $l_c(l_c+1)$ $= 2m(E-V_c)R_c^2/\hbar^2$, then

$$\sigma_f(E) \approx \pi R_c^2\left(1-\frac{V_c}{E}\right) \quad . \tag{II.4}$$

(II.3) is valid for $l_m < l_c$ (at lower energies), and (II.4) otherwise. The total reaction cross section σ_R follows (II.3) even if $l_m < l_c$ because there is no maximum angular momentum beyond which no inelastic reaction can happen. Thus, for energies for which $l_m < l_c$, $\sigma_R = \sigma_f$, and for higher energies, $\sigma_R > \sigma_f$. An example of the success of the Glas-Mosel model is given in Fig.2.

For energies far below the barrier, the lowest order energy dependence of the fusion cross section can be obtained in analogy with Gamow's[5] semiclassical derivation of the nuclear α-decay rate. Clearly, the reaction is energetically forbidden in classical mechanics and is purely a quantum effect. The s-wave transmission probability $T_0(E)$ through a potential that is constant and negative for $r < R$ and pure

Coulomb ($Z_1 Z_2 e^2/r$) for $r > R$ goes approximately as:

$$T_0(E) \propto e^{-2\pi\eta} \quad , \tag{II.5}$$

where η is the *Sommerfeld parameter*:

$$\eta = \frac{Z_1 Z_2 e^2}{\hbar v} \tag{II.6}$$

with v the center-of-mass velocity $v = (2E/m)^{1/2}$. If all $T_l(E)$ have the same energy dependence (through v and η) as $T_0(E)$, or if only the s-wave contributes appreciably to the fusion cross section, then

$$\sigma_f \propto \frac{1}{E} e^{-2\pi\eta} \quad . \tag{II.7}$$

The *astrophysical S-factor* is defined to take out this understood, model independent energy dependence:

$$S(E) = \sigma_f(E) E e^{2\pi\eta} \quad . \tag{II.8}$$

For actual systems, the definition (II.8) normally overcorrects the energy dependence of σ_f and S falls with rising E, especially for heavy ions. However, all systems exhibit the exponential dependence of σ_f on E. Therefore, inadequacies in the models for particular systems may cause little error in the fusion cross section around and above the barrier, but cause an exponential deviation of the model calculation from experimental data below the barrier.

II.2 Direct and compound nuclear reactions

A very fruitful concept in nuclear reaction theory is the distinction between *direct* and *compound nuclear* reactions.[6,7] The idea behind this distinction is the realization that the possible outcomes of nuclear collisions can be separated into two categories and that both the physical time scale of the processes that lead to a particular outcome and the physicists' models to describe them are quite different.

The first category comprises the direct reactions. These are the collisions "where not much is happening": the nuclei scatter elastically, or their surfaces might get modified (simple nuclear excitations), or a small number of nucleons is transferred between target and projectile. After the reaction, the two nuclei do not look very different from before the collision. The cross sections are mainly peaked in the forward direction. The time scales involved are relatively short, of the order of the Rutherford scattering time, i.e., scattering without the strong interaction. Accordingly, the cross sections show structure on only a relatively large bombarding energy scale. Theoretical descriptions start with the one-channel Schrödinger equation and are refined by the addition of other channels for the inelastic and transfer reactions. These additional channels involve only few nucleons and can be generally well modelled from the accumulated nuclear structure knowledge. Practical computational considerations limit the number of channels to maximally a few tens.

In the other group, the two colliding nuclei form a compound nucleus that has little in common with the original configuration (except for the overall conserved quantum numbers: energy, spin, parity, and proton and neutron number). The time

scale for the compound nucleus to decay is relatively long and the cross sections can vary more rapidly in energy than for the direct nuclear reactions. Cross sections are typically not forward peaked, but are often isotropic or at least symmetric about 90° in the center-of-mass system. The successful theoretical models for this sort of reaction are of statistical nature, and the exact low excitation energy structure of the two original nuclei is quite unimportant for the description of the compound nucleus.

This is a good point to clarify our jargon: We use the word *inelastic* always to mean inelastic scattering, namely scattering into those channels that involve (simple) target and/or projectile excitation,but not transfer of nucleons. *Inelastic cross section* thus does not refer to the whole reaction cross section, but just a part of it. In the model that we will use for the oxygen isotopes, the reactions are *elastic, inelastic, transfer* or *fusion.*

The fusion reaction clearly falls into the category of compound processes, but unitarity allows a study of this process by direct reaction theory techniques. One only has to assume that all flux removed from the direct channels (i.e., the elastic, inelastic, and few-particle transfer channels that one has designated as such) goes into fusion. The same theoretical ambiguity in the precise distinction of direct and compound nuclear reaction occurs also in the precise definition of what a fusion process is, so that the theorist has the freedom of equating the fusion probability with the formation probability for the compound nucleus. The only discrepancy occurs through the *compound elastic, compound inelastic*, and *compound transfer* reactions, in which a more or less equilibrated compound nucleus is formed, but

decays in one of the modes, e.g., the elastic, that were designated as the direct reaction channels. However, this decay probability is generally small enough to be safely neglected, because there are so many other decay channels available. The experimentalist, if he or she does not observe the recoiling compound nucleus more directly, has a non-trivial problem in determining and identifying all the decay products. Despite this conceptual arbitrariness, it is quite obvious in most heavy ion reactions how to account for the different pieces of the total reaction cross section and where to draw the line between the direct and compound nuclear reactions.

There is an alternative approach (*time-dependent Hartree-Fock*, TDHF)[8] to the direct reaction theory method for calculating the fusion cross section. In these, the compound nucleus formation is studied in detail, and one keeps track of all individual nucleons in the two colliding nuclei. This more microscopic approach certainly has some advantage over a treatment that incorporates far fewer degrees of freedom, but the precise criterion of when fusion occurs is even less clear. Furthermore, the quantum tunnelling aspect of the problem is lost, and a qualitative analysis of numerically obtained cross sections quite difficult.

Our approach is that of the direct reaction theory. There exist again two kinds of approaches in this subfield of subbarrier studies, one that uses optical potentials and the other that uses an *incoming wave boundary condition* (IWBC).

II.3 Optical potentials and the IWBC

From the foregoing discussion, we can in general write the complete scattering

state $|\Phi\rangle$ as a sum of two parts, one that is a direct reaction state (and may itself be composed of a sum over channels of the designated inelastic and transfer channels on top of the elastic channel) and the other the compound nucleus state,

$$|\Phi\rangle = |\Phi_d\rangle + |\Phi_{cn}\rangle \quad . \tag{II.9}$$

There are now two methods of calculating the fusion probability (in a sense the magnitude of the compound nuclear wave function) by solving the Schrödinger equation for the direct wave function only. In the optical potential method the inter-nuclear potential W is complex and hence non-Hermitian; as a result, unitarity is violated, and flux is removed from the direct reaction channels. By unitarity of the complete system this flux must have gone into the compound nuclear wave function, and by equating the missing direct reaction flux with the fusion flux, one has a quantitative model for the calculation of the fusion cross section. The optical potential is fitted to reproduce this and the elastic and inelastic differential cross sections.

Formally, the character of the approximation is most easily seen in the case, where direct inelastic and transfer reactions are unimportant and the direct wave function consists only of the elastic channel $|\Phi_0\rangle$. We use the projection operators P, Q from Feshbach[9], with $P + Q = 1$, $P|\Phi\rangle = |\Phi_0\rangle$, and $Q|\Phi\rangle = |\Phi_{cn}\rangle$. By projecting the Schrödinger equation $(H - E)|\Phi\rangle = 0$ onto the P and Q subspaces of the complete Hilbert space, we get the coupled equations

$$\begin{aligned} (E - H_{PP})|\Phi_0\rangle &= H_{PQ}|\Phi_{cn}\rangle \\ (E - H_{QQ})|\Phi_{cn}\rangle &= H_{QP}|\Phi_0\rangle \quad , \end{aligned} \tag{II.10}$$

where $H_{PP} = PHP$, $H_{QQ} = QHQ$, $H_{PQ} = PHQ$, and $H_{QP} = QHP$. The second of the equations (II.10) can be solved formally by a Green's function method:

$$|\Phi_{cn}\rangle = [E - H_{QQ} + i\epsilon]^{-1} H_{QP} |\Phi_0\rangle \ , \tag{II.11}$$

where there is no inhomogeneous term on the right hand side, because $|\Phi_{cn}\rangle$ contains only outgoing waves. The Schrödinger equation for the elastic channel thus becomes

$$(H_0 - E)|\Phi_0\rangle = 0 \qquad , \tag{II.12}$$

with

$$H_0 = H_{PP} + H_{PQ}[E - H_{QQ} + i\epsilon]^{-1} H_{QP} \ . \tag{II.13}$$

If H_{PP} is written as the sum of the kinetic energy and the diagonal potential, $H_{PP} = T + V$, then the optical potential operator is

$$W = V + H_{PQ}[E - H_{QQ} + i\epsilon]^{-1} H_{QP} \ . \tag{II.14}$$

W is non-local and depends on E. However, this is normally neglected and a phenomenological local, central, and energy independent form for W is used.

The IWBC method makes a different assumption: it separates the direct and compound nuclear wave functions by space. A radius r_0 is defined in the interior of the Coulomb barrier. The scattering state in the interior of the IWBC radius r_0 is assumed to be entirely compound nuclear, and outside of r_0 to be entirely direct. The potential to determine the wave function for $r > r_0$ is real; it is usually determined phenomenologically (at least in the elastic channel). The fusion flux is defined as the current of the wave function going inside at r_0. No flux is removed

artificially, since the Hamiltonian is Hermitian, and the net ingoing flux at infinity equals the net ingoing flux at r_0.

We restrict ourselves again to the case where there is only one direct channel (the elastic channel). We expand the wave function for this channel into $\frac{1}{r}\sum \chi_l(r)P_l(\cos\theta)$ (where $P_l(\cos\theta)$ is a Legendre polynomial). In the usual radial Schrödinger equation, there is a requirement of regularity of the wave function at the origin (or equivalently: $\chi_l(0) = 0$). This, together with the asymptotic scattering form at large r, gives sufficient boundary conditions to the mathematical differential equation. In the IWBC formalism, since the wave function is not extended to $r = 0$, a new boundary condition at the inner starting point of integration, i.e. at r_0, has to be found. This is the incoming wave boundary condition, namely, that the wave function near r_0, when expanded into the in- and outgoing semiclassical solution, has only an ingoing part, and the outgoing part is identical to zero, i.e.,

$$\chi_l(r) = N_l\, k_l(r)^{-\frac{1}{2}} \exp\left(-i\int_{r_0}^{r} d\bar{r} k_l(\bar{r})\right) , \tag{II.15}$$

with N_l some normalization constant and $k_l(r)$ the local semiclassical wave number

$$k_l(r) = \sqrt{\frac{2m}{\hbar^2}\big(E - V(r)\big) - \frac{l(l+1)}{r^2}} . \tag{II.16}$$

The problem is thus reduced to finding the penetrability (or transmission coefficient) for given energy and angular momentum of tunnelling through a truly one-dimensional barrier, i.e., on the whole one-dimensional space from $+\infty$ to $-\infty$(from right to left), when the wave on the right hand side consists of a part going left (the incoming flux) and a part going right (the elastically scattered or reflected part),

but to the left of the barrier only a transmitted wave going left exists. The fusion cross section in this simple case is given in terms of the transmission coefficients $T_l(E)$ by (II.1).

The motivation for the IWBC is the strong absorption inside the barrier. The IWBC also works quite well for energies slightly above the barrier and tunnelling probabilities much larger than $1/2$ ($1/2$ is a typical value for the penetrability at the top of the barrier). In general, the results for the fusion probability are insensitive to the precise location of r_0 in the interior of the barrier. This is plausible, because the truly one-dimensional problem is physically well-posed and any sensitivity to the precise location of r_0 of the barrier penetrability is due to the approximate character of the semiclassical form of the wave function in (II.15).

We prefer the IWBC method over the phenomenological optical potential for two reasons. (1) It is much more physical by providing a microscopic derivation and not just an empirical fitting of the optical potential parameters. Qualitative results in the IWBC formalism can be interpreted from the pictorial point of view of the semiclassical action integral between points inside and outside the barrier. (2) All direct reaction channels are treated on an equal footing, and the flux that goes into fusion from each of these channels is calculated in the same manner - as opposed to the optical potential, where the fusion flux is determined from different parameters in different channels. Especially for the study of different isotopes in the otherwise identical reaction, it is important to have a mechanism of flux removal from the additional channels that exist in one system but not another. Very little could be learned from just fitting different optical potentials to different isotopes.

II.4 Subbarrier fusion cross section enhancement

Many subbarrier fusion systems that have been studied are described adequately by the IWBC formalism described in the previous section or by an even simpler semiclassical calculation, in which the barrier penetrability is computed with a WKB approximation. These methods work especially well for the light systems, e.g., all experimentally known ^{1}H and ^{4}He cross sections are well reproduced (with the exception of the statically deformed ^{233}U nucleus), but also fusion of some heavier systems, such as ^{12}C+^{14}N or ^{16}O+^{27}Al causes no problems.[10] We will present another example, ^{16}O+^{16}O (cf. Fig.10), in great detail in the next chapter.

However, this analysis has failed for most of the heavier and some of the intermediate mass systems. By now, examples abound, we cite the systems of ^{16}O + different Sm isotopes[11], Ni + Sn[12], ^{40}Ar + Sm[13]. If a different isotope of the same element is substituted, the fusion probability can change dramatically, e.g., Ni + Ni[14] and Ca + Ca[15] exhibit this behavior. We show the representative results for ^{58}Ni+^{58}Ni in Fig.3. In all systems investigated so far, if the calculation fails, then the fusion cross section below the barrier is underpredicted, often by orders of magnitude. However, all these calculated fusion cross sections depend on the choice of the nuclear potential, and until the work of Balantekin, Koonin, and Negele (BKN)[16], the failure of the one-channel calculations might have been attributed to a very poor parametrization of the nuclear potential. BKN showed that with some reasonable assumptions, measured fusion cross sections as a function of energy can be inverted to give the nuclear potential in the barrier region as a function of r.

The data of systems that can be adequately desribed by a one-channel IWBC model produce a single-valued potential and a reasonable barrier, but other systems show a backbending of the potential function, i.e., two values for the potential at one value for the radius. Such unphysical behavior then proves the inadequacy of the one-channel model.

We will now briefly describe the inversion method of BKN: The total fusion cross section expressed through the partial wave penetrabilities $T_l(E)$ is given by (II.1) and three assumptions about $T_l(E)$ are made: (*i*) The $T_l(E)$ have the same form for any barrier as they would for an inverted parabola in the semiclassical approximation (the famed *Hill-Wheeler*[17] formula):

$$T_l(E) = \left[1 + e^{2S_l(E)}\right]^{-1} \quad , \tag{II.17}$$

where $S_l(E)$ is the "action" integral

$$S_l(E) = \int_{r_1}^{r_2} dr \sqrt{\frac{2m}{\hbar^2}(V(r) - E) + \frac{l(l+1)}{r^2}} \tag{II.18}$$

in the WKB approximation (the WKB approximation is valid for $S_l >> 1$). r_1 and r_2 are the classical turning points of the motion. (*ii*) The penetrability $T_l(E)$ for non-zero l is the penetrability with $l = 0$ at the shifted energy $E - l(l+1)\hbar^2/(2mR^2(E))$, where $R(E)$ is some radius between the barrier radius and the classical turning radius in the Coulomb field only; the precise location of $R(E)$ does not matter much to the end result. (*iii*) In (II.1), the sum over l can be approximated by an integral over l (this is plausible as a large number of l's contribute and the partial wave penetrabilities vary smoothly with l).

With these three reasonable assumptions, BKN are able to find the difference of the r_1 and r_2 of (II.18), and thus the barrier thickness $t(V)$ at given V in terms of the cross section as a function of E. The trick is done by a reduction of the problem to Abel's problem in classical mechanics, but the details of the derivation are unimportant here. With the assumption that the barrier shape for r larger than the barrier radius is insensitive to the exact form of the nuclear potential, r_2, the outer classical turning point, can be taken from the calculation with a reasonable nuclear potential and r_1 determined from t. The lesson to be learned is that some measured fusion cross sections, when inverted to a function $t(V)$, show a non-physical behavior in that t does not decrease fast enough when V approaches the barrier height, so that the resulting potential $V(r)$ is double-valued for some r. The interpretation of this behavior is that the one-channel model would fail to reproduce the fusion cross section no matter what potential $V(r)$ would be used.

It is therefore clear that salvation has to be sought in multi-channel calculations. A partially successful "pseudo-multi"-channel model is that of *zero-point motion*,[18] in which one-dimensional penetrabilities for different surface parameters in a vibrational model are averaged over. This model can, for example, account for most of the subbarrier fusion enhancement in the ^{16}O+Sm experiments. However, systems such as the Ni+Ni collisions cannot be explained in this way.[10]

The tendency of additional channels to enhance the fusion cross section (and not, for example, to systematically decrease it) is physically intuitive, but not really understood in detail. The physical intuition comes from the experience in quantum mechanics that when a system couples to additional degrees of freedom, the new

complete system generally has a bound state spectrum which is in part shifted up and in part shifted down in energy with respect to the bound state spectrum of the uncoupled system. This phenomenon normally occurs without regard to the sign of the coupling. Applied to the tunnelling problem this effect translates into the existence of barriers shifted in height in the different channels, with some of these channels having barriers lower than the elastic channel. The quasi-eigenstates that exhibit these shifted barriers will not necessarily be the channels with the simple degrees of freedom in terms of transfer or inelastic excitations but rather linear combinations of them, in analogy to the bound spectrum example. Another way in which lower barriers can occur is through the addition of channels that have a lower orbital angular momentum and thus a lower centrifugal potential (we will see an example of that in Chapter IV) or that have positive Q-value (such as the one-neutron transfer in $^{17}O+^{17}O$). If barriers of different height are available to the system, it tends to select dynamically those channels that facilitate compound nucleus formation or to put it differently, the system falls into the lower-energy channels during the collision. Because of the exponential dependence of the penetrability on the barrier height, such an additional channel can enhance the fusion cross section by orders of magnitude. We will now present a quantitative, yet very simple model for the barrier splitting and subbarrier fusion probability enhancement.[19]

We consider a one-dimensional system with two channels and corresponding wave functions $\chi_1(x)$ and $\chi_2(x)$. The coupled channels equations are

$$\begin{aligned} \frac{d^2}{dx^2}\chi_1(x) + \frac{2m}{\hbar^2}\big(E - V(x)\big)\chi_1(x) &= \frac{2m}{\hbar^2}V_c\chi_2(x) \\ \frac{d^2}{dx^2}\chi_2(x) + \frac{2m}{\hbar^2}\big(E - V(x)\big)\chi_2(x) &= \frac{2m}{\hbar^2}V_c\chi_1(x) \ , \end{aligned} \tag{II.19}$$

where we have assumed for simplicity that the coupling potential V_c is independent of x (this is not essential for the following argument). If we now form the linear combinations $\chi_+(x)$ and $\chi_-(x)$, such that

$$\begin{aligned}\chi_1(x) &= \frac{1}{\sqrt{2}}\Big(\chi_+(x) + \chi_-(x)\Big) \\ \chi_2(x) &= \frac{1}{\sqrt{2}}\Big(\chi_+(x) - \chi_-(x)\Big) \ ,\end{aligned} \tag{II.20}$$

then the system of equations (II.19) decouples into

$$\frac{d^2}{dx^2}\chi_\pm(x) + \frac{2m}{\hbar^2}\Big[E - \big(V(x) \pm V_c\big)\Big]\chi_\pm(x) = 0 \ . \tag{II.21}$$

Thus, the barrier without coupling, given by $V(x)$, is split into the two barriers $V(x) \pm V_c$ by the coupling; these two new barriers exist irrespective of the sign of V_c. Classically, the penetrability T is 1 if the kinetic energy is larger than the barrier height, and zero if the available energy is less than the barrier height. Quantum mechanically, this rigid step is washed out as is illustrated by the two curves in Fig.4a. V_B is the barrier height (the maximum) of the potential $V(x)$. With the correct boundary conditions for the incoming wave, the transmitted flux of the coupled system is $T = {}^1\!/_2(T_+ + T_-)$, where $T_\pm$ are the (one-channel) transmission coefficients of (II.21). Classically, these are step functions with the step at $V_B \pm V_c$, so that classically, T is 0 for $E < V_B - V_c$, 1 for $E > V_B + V_c$, and ${}^1\!/_2$ in between. Again, the steps are smoothed in the quantum mechanical treatment (cf. Fig.4b). In Fig.4c, the two quantal curves are plotted together for comparison; the coupled calculations show enhancement over the uncoupled one for energies below the barrier V_B, and the reverse is true above V_B. (The curves in Fig.4 are just schematic and not the result of an actual computation, but the numerical results of Ref.[19] bear out the same shape.)

The method of the Feynman path integral also is a valuable tool in the attempts to model multi-dimensional quantum tunnelling. Balantekin and Takigawa[20] present a model in which the Hamiltonian H consists of a one-dimensional uncoupled piece of kinetic and potential energy associated with the distance R plus an internal Hamiltonian, H_0, of one internal degree of freedom, q, plus an interaction Hamiltonian, $H_{int}(q,R)$:

$$H = -\frac{\hbar^2}{2m}\frac{\partial^2}{\partial R^2} + V(R) + H_0(q) + H_{int}(q,R)\ . \qquad \text{(II.22)}$$

By use of the Feynman path integral, the penetrability in the Hamiltonian H can be determined exactly if $H_0 + H_{int}$ can be expressed as a linear combination of the generators of a mathematical group. Examples studied by Balantekin and Takigawa include (i) a harmonic oscillator coupled linearly to the translational motion, i.e., $H_0 = -\frac{\hbar^2}{2m}\frac{\partial^2}{\partial q^2} + 1/2 m\omega^2 q^2$ and $H_{int}(q,R) = f(R)q$ for any real function $f(R)$; (ii) a harmonic oscillator quadratically coupled to the translational motion, i.e., the same form for H_0, but $f(R)q^2$ for H_{int}. The effect of the linear coupling (i) is to enhance the subbarrier penetrabilities and to hinder above-barrier transmission irrespective of the sign of the coupling formfactor, while the quadratic coupling (ii) enhances fusion at all energies, if the formfactor is negative, but diminishes fusion at all energies, if the formfactor is positive.

These model calculations are very valuable for a modelling of the subbarrier fusion process, but they do not provide any computational ease for the study of actual nuclear systems. No multi-channel calculations with physically reasonable potential couplings so far have shown an attenuation of subbarrier fusion compared with the one-channel calculations, and the experimental findings of relative fusion

cross sections are in agreement with an increase in the cross section when additional degrees of freedom are expected to be important. Nevertheless, the exact condition that the coupling matrix elements have to obey to produce enhancement remains an outstanding problem of mathematical physics. In this work, we will attempt another avenue towards solution of the nuclear tunnelling problem by a detailed quantitative analysis of one particular system, namely collisions involving the nuclei of two oxygen isotopes.

CHAPTER III

III.1 Oxygen and subbarrier fusion

Systems with two oxygen nuclei play a particularly interesting role in the subbarrier fusion field. The $^{16}O+^{16}O$ system is crucial in the prevalent theory of stellar nucleosynthesis of heavy elements; we will briefly outline that theory in Section III.3 . The systems that involve other oxygen isotopes are not fundamental in this theory as the natural abundance of ^{18}O is only 0.204% , and of ^{17}O just 0.037% . However, as we will show, a detailed understanding of the ^{16}O - ^{16}O fusion reaction is necessary because the cross section data in the experimentally accessible energy region have to be extrapolated by some theoretical model to the lower, astrophysically interesting energies. A complete prediction or reproduction of experimental data for other oxygen isotopes would instill confidence that such an understanding has been achieved.

The availability of the different isotopes and practicality of experimenting with them makes oxygen interesting from a nuclear physics point of view as well. Relative changes from one system to another can be emphasized and the differing features of the isotopes that are relevant to the fusion process can be isolated. The stable Oxygen isotopes ^{16}O, ^{17}O, and ^{18}O are particularly attractive in this regard, because ^{16}O is a doubly magic nucleus; both protons and neutrons completely fill the p shell in the nuclear shell model. This makes for a very rigid, strongly bound

nucleus without low-excitation energy states. As a doubly closed-shell nucleus, ^{16}O has a 0^+ (spin 0, positive parity) ground state.

The shell model describes ^{17}O as an ^{16}O core with an additional neutron. In the ground state, this neutron occupies the $s-d$ shell, and the first excited states of ^{17}O are expected to be single particle excitations of this valence neutron, first within the $s-d$ shell and then out of it into the $p-f$ shell. It has been found experimentally that indeed the ground state of ^{17}O has quantum numbers $\frac{5}{2}^+$ and that the excited states are a $\frac{1}{2}^+$ state with 0.871 MeV excitation energy and a $\frac{1}{2}^-$ and $\frac{5}{2}^-$ state at 3.055 MeV and 3.841 MeV, respectively. All other states lie above decay threshold into ^{16}O+n. All this is more or less expected from the naive shell model with spin-orbit coupling (only the $p_{3/2}$ and $f_{7/2}$ states would be expected to be lower in energy than the $p_{1/2}$ and $f_{5/2}$, respectively, and there should be a $d_{3/2}$ state).

^{18}O is an even-even nucleus like ^{16}O and has a 0^+ ground state, too, because the two $d_{5/2}$ valence neutrons couple to total angular momentum 0. The excited states are determined by the configuration of the valence neutrons, the two first excitations are $(d_{5/2})^2$ coupled to 2^+ (with some $(s_{1/2}d_{5/2})$ admixture) and 4^+, the next one $(s_{1/2})^2$ coupled to 0^+.

The energy levels of ^{17}O and ^{18}O with respect to their decay threshold into ^{16}O and one or two neutrons, respectively, are shown in Fig.5. There are additional levels in ^{18}O that we have left out in the diagram.

The most interesting combinations of the oxygen isotopes for fusion studies are:

(a) $^{16}O + {}^{16}O$: This is the astrophysically important case. The two nuclei are very rigid and internal degrees of freedom are expected to be largely irrelevant to the fusion process. Hence, this reaction can provide the calibration of the core-core potential for all other cases.

(b) $^{17}O + {}^{16}O$: The relatively clean character of the ground and first excited state as single particle states in ^{17}O adds clearly defined degrees of freedom. The coherent addition of direct elastic and transfer elastic (and equivalently for the inelastic) amplitudes should provide a rich structure in the elastic (and inelastic) angular distributions.

(c) $^{18}O + {}^{16}O$: Pair transfer takes over from single nucleon transfer in (b) because the Q-value for $^{18}O+{}^{16}O \rightarrow {}^{17}O+{}^{17}O$ is large and negative (3.9 MeV).

(d) $^{18}O + {}^{18}O$: This system might show the onset of a more complicated coupling scheme with many important degrees of freedom as they occur typically in the subbarrier fusion of the very heavy ions.

(e) $^{17}O + {}^{17}O$: The nucleon transfer into $^{16}O+ {}^{18}O$ has positive Q-value, i.e., is exoergic. A very large enhancement of the low-energy fusion cross section can be expected when the system falls into this transfer channel and sets free a considerable amount of energy. The quantitative features of channels with positive Q-values have been studied very little to date.

We believe that oxygen lies in the golden middle between the light nuclei, whose nuclear structure is well understood, but whose fusion is adequately described by the simple one-channel model, and the very heavy ions with interesting fusion behavior, but relatively poorly understood nuclear structure. Furthermore, we hope that it is

easier to disentangle structure and dynamics and to isolate the important degrees of freedom in simpler systems than the very heavy ions. As we have shown in (a) through (e), all of the interesting features suggested so far are already exhibited in the O+O system. Another system of similar interest (and at least equal astrophysical importance) consists of the carbon isotopes, but here the supposedly simple $^{12}C - ^{12}C$ reaction is plagued by resonances in the cross sections and the nucleus ^{14}C is radioactive, which poses some experimental problems. Unfortunately, even if we succeed in modelling the oxygen system, this will not automatically warrant that the same methods can be applied to the very heavy ions, because their greater complexity might render computational methods impractical.

III.2 Experimental program at Caltech

Because of its astrophysical importance, measurements of the $^{16}O + ^{16}O$ subbarrier fusion cross section were performed in the W. K. Kellogg Radiation Laboratory in the seventies.[21,22] However, there was a discrepancy at the lowest energies between the Caltech data and those of Hulke *et al.*,[23] and the extrapolation to even lower energies remains rather ambiguous. Furthermore, the whole field of subbarrier fusion had gained considerable attention within the nuclear physics community since then.[2] Therefore, in 1983 a program was initiated at Caltech to measure the cross sections systematically between different oxygen isotopes.

At the writing of this thesis, data have been taken for the systems $^{16}O+ ^{16}O$, $^{17}O+^{16}O$, $^{18}O+^{16}O$, and $^{18}O+^{18}O$. The measurements for $^{18}O + ^{18}O$ are not analyzed yet, as this experiment has proven to be much more difficult than the other

three. The results for the first two systems have been published,[24] and a review of the experiments for the first three systems has been submitted for publication.[25]

In the experiments, total gamma ray yields are measured. This way, fusion, inelastic, and transfer cross sections are determined simultaneously. Specific γ ray lines correspond to specific transitions in the reaction products and can be identified experimentally. The γ ray yields are converted into fusion cross sections by use of a statistical model (Hauser-Feshbach formalism) for the formation and decay of the compound nucleus. The analysis of the $^{18}O+^{18}O$ raw data is so difficult because of the large number of gamma ray peaks and the necessity to incorporate three-step decays into the Hauser-Feshbach scheme (one- and two-step decays were sufficient for the other three systems). Running time considerations limit the measurements to cross sections of a few μb and above; this sets a lower limit of about 6.5 MeV on the feasible center-of-momentum energies.

For $^{17}O+^{16}O$ and $^{18}O+^{16}O$, the target was chosen to be the ^{16}O nucleus, because it is much easier to separate beams of mixed isotopes than to maintain high enrichment of the targets with a rare isotope. For $^{18}O+^{18}O$, target enrichment was obviously unavoidable and could be achieved. However, the expense and difficulty in manufacturing ^{17}O targets makes the ^{17}O - ^{17}O experiment the most intricate one of any of the projectile-target combinations from the set ^{16}O, ^{17}O, ^{18}O, because of the low natural ^{17}O abundance.

The results from Thomas *et al.* are shown in Figs.6 and 7. Fig.6 displays the three measured fusion cross sections and the two total inelastic cross sections. The inelastic cross sections were determined from just one γ ray intensity each, namely

for ^{17}O the 0.87 MeV transition from the first excited to the ground state and for ^{18}O the 1.98 MeV transition from the first excited to the ground state. Other γ ray lines from the oxygen nuclides could not be found in the spectra. The measured fusion cross sections were inverted by the BKN method and the resulting potential barriers are plotted in Fig.7. Whereas the ^{16}O+^{16}O and ^{18}O+^{16}O potentials are single-valued, that of ^{17}O+^{16}O is not, and thus, this system cannot be described successfully in a one-channel model.

III.3 Oxygen burning in stars

We will now give a short summary of the astrophysical motivation for our work. It is believed that the nucleosynthesis that produced today's observed elemental abundances in the solar system occurs in more or less separate groups of reactions at different stages in the development of certain types of stars.[26] The first such group is the hydrogen burning that produces ^{4}He via the *p-p chain* or the *C-N-O cycle*. If enough helium has accumulated in the core of the star and if the hydrogen burning in an outside shell has compressed and heated this core sufficiently, then helium burning with main end products ^{12}C and ^{16}O will occur. For stars with initial mass of at least about eight times that of the sun, carbon burning (mainly $^{12}\mathrm{C}+^{12}\mathrm{C}$ and $^{12}\mathrm{C}+^{16}\mathrm{O}$) is the next stage, followed by neon burning (mainly $^{20}\mathrm{Ne}+\gamma \rightarrow ^{16}\mathrm{O}+\alpha$ and $^{20}\mathrm{Ne}+\alpha \rightarrow ^{24}\mathrm{Mg}+\gamma$). If the star had an initial mass of at least about 15 times that of the sun, static oxygen burning will take over, followed by a short period of silicon burning.

The temperature of oxygen burning has been calculated to be about 2×10^9 K

for a star of 25 solar masses.[27] The interaction rate is proportional to the velocity averaged product $\langle \sigma v \rangle$ of (center-of-mass) cross section and velocity.[28] For a Maxwell-Boltzmann velocity distribution, this product becomes (with the center-of-momentum energy E as the integration variable):

$$\langle \sigma v \rangle = \sqrt{\frac{8}{\pi M (k_B T)^3}} \int_0^\infty E \sigma(E) \exp(-\frac{E}{k_B T})\, dE \quad ; \tag{III.1}$$

M is the reduced mass of the nuclei, k_B is the Boltzmann constant, and T the temperature. If one assumes the S-factor to be approximately independent of E, the integral in (III.1) becomes

$$S(E_0) \int_0^\infty \exp\left(-\frac{E}{k_B T} - \sqrt{\frac{E_G}{E}}\right) dE \quad , \tag{III.2}$$

where E_G is the *Gamow energy*

$$E_G = (2\pi\alpha Z_1 Z_2)^2 \, \frac{Mc^2}{2} \quad , \tag{III.3}$$

with $\alpha = e^2/\hbar c$, the fine structure constant. E_0 in (III.2) is the energy at which the integrand peaks; i.e., at the minimum of $E/(k_B T) + \sqrt{E_G/E}$, hence

$$E_0 = \left[\tfrac{1}{2}\, k_B T E_G{}^{1/2}\right]^{\frac{2}{3}} \quad . \tag{III.4}$$

The peak of the integrand has a full width at half height:

$$\Delta E_0 = 4\left[E_0 k_B T/3\right]^{1/2} \quad . \tag{III.5}$$

For $^{16}O + {}^{16}O$ at 10^9 K one finds $E_0 = 3.1$ MeV and $\Delta E_0 = 1.2$ MeV, and at 3×10^9 K, $E_0 = 6.4$ MeV and $\Delta E_0 = 3.0$ MeV.[26] Any calculation of the rate of

oxygen burning in such a star would thus require some knowledge of the fusion cross section down to about 3 MeV or even farther. However, no laboratory data below 6.5 MeV have been taken (the s-wave barrier is at 10.2 MeV). Therefore, an extrapolation of the available data to lower energy is necessary. A qualitative theoretical understanding of the reaction and a good fit to the available data is a prerequisite to any extrapolation of the quality required for quantitative astrophysical calculations. Fig.8 gives an impression of the scope of the extrapolation involved.

III.4 ^{16}O+^{16}O calculation

We use the scattering formalism from Ref.[29] amended to include the IWBC and the symmetry of the two identical bosons (spin 0) ^{16}O. Both nuclei are treated as elementary, i.e., point-like particles interacting through a potential $V(r)$, where r is the magnitude of the separation vector $\vec{r}$ between the two nuclei. The stationary scattering wave function for distinguishable particles in the center-of-mass frame is

$$\Psi_D(\vec{r}) = \frac{1}{2kr}\sum_{l=0}^{\infty} (2l+1) i^{l+1} \psi_l(r) P_l(\cos\theta) \quad , \tag{III.6}$$

where $k = (2ME/\hbar^2)^{1/2}$ is the wave number (M is the reduced mass and E the center-of-mass energy), and P_l is a Legendre polynomial. The $\psi_l(r)$ are the solutions of the partial wave Schrödinger equations

$$\left[-\frac{\hbar^2}{2M}\frac{d^2}{dr^2} + \frac{\hbar^2 l(l+1)}{2Mr^2} + V(r) - E\right]\psi_l(r) = 0 \tag{III.7}$$

with the IWBC at an inner radius r_0 and asymptotic behavior for large r such that

$$\psi_l \sim u_l^{(-)}(kr) - S_l \exp(2i\sigma_l)\, u_l^{(+)}(kr) \quad . \tag{III.8}$$

$u_l^{(+)}(kr)$ and $u_l^{(-)}(kr)$ are the outgoing and incoming spherical Coulomb functions, i.e., the eigenfunctions of the partial wave Schrödinger equations with potential $(Z_1\, Z_2\, e^2)/r$; σ_l is the Coulomb phase shift

$$\sigma_l = \arg\Gamma(l+1+i\eta) \quad . \tag{III.9}$$

The IWBC is the reason why the absolute value of S_l can be less than unity and S_l cannot be written as $\exp(2i\delta_l)$ with real phase shifts δ_l. The deviation of $|S_l|$ from one is a measure for the amount of flux removed from the elastic channel and determines the fusion cross section.

For the case of identical bosons, instead of $\Psi_D(\vec{r})$, the symmetric wave function $\Psi(\vec{r}) = \Psi_D(\vec{r}) + \Psi_D(-\vec{r})$ has to be used. Since $P_l(\cos(\pi-\theta)) = (-)^l P_l(\cos\theta)$,

$$\Psi(\vec{r}) = \frac{1}{kr}\sum_{l\,even}(2l+1)i^{l+1}\psi_l(r)\,P_l(\cos\theta) \quad . \tag{III.10}$$

From (III.10),with the asymptotic behavior (III.8), we find for the nuclear scattering amplitude

$$f_N(\theta) = \frac{1}{ik}\sum_{l\,even}(2l+1)e^{2i\sigma_l}(S_l-1)P_l(\cos\theta) \quad . \tag{III.11}$$

The elastic cross section is the square of the sum of f_N and the symmetric Coulomb amplitude f_C^s,

$$\frac{d\sigma}{d\Omega} = |f_N(\theta) + f_C^s(\theta)|^2 \quad . \tag{III.12}$$

The symmetric Coulomb amplitude is the sum of the usual Rutherford amplitudes at angles θ and $(\pi-\theta)$:

$$f_C^s(\theta) = -\frac{\eta}{2k}\left[\frac{\exp(-i\,\eta\,\ln(\sin^2\theta/2)+2i\sigma_0)}{\sin^2(\theta/2)} + \frac{\exp(-i\,\eta\,\ln(\cos^2\theta/2)+2i\sigma_0)}{\cos^2(\theta/2)}\right] \quad . \tag{III.13}$$

(III.12) can be rewritten as

$$\frac{d\sigma}{d\Omega} = |\, f_N(\theta)\,|^2 + |f_C^s(\theta)\,|^2 + 2\Re\left[\left(f_N(\theta)\right)^* f_C^s(\theta)\right] \quad , \tag{III.14}$$

and $|\, f_C^s(\theta)\,|^2$ is easily evaluated as the symmetric Rutherford cross section:

$$\frac{d\sigma_0}{d\Omega} = |\, f_C^s(\theta)\,|^2 = \left(\frac{\eta}{2k}\right)^2 \times \left[\frac{1}{\sin^4(\theta/2)} + \frac{1}{\cos^4(\theta/2)} + \frac{2}{\cos^2(\theta/2)\,\sin^2(\theta/2)} \cos\Big(\eta \ln(\tan^2(\theta/2))\Big)\right] \tag{III.15}$$

The total elastic cross section $\int d\Omega(d\sigma/d\Omega)$ diverges, because we do not cut off the Coulomb potential in $V(r)$ for large r. The scattering cross section $d\sigma$ is defined as the probability per unit time that the projectile will pass through a surface element $r^2 d\Omega$ divided by the incoming current density. In analogy, the total fusion cross section in the IWBC formalism is the integral over the spherical surface at the IWBC radius r_0 of the probability per unit time that the particle passes through a surface element on the sphere divided by the incoming current density. The expression for the scattering cross section as the square of $f(\theta)$ (if the outgoing wave is written as $\Psi(\theta, r) = f(\theta)\exp(ikr)/r$) follows from the calculation of the local radial current density per surface element $r^2 d\Omega$, namely $\vec{j} = \frac{i\hbar}{2m}(\Psi\vec{\nabla}\Psi^* - \Psi^*\vec{\nabla}\Psi)$, dotted into the surface element. This product is the probability dw_s per unit time that the particle passes through $r^2 d\Omega$. Thus,

$$dw_s = \vec{j}\cdot\hat{n}r^2 d\Omega = \frac{\hbar k}{M}|f(\theta)|^2 d\Omega \quad , \tag{III.16}$$

where $\hat{n}$ is the unit vector perpendicular to $d\Omega$ and pointing outwards. $(dw_s/d\Omega)$ divided by the incoming current density $\hbar k/M$ gives the cross section $d\sigma/d\Omega =$

$|f(\theta)|^2$. Analogously, we find for the total fusion probability w_f per unit time

$$w_f = -\int r^2 d\Omega \frac{i\hbar}{2M}\left(\Psi\frac{\partial}{\partial r}\Psi^* - \Psi^*\frac{\partial}{\partial r}\Psi\right) \quad , \tag{III.17}$$

where the integral is over the spherical surface at r_0, and the minus sign in front of the integral stems from the fact that we are now considering an ingoing instead of an outgoing flux. If we insert (III.6) into (III.17), and use the IWBC for the ψ_l, we find after integration over $d\Omega$ (using $\int d\Omega P_l(\cos\theta)P_{l'}(\cos\theta) = 4\pi\delta_{ll'}/(2l+1)$) for the total fusion cross section for distinguishable particles (cf. (II.1)):

$$\sigma_{fD} = \frac{Mw_f}{\hbar k} = \frac{\pi}{k^2}\sum_{all\ l}(2l+1)T_l \quad , \tag{III.18}$$

where

$$T_l = \frac{k_l(r_0)}{k}|\psi_l(r_0)|^2 \tag{III.19}$$

is the transmission coefficient. For identical bosons we find (cf. (II.6))

$$\sigma_f = \frac{2\pi}{k^2}\sum_{l\ even}(2l+1)T_l \quad , \tag{III.20}$$

the factor 2 is a product of a 4 from the squared wave function (cf. (III.8) and (III.13)) times a factor $\frac{1}{2}$ that must be included to compensate for double-counting in the same way that a total (finite-range potential) scattering cross section of identical particles is half the integral over all solid angle of the differential cross section. If the penetrability coefficients vary slowly in l (and if thus lots of partial waves contribute), then σ_f approximately equals σ_{fD} in accordance with the correspondence principle of quantum mechanics. Because of unitarity (and more about that in the next chapter)

$$T_l = 1 - |S_l|^2 \quad . \tag{III.21}$$

According to (III.7) we numerically integrate the ψ_l outwards from the IWBC radius r_0 to some radius r_1 far outside the range of the nuclear potential, but still inside the range of the centrifugal and necessarily the Coulomb potential. At r_0, the logarithmic derivative of ψ_l is fixed by the IWBC, and near r_1, ψ_l is matched to $u_l^{(-)}(kr)$ and $u_l^{(+)}(kr)$ and then normalized so that its coefficient of $u_l^{(-)}(kr)$ equals unity (cf. (III.8)).

Results of the calculation are shown in Figs.9-12. We used a Woods-Saxon potential $V_N(r) = -V_0/[1 + \exp((r - R)/a)]$ plus a point-point Coulomb potential for V. This potential has the following relationship of the maximum of the s-wave barrier R_B, the potential range R, the diffuseness a, and the depth V_0:

$$R = R_B - a \ln\left(\kappa - 1 + \sqrt{\kappa^2 - 2\kappa}\right) \quad , \tag{III.22}$$

with

$$\kappa = \frac{R_B^2 V_0}{2 Z_1 Z_2 e^2 a} \quad . \tag{III.23}$$

Thomas *et al.*[25] have fitted the Woods-Saxon parameters to their measured fusion cross section with a least-χ^2 approach. Since the fusion cross section is sensitive only to the barrier region of the potential and not to the interior region, equally good χ^2 fits were obtained from widely different depths V_0. Therefore, Thomas *et al.* fixed V_0 at 50 MeV and fitted the potential range R and diffuseness a. They find the lowest χ^2 per degree of freedom to be 1.66 at R =6.51 fm and a =0.46 fm. The s-wave potential $V(r)$ is plotted in Fig.9, and the calculated fusion cross section in Fig.10. R =6.51 fm is equivalent to an R_0 =1.29 fm in the usual parametrization $R = R_0(A_1^{\frac{1}{3}} + A_2^{\frac{1}{3}})$, where A_1 and A_2 are the mass numbers of the two nuclei, i.e., 16

for both in our case. The values for V_0 and R_0 are typical for the real part of optical potentials that are used for heavy ions in this region of the periodic table. However, the diffuseness is rather small; typically optical potentials have a larger than 0.6 fm. Thomas's potential also reproduces the elastic scattering cross section at 90° (cf. Fig.11) measured by Spinka and Winkler.[21] Christensen and Switkowski[30] claimed that such a simultaneous fit to fusion and elastic data is impossible with a simple Woods-Saxon form of the potential. Apparently, they restricted their parameter search to the region of larger diffuseness. Recently, it was discovered for the system ^{16}O+ ^{208}Pb that a simultaneous fit to fusion and scattering data in the IWBC formalism requires a much steeper potential than used before in optical model calculations.[31] Fig.12 shows the elastic angular distribution for ^{16}O+^{16}O at 13 MeV together with the simple symmetric Rutherford cross section ($d\sigma_0/d\Omega$); the data are from an old paper by Bromley *et al.*,[32] and it is very difficult to read the data points from their published figure. In any case, there is reasonable agreement between the calculation and experiment. Most of the cross section is just $d\sigma_0/d\Omega$, but also the deviations of the data from $d\sigma_0/d\Omega$ are at least qualitatively reproduced. For $E = 10$ MeV, the cross section is practically identical to the symmetric Rutherford cross section.

Instead of a point-point Coulomb potential, a more sophisticated version can be used that will model the extended charge densities of the colliding nuclei (e.g., as two uniformly charged spheres) and modify the potential at short range, when the charge densities overlap, accordingly. However, because of the insensitivity of the calculated cross section to the interior of the potential, any such modification will

have negligible effect. We believe that Thomas *et al.* used a point-point Coulomb force when they fitted their parameters, and so we also keep this simple form.

The results of the calculation are also insensitive to the location of the IWBC radius r_0. We found a change of less than about 1% in both the fusion and 90° elastic cross sections when r_0 is varied from 5.0 to 5.5 fm. Convergence in the angular momentum is satisfactory when partial waves up to $l = 16$ are taken into account; for $E = 14$ MeV, a lower maximum l would cause a noticeable error. For the integration of the wave function we use the Numerov algorithm[33] whose local numerical error goes as the sixth power of the step size. A step size of 0.01 fm proved more than sufficient. As a numerical check, we calculated T_l directly from (III.19) and also from (III.21); the resulting values can be made as close to each other as one might desire by decreasing the step size and are in excellent agreement for our choice. An outside matching radius of 12 fm is far enough from the range of the Woods-Saxon potential.

In summary, the $^{16}O+^{16}O$ fusion cross section can be well reproduced by a one-channel IWBC calculation. When the potential is adjusted to give a best fit to these data, the 90° elastic cross section is also reproduced. Our expectation of the stiffness of the ^{16}O nuclei in a subbarrier collision is thus confirmed; internal degrees of freedom do not seem to play an important role.

CHAPTER IV

We will now develop an unified model for $^{17}O + {}^{16}O$ and simultaneously calculate the fusion, elastic, and inelastic cross sections.

IV.1 The Hamiltonian

We will treat the reaction as a 3-body problem, where the three bodies are the neutron outside the closed shell in ^{17}O and two ^{16}O nuclei, which we treat as inert cores (or "elementary" particles) without the possibility of internal excitations. This assumption is reasonable, because the first excited state in ^{16}O is 6.04 MeV above the ground state, compared with 0.87 MeV for ^{17}O. However, for small inter-nuclear distances the Pauli principle between nucleons of the different cores (or between the extra neutron and an ^{16}O core) becomes important. We will neglect this, as we will consider only bombarding energies at which the two nuclei do not strongly overlap in the direct reactions and we will treat the fusion reaction and thus the compound nucleus with an IWBC, in which the details of the compound nuclear wave function are lost anyhow. We will treat the symmetry between the two identical bosons ^{16}O exactly, though.

We denote the two cores as "1" and "2" and the extra neutron as "n" and use $\vec{R}$, $\vec{r}$, and $\vec{r} - \vec{R}$ for the relative position vectors, as in Fig.13. The Hamiltonian $\mathcal{H}$

for the system is

$$\mathcal{H} = T_1 + T_2 + T_n + V_1 + V_2 + V_c \quad , \tag{IV.1}$$

where T_i is the kinetic energy for particle i, V_i the potential between "n" and i, and V_c the potential between the cores "1" and "2". We will neglect the recoil correction that stems from the change in masses and hence in the center-of-mass coordinates in a rearrangement collision. These corrections are of order $M_n/M_1 = \frac{1}{16}$, where M_i is the mass of particle i. In this approximation no differentiation between $\vec{R}$ and the position vector between ^{17}O (the center-of-mass of one ^{16}O and "n") and the other ^{16}O exists. While an expansion of the recoil in M_n/M_1 is possible,[34] the complete neglect of terms of order M_n/M_1 makes the expressions more tractable and greatly reduces the magnitude of the numerical computations.

The Hamiltonian thus becomes

$$\mathcal{H} = T_{cm} + H \quad , \tag{IV.2}$$

where T_{cm} is the total center-of-mass kinetic energy and

$$H = T + T_n + V_1 + V_2 + V_c \quad , \tag{IV.3}$$

where T is the kinetic energy of the relative motion between "1" and "2".

IV.2 The wave function

The stationary scattering state is

$$|\Phi(R)\rangle = \sum_i \phi_i(R)\,|\,i\rangle \quad , \tag{IV.4}$$

the sum over the products of a radial wave function ϕ_i of the inter-nuclear distance $R = |\vec{R}|$ and an internal state $|i\rangle$ of ^{17}O and ^{16}O containing also the wave function of the angles of the vector $\vec{R}$. The label i characterizes (1) the partition γ (whether the neutron belongs to particle "1" or "2"; these partitions are called α and β, respectively), (2) the eigenstate of ^{17}O, and (3) the eigenstate of orbital angular momentum L associated with the vector $\vec{R}$. The internal spin of the ^{17}O nucleus and the orbital angular momentum are coupled so that $|i\rangle$ is an eigenstate of total angular momentum J and its component J_z along some fixed axis. If the sum in (IV.4) is to be taken over a complete set of eigenstates of ^{17}O and all angular momenta L, then $|\Phi(R)\rangle$ is the exact scattering state within our model, i.e., when we consider only single particle excitations of the extra neutron in ^{17}O and one-neutron transfer. Of course, we will truncate the series (IV.4) quite severely and thus restrict the subspace of possible wave functions.

The eigenstates $|i\rangle$ of the single particle Hamiltonian have the property that for states with the ^{17}O on the left (α states)

$$\left(T_n + V_1\right)|i(\alpha)\rangle = \epsilon_i\,|i(\alpha)\rangle \qquad , \tag{IV.5}$$

and for the ^{17}O on the right

$$\left(T_n + V_2\right)|i(\beta)\rangle = \epsilon_i\,|i(\beta)\rangle \qquad , \tag{IV.6}$$

where ϵ_i is the single particle energy of the neutron in the ^{17}O nucleus in the state i. α and β states are not orthogonal because of the different origin for the single particle wave function.

IV.3 The adiabatic approximation

The Schrödinger equation

$$(H - E)\,|\Phi(R)\rangle = 0 \tag{IV.7}$$

is transformed into a set of coupled equations by multiplication by each of the $|i\rangle$, i.e.,

$$\langle i|\, H - E\,|\Phi(R)\rangle = 0 \qquad \text{for all } i. \tag{IV.8}$$

The adiabatic (or *Born-Oppenheimer*) approximation consists of letting T operate only on the explicit dependence of $|\Phi(R)\rangle = \sum \phi_j(R)|j\rangle$ upon $\vec{R}$ (namely upon the radial wave function $\phi_j(R)$) and the orbital angular momentum part of $|j\rangle$, but not on the intrinsic structure of $|j\rangle$. Thus, when the Laplacian that occurs in the kinetic energy operator is expanded into radial and angular parts,

$$\nabla^2 = \frac{1}{R}\frac{\partial^2}{\partial R^2}R - \frac{\vec{L}^2}{\hbar^2 R^2} \qquad , \tag{IV.9}$$

then

$$T\phi_j(R)\,|j\rangle \approx |j\rangle\left(-\frac{\hbar^2}{2mR}\frac{d^2}{dR^2}R + \frac{\hbar^2 L_j(L_j+1)}{2mR^2}\right)\phi_j(R) = |j\rangle\, T^j\phi_j(R) \qquad , \tag{IV.10}$$

where m is the reduced mass, and L_j gives the angular momentum of the state $|j\rangle$, $\vec{L}^2\,|j\rangle = \hbar^2 L_j(L_j+1)\,|j\rangle$. (IV.10) is only an approximation, because the states $|j\rangle$ are functions of R. Combining (IV.3), (IV.5),(IV.6),(IV.8), and (IV.10), and letting $T_n + V_2$ operate on the right yields

$$\sum_j \left[\langle i|j\rangle\left(\epsilon_j - E + T^j + V_c\right)\phi_j(R) + \langle i|V_{(j)}|j\rangle\phi_j(R)\right] = 0 \qquad . \tag{IV.11}$$

Here, $V_{(j)} = V_1$, if $|j\rangle = |j(\beta)\rangle$ is a right (a β) state and $V_j = V_2$ for an α state. If we define $g_{ij} = \langle i|j\rangle$, $f_{ij} = \langle i|V_{(j)}|j\rangle$, and $\psi_j(R) = (\epsilon_j - E + T^j + V_c)\phi_j(R)$, then we can interpret g and f as matrices and ϕ and ψ as column vectors and write the set of equations (IV.11) as:

$$g\psi + f\phi = 0 \tag{IV.12}$$

or equivalently

$$\psi = -g^{-1}f\phi \quad . \tag{IV.13}$$

In more explicit notation, (IV.13) can be brought into the form

$$\Big(\epsilon_i - E + T^i + V_c + \sum_j (g^{-1})_{ij}\langle j|V_{(i)}|i\rangle\Big)\phi_i(R) = -\sum_{k\neq i}\sum_j (g^{-1})_{ij}\langle j|V_{(k)}|k\rangle\phi_k(R) \tag{IV.14}$$

for all i. The set of coupled channels equations (IV.14) is very typical in direct nuclear reaction theory (cf. (II.19)), the left hand side of each equation is the usual one-channel Schrödinger equation, and the right hand side is an inhomogeneous term that couples the wave function on the left hand side to all others. However, (IV.14) is a homogeneous system of differential equations for the total wave function (the sum over all channel wave functions). A set of equations like (IV.14) is used in almost all multi-channel subbarrier fusion calculations that include transfer. However, the explicit set (IV.14) does not admit a conserved current, as we will show next.

IV.4 Violation of unitarity in the adiabatic approximation

Flux non-conservation is already exhibited by a one-dimensional model, so, to avoid the obfuscating aspects of the angular momenta, we will treat the one-

dimensional case in this and the next section. It will become clear how to extend this proof to the full three-dimensional case when we derive the full matrix elements between the states $|i\rangle$. If we use R as the Cartesian coordinate, then the equations look very similar to the above if we substitute the one-dimensional wave function $\chi(R)$ for the product $R\phi(R)$. The simplifying feature is that the kinetic energy operator does not include a centrifugal potential and is thus the same in all channels.

The generalized radial flux in the case of non-orthogonal states is proportional to the quantity

$$F = \sum_{i,j} \left[\langle i|j\rangle \left(\chi_i^* \frac{d}{dR}\chi_j - \chi_j \frac{d}{dR}\chi_i^* \right) \right] \quad , \tag{IV.15}$$

if the $\langle i|j\rangle$ are real. We will show later that this choice of phase is indeed possible (and that the $\langle i|V_{(j)}|j\rangle$ then become real, too), and we will restrict our analysis to this convention. We will now prove that neither F nor an "orthogonal" substitute

$$\bar{F} = \sum_i \left(\chi_i^* \frac{d}{dR}\chi_i - \chi_i \frac{d}{dR}\chi_i^* \right) \tag{IV.16}$$

is conserved by the adiabatic equations. If we insert (IV.10) into (IV.11), the adiabatic equations in terms of the χ_i become:

$$\sum_j \left[\langle i|j\rangle \left(-\frac{\hbar^2}{2m}\frac{d^2}{dR^2} + \epsilon_j - E + V_c \right) \chi_j(R) + \langle i|V_{(j)}|j\rangle \chi_j(R) \right] = 0 \, . \tag{IV.17}$$

We will at first calculate the radial derivative of F, then that of $\bar{F}$:

$$\frac{dF}{dR} = \sum_{i,j} \left[\langle j|i\rangle \left(\chi_i^* \frac{d^2}{dR^2}\chi_j - \chi_j \frac{d^2}{dR^2}\chi_i^* \right) + \left(\chi_i^* \frac{d}{dR}\chi_j - \chi_j \frac{d}{dR}\chi_i^* \right) \frac{d}{dR}\langle j|i\rangle \right] . \tag{IV.18}$$

We proceed from (IV.17) in a similar fashion to the proof of flux conservation for the simple one-channel Schrödinger equation, we multiply (IV.17) by χ_i^* and sum

over all i, the result is

$$\sum_{i,j}\left[\langle i|j\rangle\,\chi_i^*\Big(-\frac{\hbar^2}{2m}\frac{d^2}{dR^2}+\epsilon_j-E+V_c(R)\Big)\chi_j+\langle i|V_{(j)}|j\rangle\chi_i^*\chi_j\right]=0\ . \qquad \text{(IV.19)}$$

Instead of (IV.17), we could derive an analogous equation for the complex conjugate wave function if we let $T+V_i$ operate on the bra state and interchange the indices i and j, i.e.

$$\sum_{i}\left[\langle i|j\rangle\,\Big(\epsilon_j-E-\frac{\hbar^2}{2m}\frac{d^2}{dR^2}+V_c\Big)\chi_i^*(R)+\langle i|V_{(i)}|j\rangle\chi_i^*(R)\right]=0\ . \qquad \text{(IV.20)}$$

We multiply (IV.20) by χ_j, sum over all j and subtract the resulting equation from (IV.19), hence

$$\frac{\hbar^2}{2m}\sum_{i,j}\langle i|j\rangle\Big(\chi_i^*\frac{d^2}{dR^2}\chi_j-\chi_j\frac{d^2}{dR^2}\chi_i^*\Big)=\sum_{i,j}\left[\langle i|j\rangle(\epsilon_j-\epsilon_i)+\langle i|V_{(j)}-V_{(i)}|j\rangle\right]\chi_i^*\chi_j\ . \qquad \text{(IV.21)}$$

Hermiticity (or, by our choice of phase: symmetry) of the sum of operators V_1, V_2, and T_n requires that

$$\langle i|\Big(V_1+V_2+T_n|j\rangle\Big)=\Big(\langle i|V_1+V_2+T_n\Big)|j\rangle \qquad , \qquad \text{(IV.22)}$$

or, equivalently,

$$\langle i|j\rangle(\epsilon_j-\epsilon_i)+\langle i|V_{(j)}-V_{(i)}|j\rangle=0 \qquad . \qquad \text{(IV.23)}$$

Therefore, in the adiabatic approximation,

$$\sum_{i,j}\langle i|j\rangle\Big(\chi_i^*\frac{d^2}{dR^2}\chi_j-\chi_j\frac{d^2}{dR^2}\chi_i^*\Big)=0 \qquad , \qquad \text{(IV.24)}$$

and if we insert (IV.24) into (IV.18)

$$\frac{dF}{dR}=\sum_{i,j}\Big(\chi_i^*\frac{d}{dR}\chi_j-\chi_j\frac{d}{dR}\chi_i^*\Big)\frac{d}{dR}\langle j|i\rangle \qquad . \qquad \text{(IV.25)}$$

Although the terms involving $\frac{d}{dR}\langle i|j\rangle$ were neglected in the derivation of (IV.11) from the general Hamiltonian and wave function, the $\langle i|j\rangle$ that are inserted into (IV.11) are not constant in R (precisely herein lies the inconsistency), and, by (IV.25), F is not conserved.

This is perhaps not surprising, but it is surprising that $\bar{F}$ is also not conserved. (IV.11) can be abbreviated to the following equations for the χ_i:

$$\frac{d^2}{dR^2}\chi_i + a_i\chi_i + \sum_j h_{ij}\chi_j = 0 \qquad , \tag{IV.26}$$

where h is the matrix product of the inverse of the overlap and, for symmetry let us say $\epsilon_j\delta_{ij} + \langle i|V_{(j)}|j\rangle = \epsilon_i\delta_{ij} + \langle j|V_{(i)}|i\rangle$. If h were Hermitian, (IV.24) would prove the conservation of $\bar{F}$ as follows: Multiply (IV.24) by χ_i^* and sum over all i, then form the complex conjugate of (IV.24), multiply by χ_i and again sum over all i, the difference of the two resulting equations - by Hermiticity of h - has just $d\bar{F}/dR$ on the left hand side and zero on the right hand side. However, h as the product of two Hermitian matrices does not have to be Hermitian itself. If one forms Hermitian matrices A_{ij} and B_{ij} as inner products of self-adjoint operators A and B in an orthonormal basis, the matrix product $\sum_j A_{ij}B_{jk}$ is Hermitian if and only if A and B commute. However, this is not true for non-orthogonal basis states such as those we are dealing with here. Therefore, $d\bar{F}/dR \neq 0$ if $\langle i|j\rangle \neq \delta_{ij}$.

We consider the failure of the adiabatic equations to conserve flux to be a very serious deficiency. The principle of the IWBC equates the flux at the inner radius with the fusion flux, but if the model equations are not unitary, the fusion flux defined in this way will not equal the total flux removed from the explicit reaction channels. This inequality would bring our whole program into question,

as we intend to calculate fusion, elastic, and inelastic cross section in a consistent way. Therefore, our original equations (IV.8) have to be solved without neglect of the non-centrifugal terms of $\langle i|T|j\rangle$, i.e., without using the approximation (IV.10). Not only will this restore unitarity, but it will mean one approximation less, always a desirable effect. However, the price to be paid is not only a cluttering of analytic expressions, but also considerable complications in the numerical work that we will encounter.

IV.5 Unitarity of the non-adiabatic equations

We will now show that the non-adiabatic equations conserve flux, as they should, because our original Hamiltonian (IV.3) is self-adjoint. Again, we restrict ourselves to the one-dimensional case; the result does not change in three dimensions, but the expressions are less lucid.

We now measure the position of "n" from the center between "1" and "2". If we denote the corresponding position vector by $\vec{r}$, the single particle wave function of α states will then be $\chi(r+R/2)$, of β states $\chi(r-R/2)$. Our set of equations is:

$$\sum_j \Big[-\frac{\hbar^2}{2m}\Big(\Big\langle i\Big|\frac{\partial^2}{\partial R^2} j\Big\rangle \chi_j + 2\Big\langle i\Big|\frac{\partial}{\partial R} j\Big\rangle \frac{d\chi_j}{dR}\Big) + \langle i|j\rangle\Big(\epsilon_j - E - \frac{\hbar^2}{2m}\frac{d^2}{dR^2} + V_c\Big)\chi_j + \langle i|V_{(j)}|j\rangle\chi_j\Big] = 0\ , \tag{IV.27}$$

where

$$\Big\langle i\Big|\frac{\partial^2}{\partial R^2} j\Big\rangle = \int dr\, \chi_i^*(r \pm R/2)\frac{\partial^2}{\partial R^2}\chi_j(r \pm R/2) \quad , \tag{IV.28}$$

and

$$\Big\langle i\Big|\frac{\partial}{\partial R} j\Big\rangle = \int dr\, \chi_i^*(r \pm R/2)\frac{\partial}{\partial R}\chi_j(r \pm R/2) \tag{IV.29}$$

produce the new terms that are not in the adiabatic equations. The sign in the argument of the wave function depends on the partition of the wave function, plus and minus for α and β states, respectively. The complex conjugate to (IV.27) is

$$\sum_i \Big[-\frac{\hbar^2}{2m}\Big(\Big\langle \frac{\partial^2}{\partial R^2} i \Big| j \Big\rangle \chi_i^* + 2\Big\langle \frac{\partial}{\partial R} i \Big| j \Big\rangle \frac{d\chi_i^*}{dR}\Big) + \langle i|j\rangle \Big(\epsilon_i - E - \frac{\hbar^2}{2m}\frac{d^2}{dR^2} + V_c\Big)\chi_i^* + \langle i|V_{(i)}|j\rangle \chi_i^* \Big] = 0 \quad . \quad (IV.30)$$

We multiply (IV.27) by χ_i^* and sum over all i, and analogously multiply (IV.30) by χ_j and sum over all j; the difference between the two resulting equations becomes

$$\frac{\hbar^2}{2m}\sum_{i,j}\Big[\Big(\Big\langle i\Big|\frac{\partial^2}{\partial R^2} j\Big\rangle - \langle \frac{\partial^2}{\partial R^2} i \Big| j\rangle\Big)\chi_i^*\chi_j + 2\Big(\Big\langle i\Big|\frac{\partial}{\partial R} j\Big\rangle \chi_i^* \frac{d\chi_j}{dR} - \Big\langle \frac{\partial}{\partial R} i\Big| j\Big\rangle \frac{d\chi_i^*}{dR}\chi_j\Big) + \langle i|j\rangle\Big(\chi_i^*\frac{d^2\chi_j}{dR^2} - \frac{d^2\chi_i^*}{dR}\chi_j\Big)\Big] = 0 \,, \quad (IV.31)$$

when we use (IV.23). Partial integration on (IV.27) proves that $\Big\langle i\Big|\frac{\partial^2}{\partial R^2} j\Big\rangle = \Big\langle \frac{\partial^2}{\partial R^2} i\Big| j\Big\rangle$. Also, (IV.27) and (IV.28) do not connect states with equal partition, but opposite parity of the single particle wave function; and, for equal parity of χ_i and χ_j, $\langle \frac{\partial}{\partial R} i|j\rangle = \langle i|\frac{\partial}{\partial R} j\rangle = 0$. Therefore, we only need to consider the case of opposite partition for the terms $\langle \frac{\partial}{\partial R} i|j\rangle$ and $\langle i|\frac{\partial}{\partial R} j\rangle$, and again these amplitudes are equal by proof of partial integration on (IV.28). Thus,

$$\frac{\partial}{\partial R}\langle i|j\rangle = \Big\langle \frac{\partial}{\partial R} i\Big| j\Big\rangle + \Big\langle i\Big|\frac{\partial}{\partial R} j\Big\rangle = 2\Big\langle i\Big|\frac{\partial}{\partial R} j\Big\rangle = 2\Big\langle \frac{\partial}{\partial R} i\Big| j\Big\rangle \,, \quad (IV.32)$$

so that the expression in (IV.31) becomes just the derivative of the flux (IV.15), since the radial derivative of R times the three-dimensional wave function is precisely

equivalent to the one-dimensional wave function (and hence using the same notation for them justified). Therefore, $\partial F/\partial R$ vanishes, or F is conserved.

IV.6 Formfactors

The matrix elements of various operators between the states $|i\rangle$ are needed as input into the coupled channels equations. These matrix elements are called formfactors, they are functions of R and depend on the single particle eigenstate and the coupled angular momenta. We will now derive the analytic form of these matrix elements for three dimensions.

For the derivation of the formfactors, the starting point is the Hamiltonian (IV.3) and the scattering state $|\Phi\rangle = \frac{1}{R}\sum_j \chi_j(R)|j\rangle$; we multiply (IV.8) by R and gain

$$\sum_j \left\langle i \middle| \left(-\frac{\hbar^2}{2m} R\nabla^2 \frac{1}{R} + V_c(R) + \epsilon_j - E + V_{(j)}(R) \right) \chi_j(R) \middle| j \right\rangle = 0 \,. \qquad \text{(IV.33)}$$

In (IV.33), ∇^2 operates both on χ_j/R and on $|j\rangle$. By the product rule for derivatives, this will produce $(\chi_j/R)\nabla^2|j\rangle + |j\rangle\nabla^2(\chi_j/R) + 2(\vec{\nabla}|j\rangle)\cdot(\vec{\nabla}(\chi_j/R))$. Since in the last term the gradient operates on a radial function only, and since the gradient in spherical polar coordinates is $\hat{R}\frac{\partial}{\partial R}$ plus parts perpendicular to $\hat{R}$ (the unit vector in the direction of $\vec{R}$) that do not involve $\frac{\partial}{\partial R}$, only the radial component of the dot product of the two gradients, i.e., $2(\frac{\partial}{\partial R}|j\rangle)(\frac{\partial}{\partial R}(\chi_j/R))$, contributes.

Another method of treating the term involving $\langle i|R\nabla^2\frac{1}{R}\chi_j|j\rangle$ exists and might *a priori* look even simpler: By (IV.9), the above matrix element of the Laplacian is simply $\langle i|\frac{\partial^2}{\partial R^2}\chi_j|j\rangle - \chi_j/(\hbar^2R^2)\langle i|\vec{L}^2|j\rangle$, and the product rule of differentiation can

now be applied to $\chi_j|j\rangle$ in $\frac{\partial}{\partial R}$ instead of the gradient. However, this second method of evaluating the Laplacian turns out to be no easier, because we will expand the state $|j\rangle$ in the sum of products of an internal state times an angular wave function, and it is easier to use the product rule on these products for the Laplacian than for $\vec{L}^2$ and $\frac{\partial^2}{\partial R^2}$. In the end, as both methods will require roughly the same amount of algebra, neither one is a neat step towards a simple formalism. We choose the first method.

Thus, the required operators between the states $\langle i|$ and $|j\rangle$ are: The Laplacian ∇^2 and radial gradient $\frac{\partial}{\partial R}$, the potential $V_{(i)}$, and the unit operator (for the overlap). The bra and ket states of the matrix elements can have either the same or opposite partition, the first case produces the inelastic excitations, the second the transfer reactions.

A new choice of coordinates facilitates the derivation; in fact, two coordinate systems are needed: an external fixed system (x, y, z) and - rotated with respect to it - an intrinsic system $(\bar{x}, \bar{y}, \bar{z})$. The angles in spherical polar coordinates of any vector $\vec{v}$ are denoted θ_v, φ_v and $\bar{\theta}_v$, $\bar{\varphi}_v$ in the external and intrinsic system, respectively. Particle "1" lies at the origin, particle "2" is separated by $\vec{R}$, the neutron by $\vec{r}$, as in Fig.13. The intrinsic frame has the $\bar{z}$-axis parallel to $\vec{R}$ and the $\bar{y}$-axis in the x-y plane so that the angle between the positive y-axis and positive $\bar{y}$-axis is less than or equal to $\pi/2$. The components of $\vec{R}$ and $\vec{r}$ serve as independent coordinates. With our choice of the origin, the single particle wave function (of the neutron) takes argument $\vec{r}$ in an α state and argument $(\vec{r} - \vec{R})$ in β states. This independence of $\vec{R}$ of the α states makes this particular representation useful for

the derivation of the formfactors. Unfortunately, a more symmetric representation between α and β states is needed below; the transformation is described in Section IV.7 .

For convenience, we will often abbreviate the pair θ_v, φ_v by Ω_v and $\int_0^{2\pi} d\varphi_v$ $\int_{-1}^{1} d(\cos\theta_v)$ by $\int d\Omega_v$. Whenever the notation $\langle a_1|O|a_2\rangle$ is ambiguous for some operator O, we will always mean O to operate on the right. We can write for our states:

$$|j\rangle = |(IL)J\mu\gamma\rangle = \sum_{M_I,M_L} \langle IM_I LM_L|J\mu\rangle Y_{LM_L}(\Omega_R)|IM_I\gamma\rangle \ . \qquad \text{(IV.34)}$$

γ is either α or β, depending on the partition. The $Y_{LM}(\Omega_R)$ are the usual spherical harmonics defined by $\vec{L}^2 Y_{LM}(\Omega_R) = \hbar^2 L(L+1)Y_{LM}$, $L_z Y_{LM}(\Omega_R) = M\hbar Y_{LM}(\Omega_R)$, and $\int d\Omega_R Y^*_{LM}(\Omega_R)Y_{LM}(\Omega_R) = 1$. I is the spin of the ^{17}O nucleus, L the relative angular momentum between the ^{17}O and ^{16}O nuclei, M_I, M_L the corresponding projections onto the z-axis. In the state $|j\rangle$, I and L are coupled to total angular momentum J with projection μ. Instead of keeping an extra index on these labels to differentiate between the quantum numbers of $|j\rangle$ and $\langle i|$, we mark those of the bra state by a $'$ symbol.

The matrix element of the operator X is thus:

$$\begin{aligned}\left\langle (I'L')J'\mu'\gamma'|X|(IL)J\mu\gamma\right\rangle_R &= \sum_{M'_I,M'_L}\sum_{M_I,M_L} \langle I'M'_I L'M'_L|J'\mu'\rangle \\ \times \langle IM_I LM_L|J\mu\rangle &\int d\Omega_R Y^*_{L'M'_L}(\Omega_R)\langle I'M'_I\gamma'|X|IM_I\gamma\rangle_{\vec{R}} Y_{LM_L}(\Omega_R) \ .\end{aligned} \qquad \text{(IV.35)}$$

The amplitude on the left hand side depends only on the magnitude of the vector $\vec{R}$, whereas the amplitude under the integral sign depends also on Ω_R. The operator X can be any of the following:

(i) The radial gradient $\frac{\partial}{\partial R}$, or

(ii) the Laplacian ∇^2, or

(iii) the unit operator 1 (for the overlap), or

(iv) $V_1 = v(r)$ or $V_2 = v(|\vec{r} - \vec{R}|)$, where v is the potential function between "n" and ^{16}O: V_1 if $\gamma = \beta$ and V_2 for $\gamma = \alpha$.

If X contains derivatives, (IV.35) has to be interpreted such that the derivative acts both on $|IM_I\gamma\rangle$ and on $Y_{LM_L}(\Omega_R)$, and it acts on the right only. At first, we will investigate the effect of the derivative operators on the spherical harmonics. Case *(i)* is trivial, as the radial derivative of a function of the angles vanishes, $\frac{\partial}{\partial R} Y_{LM}(\Omega_R) = 0$. Thus,

$$\begin{aligned} &\int d\Omega_R Y^*_{L'M'_L}(\Omega_R) \left\langle I'M'_I\gamma' \middle| \frac{\partial}{\partial R} \middle| IM_I\gamma \right\rangle Y_{LM_L}(\Omega_R) \\ &\quad = \int d\Omega_R Y^*_{L'M'_L}(\Omega_R) Y_{LM_L}(\Omega_R) \left\langle I'M'_I\gamma' \middle| \frac{\partial}{\partial R} \middle| IM_I\gamma \right\rangle . \end{aligned} \tag{IV.36}$$

Case *(ii)* becomes tractable after the Laplacian is split into radial and angular components by (IV.9). Clearly, only the angular momentum operator contributes on the Y_{LM}'s. If $\gamma = \alpha$ in (IV.35), then the Laplacian acts only on the Y_{LM}'s because of the independence of $|IM_I\alpha\rangle$ on $\vec{R}$. Hence,

$$\left\langle (I'L')J'\mu'\gamma' | \nabla^2 | (IL)J\mu\alpha \right\rangle = -\frac{L(L+1)}{R^2} \left\langle (I'L')J'\mu'\gamma' \middle| (IL)J\mu\alpha \right\rangle . \tag{IV.37}$$

For any two functions f and g of Ω, $\int d\Omega f(\nabla^2 g) = \int d\Omega g(\nabla^2 f)$. (This is most easily seen by expanding f and g in the eigenfunctions of the angular Laplacian, the spherical harmonics.) Then, (IV.35) can be evaluated for $\gamma' = \alpha$ by letting the Laplacian operate on the left:

$$\left\langle (I'L')J'\mu'\alpha | \nabla^2 | (IL)J\mu\gamma \right\rangle = -\frac{L'(L'+1)}{R^2} \left\langle (I'L')J'\mu'\alpha \middle| (IL)J\mu\gamma \right\rangle . \tag{IV.38}$$

(IV.37) and (IV.38) do not contradict each other for $\gamma' = \gamma = \alpha$, because $\langle (I'L')J'\mu'\alpha | (IL)J\mu\alpha \rangle$ vanishes for $L' \neq L$ (cf. below). For $\gamma' = \gamma = \beta$ in (IV.35), the Laplacian on the product $|IM_I\beta\rangle Y_{LM_L}(\Omega_R)$ must be evaluated by the product rule; of the three terms that are created thus, the one containing $\langle I'M'_I\beta|\vec{\nabla}|IM_I\beta\rangle$ vanishes because of parity conservation, the remaining two terms give:

$$\begin{aligned}\int d\Omega_R Y^*_{L'M'_L}(\Omega_R)\langle I'M'_I\beta|\nabla^2|IM_I\beta\rangle Y_{LM_L}(\Omega_R) \\ = -\frac{L(L+1)}{R^2}\int d\Omega_R Y^*_{L'M'_L}(\Omega_R)Y_{LM_L}(\Omega_R)\langle I'M'_I\beta|IM_I\beta\rangle \\ + \int d\Omega_R Y^*_{L'M'_L}(\Omega_R)Y_{LM_L}(\Omega_R)\langle I'M'_I\beta|\nabla^2|IM_I\beta\rangle \ .\end{aligned} \tag{IV.39}$$

The first summand in (IV.39), when inserted into (IV.35), will give $-L(L+1)/R^2$ $\langle (I'L')J'\mu'\beta | (IL)J\mu\beta \rangle$. We have thus successfully treated the effect of the operators on the angular wave function in $\vec{R}$, what remains is to calculate the amplitudes $\langle I'M'_I\gamma'|X|IM_I\gamma\rangle$ as functions of $\vec{R}$ for the four choices of X.

We will calculate these amplitudes in the expansion

$$\langle I'M'_I\gamma'|X|IM_I\gamma\rangle_{\vec{R}} = \sum_{\Lambda,\nu} x_{\Lambda\nu}(R)Y_{\Lambda\nu}(\Omega_R) \quad , \tag{IV.40}$$

where indices to show the dependence of x on I', I, etc. are omitted. After insertion of (IV.40) into (IV.35) (or of (IV.38) into (IV.36) or(IV.37) and then into (IV.35) in cases *(i)* and *(ii)*, respectively), the integrand in (IV.35) is a product of three spherical harmonics, whose integral is easily evaluated:

$$\begin{aligned}\int d\Omega_R Y^*_{L'M'_L}(\Omega_R)Y_{LM_L}(\Omega_R)Y_{\Lambda\nu}(\Omega_R) \\ = (-)^{M'_L}\left[\frac{(2L'+1)(2L+1)(2\Lambda+1)}{4\pi}\right]^{\frac{1}{2}}\begin{pmatrix} L' & L & \Lambda \\ 0 & 0 & 0\end{pmatrix}\begin{pmatrix} L' & L & \Lambda \\ -M'_L & M_L & \nu\end{pmatrix} ;\end{aligned} \tag{IV.41}$$

where

$$\begin{pmatrix} j_1 & j_2 & j_3 \\ m_1 & m_2 & m_3 \end{pmatrix} = (-)^{j_1-j_2-m_3}(2j_3+1)^{-\frac{1}{2}}\langle j_1 m_1 j_2 m_2 | j_3 - m_3\rangle \qquad \text{(IV.42)}$$

is the usual Wigner 3-j symbol. We begin the calculations of $\langle I'M_I'\gamma'|X|IM_I\gamma\rangle$ with the case of $\gamma' = \gamma = \alpha$ (an inelastic excitation of the ^{17}O nucleus on the left).

In our representation, α states do not depend explicitly on $\vec{R}$, hence, $\vec{\nabla}|IM_I\alpha\rangle = 0$, and $\nabla^2|IM_I\alpha\rangle = 0$. The $|IM_I\alpha\rangle$ are also orthonormal, i.e. $\langle I'M_I'\alpha|IM_I\alpha\rangle = \delta_{II'}\delta_{M_IM_I'}$. Thus, only $f(\vec{R}) = \langle I'M_I'\alpha|\, v(|\vec{r}-\vec{R}|)\,|IM_I\alpha\rangle$ remains. Sometimes it is just $f(\vec{R})$ and not the complete amplitude on the left hand side of (IV.35) that is referred to as the formfactor. In order to calculate $f(\vec{R})$ we need to disentangle the state $|IM_I\gamma\rangle$:

$$|IM_I\gamma\rangle = \psi_I(r)\mathcal{Y}^{M_I}_{l,s=1/2,I}(\Omega_r) \qquad , \qquad \text{(IV.43)}$$

where ψ_I is the single particle radial wave function of the neutron in ^{17}O with a phase convention so that the ψ_I are real; with this choice of phase all formfactors are real, too. $\mathcal{Y}^m_{lsj}$ is the usual spin spherical harmonic

$$\mathcal{Y}^m_{lsj} = \sum_{m_l,m_s}\langle lm_l sm_s|jm\rangle Y_{lm_l}\sigma_{sm_s} \qquad , \qquad \text{(IV.44)}$$

σ being the spin matrix (*not* a Pauli matrix). The spin $s = \frac{1}{2}$ of the neutron and the angular momentum l of the single particle wave function couple to the total spin I of the ^{17}O nucleus. l is determined by I. This coupling is only possible and (IV.42) is only valid if m_l and m_s are good quantum numbers in the potential $v(r)$, in particular, $v(r)$ must not contain a spin-orbit coupling term. Now,

$$\begin{aligned} f(\vec{R}) = &\sum_{m_l,m_s}\sum_{m_l',m_s'}\langle lm_l\,{}^1\!/_2 m_s|IM_I\rangle\langle l'm_l'\,{}^1\!/_2 m_s'|I'M_I'\rangle \\ &\times\int r^2 dr\psi^*_{I'}(r)\psi_I(r)\int d\bar{\Omega}_r v(|\vec{r}-\vec{R}|)Y^*_{l'm_l'}(\Omega_r)Y_{lm_l}(\Omega_r)\sigma^\dagger_{\frac{1}{2}m_s'}\cdot\sigma_{\frac{1}{2}m_s}\ . \end{aligned} \qquad \text{(IV.45)}$$

The argument of v is the distance between "n" and "2", namely $|\vec{r}-\vec{R}|=[r^2+R^2-2rR\cos\bar{\vartheta}_r]^{1/2}$. The angular integral in (IV.45) is most easily evaluated by expressing the product of two spherical harmonics as the sum over the products of one spherical harmonic times Wigner 3-j symbols, i.e.

$$Y^*_{l'm'_l}(\Omega_r)Y_{lm}(\Omega_r)=(-)^{m'_l}\sum_{\Lambda\nu}(-)^{\nu}\Big[\frac{(2l'+1)(2l+1)(2\Lambda+1)}{4\pi}\Big]^{\frac{1}{2}} \begin{pmatrix} l' & l & \Lambda \\ 0 & 0 & 0 \end{pmatrix}\begin{pmatrix} l' & l & \Lambda \\ -m'_l & m_l & -\nu \end{pmatrix} Y_{\Lambda\nu}(\Omega_r)\ , \tag{IV.46}$$

and rotating the $Y_{\Lambda\nu}(\Omega_r)$ to the intrinsic frame by

$$Y_{\Lambda\nu}(\Omega_r)=\sum_{\nu'}\mathcal{D}^{(\Lambda)}_{\nu'\nu}(0,\theta_R,\varphi_R)Y_{\Lambda\nu'}(\bar{\Omega}_r)\ . \tag{IV.47}$$

The $\mathcal{D}^{(j)}_{m'm}$ are the rotation matrices as defined in Edmonds[35] (i.e., $\mathcal{D}^{(j)}_{m'm}(\alpha,\beta,\gamma)$ $=\langle jm'|\exp(i\alpha J_z/\hbar)\exp(i\beta J_y/\hbar)\exp(i\gamma J_z/\hbar)|jm\rangle$); $\gamma=\varphi_R$, $\beta=\theta_R$, and $\alpha=0$ are the Euler angles associated with a rotation from the external to the intrinsic frame. Now the integral over $d\bar{\varphi}_r$ can be performed:

$$\int_0^{2\pi}d\bar{\varphi}_r Y_{\Lambda\nu'}(\bar{\theta}_r,\bar{\varphi}_r)=\sqrt{\pi(2\Lambda+1)}P_\Lambda(\cos\bar{\theta}_r)\delta_{\nu'0}\ . \tag{IV.48}$$

The remaining rotation matrix is proportional to a spherical harmonic,

$$\mathcal{D}^{(\Lambda)}_{0\nu}(0,\theta_R,\varphi_R)=\sqrt{\frac{4\pi}{2\Lambda+1}}Y_{\Lambda\nu}(\theta_R,\varphi_R)\ . \tag{IV.49}$$

By combining (IV.45)-(IV.49) and summing over the m's using $\sigma^{\dagger}_{\frac{1}{2}m'_s}\cdot\sigma_{\frac{1}{2}m_s}=\delta_{m'_s m_s}$ we find

$$f(\vec{R})=\sqrt{\pi}(-)^{1/2-M_I}\sum_{\Lambda,\nu}\big[(2I+1)(2I'+1)(2l+1)(2l'+1)(2\Lambda+1)\big]^{\frac{1}{2}} \begin{pmatrix} I' & I & \Lambda \\ -M'_I & M_I & -\nu \end{pmatrix}\begin{pmatrix} I' & I & \Lambda \\ 0 & 0 & 0 \end{pmatrix}\begin{Bmatrix} I' & I & \Lambda \\ l' & l & 1/2 \end{Bmatrix} Y_{\Lambda\nu}(\theta_R,\varphi_R)J_{I'I\Lambda}(R)\ , \tag{IV.50}$$

where

$$J_{I'I\Lambda}(R) = \int_0^\infty r^2 dr \psi_{I'}(r)\psi_I(r) \int_{-1}^{1} d(\cos\bar{\theta}_r) v(|\vec{r}-\vec{R}|) P_\Lambda(\cos\bar{\theta}_r) \ , \qquad \text{(IV.51)}$$

and the curly bracket is a Wigner 6-j symbol. We can now insert (IV.50) as the amplitude in the right hand side of (IV.35) for $X = V_2$ and perform the integral over $d\Omega_r$ of three spherical harmonics and more tedious sums over angular momentum projections, the net result is:

$$\langle (I'L')J'\mu'\alpha|V_2|(IL)J\mu\alpha\rangle$$
$$= \delta_{JJ'}\delta_{\mu'\mu}(-)^{J-1/2}\,1/2\left[(2I+1)(2I'+1)(2L+1)(2L'+1)(2l+1)(2l'+1)\right]^{\frac{1}{2}}$$
$$\sum_\Lambda (-)^\Lambda (2\Lambda+1) \begin{pmatrix} l' & l & \Lambda \\ 0 & 0 & 0 \end{pmatrix} \begin{pmatrix} L' & L & \Lambda \\ 0 & 0 & 0 \end{pmatrix} \begin{Bmatrix} I & I' & \Lambda \\ l' & l & 1/2 \end{Bmatrix} \begin{Bmatrix} I & I' & \Lambda \\ L' & L & J \end{Bmatrix} J_{I'I\Lambda} \ . \qquad \text{(IV.52)}$$

The 3-j symbols ensure parity conservation, because $\begin{pmatrix} a & b & c \\ 0 & 0 & 0 \end{pmatrix} = 0$ if $a+b+c$ is odd. As a check, we can substitute the constant 1 for the function v in (IV.51), then $J_{I'I\Lambda}(R) = 2\delta_{II'}\delta_{\Lambda 0}$ and in (IV.52) we find indeed after insertion of the analytic expression for the Wigner 6-j symbols with $\Lambda = 0$ and some albegra that $\langle I'M_I'\alpha|IM_I\alpha\rangle = \delta_{II'}\delta_{MM_I'}$ and

$$\langle (I'L')J'\mu'\alpha|(IL)J\mu\alpha\rangle = \delta_{JJ'}\delta_{\mu\mu'}\delta_{II'}\delta_{LL'} \qquad \text{(IV.53)}$$

as expected.

If we consider β instead of α states, the overlap does not change,

$$\langle (I'L')J'\mu'\alpha|(IL)J\mu\alpha\rangle = \langle (I'L')J'\mu'\beta|(IL)J\mu\beta\rangle \qquad ; \qquad \text{(IV.54)}$$

the same is true for the potential matrix element if we consider the potential from the other ^{16}O nucleus:

$$\langle (I'L')J'\mu'\alpha|V_2|(IL)J\mu\alpha\rangle = \langle (I'L')J'\mu'\beta|V_1|(IL)J\mu\beta\rangle \qquad . \qquad \text{(IV.55)}$$

(IV.54) and (IV.55) become evident if one performs the change of integration variables $\vec{R} \rightarrow -\vec{R}$, i.e., $\theta_R \rightarrow \pi - \theta_R$ and $\varphi_R \rightarrow \pi + \varphi_R$ under the integral over $d\Omega_R$ and substitutes $\vec{r}+\vec{R}$ for $\vec{r}$ and $\vec{r}$ for $\vec{r}-\vec{R}$ under the integral over $d\Omega_R$. Therefore, we have now derived all inelastic formfactors with the exception of the derivatives between β states and we will now continue with the transfer formfactors.

Whereas α states are described by (IV.43), for β states Ω_{r-R} and $|\vec{r}-\vec{R}|$ must be substituted for Ω_r and r. Consequently, $|IM_I\beta\rangle$ depends on $\vec{R}$, so that $\nabla^2|IM_I\beta\rangle$ and $\vec{\nabla}|IM_I\beta\rangle$ do not vanish; furthermore, the $|IM_I\beta\rangle$ are not orthogonal to the $|I'M'_I\alpha\rangle$. We have to calculate the right hand side of (IV.35) for $\gamma' \neq \gamma$ and the four different choices of X listed below (IV.35).

Starting with the radial integral, we find for the radial derivative formfactor that the integral in (IV.35) becomes $\delta_{LL'}\delta_{M_L M'_L}\langle I'M'_I\gamma'|\frac{\partial}{\partial R}|IM_I\gamma\rangle$, this expression vanishes for $\gamma = \alpha$; and for $\gamma = \beta$ and $\gamma' = \alpha$ the derivative can be taken in front of the matrix element and even in front of the whole expression on the right hand side of (IV.35), thus

$$\left\langle (I'L')J'\mu'\beta\middle|\frac{\partial}{\partial R}\middle|(IL)J\mu\alpha\right\rangle = 0\ , \tag{IV.56}$$

and

$$\left\langle (I'L')J'\mu'\alpha\middle|\frac{\partial}{\partial R}\middle|(IL)J\mu\beta\right\rangle = \frac{\partial}{\partial R}\left\langle (I'L')J'\mu'\alpha\middle|(IL)J\mu\beta\right\rangle\ . \tag{IV.57}$$

So the case *(i)* gets reduced to the case *(iii)*. It is partly for this reason, why we chose this representation.

$$\langle I'M'_I\beta|\vec{\nabla}|IM_I\beta\rangle = 0 \qquad , \tag{IV.58}$$

by reason of parity. (Formally, $\langle I'M'_I\beta|\vec{\nabla}|IM_I\beta\rangle \sim \int d^3\vec{r}\psi_{I'}(|\vec{r}-\vec{R}|)\ Y^*_{l'm'_l}(\Omega_{r-R})$ $\vec{\nabla}\psi_I(|\vec{r}-\vec{R}|)\ Y_{lm_l}(\Omega_{r-R})$, but the gradient with respect to $\vec{r}$ equals minus the gradient with respect to $(\vec{r}-\vec{R})$, under a substitution of variables, the integral transforms to $\int d^3\vec{x}\,\psi_{I'}(x)\ Y^*_{l'm'_l}(\Omega_x)\ \vec{\nabla}_x\psi_I(x)\ Y_{lm_l}(\Omega_x)$, and evidently, if the two states have equal parity, the integral vanishes.)

In case (iii), i.e., if $X=\nabla^2$, the integral for $\gamma'=\gamma=\beta$ becomes

$$\langle I'M'_I\beta|\nabla^2|IM_I\beta\rangle = \delta_{II'}\delta_{M_IM'_I}T_I \qquad , \tag{IV.59}$$

where

$$T_I = \int_0^\infty x^2dx\psi_{I'}(x)\Big(\frac{1}{x}\frac{\partial^2}{\partial x^2}x - \frac{l(l+1)}{x^2}\Big)\psi_I(x) \qquad . \tag{IV.60}$$

T_I is a constant independent of $\vec{R}$. Obviously, as the α state is independent of $\vec{R}$,

$$\langle I'M'_I\beta|\nabla^2|IM_I\alpha\rangle = 0 \qquad . \tag{IV.61}$$

For the same reason,

$$\langle I'M'_I\alpha|\nabla^2|IM_I\beta\rangle = \nabla^2\langle I'M'_I\alpha|IM_I\beta\rangle \qquad . \tag{IV.62}$$

For cases (iii) and (iv), we have to calculate $\langle I'M'_I\alpha|X|IM_I\beta\rangle$ with X either 1 or V_1. The expression of the amplitude in terms of the single particle wave function is:

$$\langle I'M'_I\alpha|X|IM_I\beta\rangle = \sum_{m_l,m_s}\sum_{m'_lm'_s}\langle lm_l\,{}^1\!/_2m_s|IM_I\rangle\langle l'm'_l\,{}^1\!/_2m'_s|I'M'_I\rangle$$
$$\int d^3\vec{r}\psi_{I'}(r)Y^*_{l'm'_l}(\Omega_r)x(r)\psi_I(|\vec{r}-\vec{R}|)Y_{lm_l}(\Omega_{r-R})\sigma^\dagger_{\frac{1}{2}m'_s}\sigma_{\frac{1}{2}m_s} \qquad , \tag{IV.63}$$

with $x(r) = v(r)$ or $x(r) \equiv 1$. We rotate to the intrinsic frame by the transformation (IV.49), i.e.

$$Y^*_{l'm'_l}(\theta_r, \varphi_r) = \sum_{\bar{m}'_l} [\mathcal{D}^{(l')}_{\bar{m}'_l m'_l}(0, \theta_R, \varphi_R)]^* Y^*_{l'\bar{m}'_l}(\bar{\theta}_r, \bar{\varphi}_r) \ , \tag{IV.64}$$

and

$$Y_{lm_l}(\theta_{r-R}, \varphi_{r-R}) = \sum_{\bar{m}_l} \mathcal{D}^{(l)}_{\bar{m}_l m_l}(0, \theta_R, \varphi_R) Y_{l\bar{m}_l}(\bar{\theta}_{r-R}, \bar{\varphi}_r) \ , \tag{IV.65}$$

since $\bar{\varphi}_r = \bar{\varphi}_{r-R}$ by choice of R as the z-axis. Also, $|\vec{r} - \vec{R}|$ does not depend on $\bar{\varphi}_r$. This allows us to perform the integral over $d\bar{\varphi}_r$ (cf. (IV.48)):

$$\int_0^{2\pi} d\bar{\varphi} Y^*_{l'\bar{m}'_l}(\bar{\theta}_r, \bar{\varphi}_r) Y_{l\bar{m}_l}(\bar{\theta}_{r-R}, \bar{\varphi}_r) = 2\pi \delta_{\bar{m}_l \bar{m}'_l} Y^*_{l'\bar{m}_l}(\bar{\theta}_r, 0) Y_{l\bar{m}_l}(\bar{\theta}_{r-R}, 0) \ . \tag{IV.66}$$

If $\bar{m}_l = \bar{m}'_l$, the product of the rotation matrices in (IV.64) and (IV.65) can be written as a sum over spherical harmonics,

$$\begin{aligned} [\mathcal{D}^{(l')}_{\bar{m}_l m'_l}(0, \theta_R, \varphi_R)]^* \mathcal{D}^{(l)}_{\bar{m}_l m_l}(0, \theta_R, \varphi_R) = \sum_{\Lambda, \nu} \sqrt{4\pi(2\Lambda+1)} (-)^{\bar{m}_l - m'_l + \nu} \\ \begin{pmatrix} l & l' & \Lambda \\ \bar{m}_l & -\bar{m}_l & 0 \end{pmatrix} \begin{pmatrix} l & l' & \Lambda \\ m_l & -m'_l & -\nu \end{pmatrix} Y_{\Lambda\nu}(\theta_R, \varphi_R) \ , \end{aligned} \tag{IV.67}$$

so that the integral in (IV.63) becomes:

$$I_0 = 4\pi^{\frac{3}{2}} \sum_{\Lambda\nu} (-)^{\nu - m'_l} \sqrt{2\Lambda+1} \begin{pmatrix} l & l' & \Lambda \\ m_l & -m'_l & -\nu \end{pmatrix} Y_{\Lambda\nu}(\theta_R, \varphi_R) \mathcal{I}^{(x)}_{I'I\Lambda}(R) \ , \tag{IV.68}$$

where

$$\begin{aligned} \mathcal{I}^{(x)}_{I'I\Lambda}(R) = \sum_{\bar{m}_l} (-)^{\bar{m}_l} \begin{pmatrix} l & l' & \Lambda \\ \bar{m}_l & -\bar{m}_l & 0 \end{pmatrix} \int_0^\infty r^2 dr \int_{-1}^1 d(\cos\bar{\theta}_r) \\ \psi_{I'}(r) x(r) \psi_I(|\vec{r} - \vec{R}|) Y^*_{l'\bar{m}_l}(\bar{\theta}_r, 0) Y_{l\bar{m}_l}(\bar{\theta}_{r-R}, 0) \ , \end{aligned} \tag{IV.69}$$

with $|\vec{r} - \vec{R}| = [r^2 + R^2 - 2rR\cos\bar{\theta}_r]^{\frac{1}{2}}$ and $\cos(\bar{\theta}_{r-R}) = (rR\cos\bar{\theta}_r - R^2)/(|\vec{r} - \vec{R}|\, R)$. $\hbar\Lambda$ is the angular momentum that is transferred between the two nuclei. Now,

(IV.68) and (IV.69) enable us to evaluate the Laplacian of I_0:

$$\nabla^2 I_0 = 4\pi^{3/2} \sum_{\Lambda,\nu} (-)^{\nu-m_l'} \sqrt{2\Lambda+1} \begin{pmatrix} l & l' & \Lambda \\ m_l & -m_l' & -\nu \end{pmatrix} Y_{\Lambda\nu}(\theta_R, \varphi_R) \left(\frac{1}{R} \frac{\partial^2}{\partial R^2} R - \frac{\Lambda(\Lambda+1)}{R^2} \right) \mathcal{I}^{(x)}_{I'I\Lambda}(R) \ . \tag{IV.70}$$

Thus, the expansion (IV.40) is found, and after integration of the three spherical harmonics and some angular momentum algebra, just as for the inelastic case, we finally obtain:

$$\begin{aligned} &\langle (I'L')J'\mu'\alpha|X|(IL)J\mu\beta\rangle \\ &\quad = 2\pi(-)^{J-1/2} \delta_{JJ'}\delta_{\mu\mu'} \left[(2I+1)(2I'+1)(2L+1)(2L'+1)\right]^{\frac{1}{2}} \\ &\quad \sum_{\Lambda=0}^{\infty} (-)^{\Lambda}(2\Lambda+1) \begin{pmatrix} L' & L & \Lambda \\ 0 & 0 & 0 \end{pmatrix} \begin{Bmatrix} I & I' & \Lambda \\ L' & L & 1/2 \end{Bmatrix} \begin{Bmatrix} I & I' & \Lambda \\ l' & l & J \end{Bmatrix} \mathcal{I}^{(x)}_{I'I\Lambda}(R) \ . \end{aligned} \tag{IV.71}$$

We can check this formula for $x = 1$ by letting R approach 0, where we find $\mathcal{I}^{(1)}_{I'I\Lambda}(0)$ $= \sqrt{2l+1}/(2\pi)\delta_{II'}\delta_{\Lambda 0}$, and thus $\delta_{JJ'}\ \delta_{\mu\mu'}\ \delta_{II'}\ \delta_{LL'}$ for the complete matrix element in (IV.35) for $X = 1$ and $R = 0$. Also, we find that the "small" matrix element $\langle I'M_I'\alpha|\vec{L}^2/\hbar^2|IM_I\beta\rangle$ produces the following "complete" matrix element that will be useful later:

$$\begin{aligned} &\langle (I'L')J'\mu'\alpha|D|(IL)J\mu\beta\rangle \\ &= 2\pi(-)^{J-1/2} \delta_{JJ'}\delta_{\mu\mu'} \left[(2I+1)(2I'+1)(2L+1)(2L'+1)\right]^{\frac{1}{2}} \\ &\sum_{\Lambda=0}^{\infty} (-)^{\Lambda}\Lambda(\Lambda+1)(2\Lambda+1) \begin{pmatrix} L' & L & \Lambda \\ 0 & 0 & 0 \end{pmatrix} \begin{Bmatrix} I & I' & \Lambda \\ L' & L & 1/2 \end{Bmatrix} \begin{Bmatrix} I & I' & \Lambda \\ l' & l & J \end{Bmatrix} \mathcal{I}^{(x)}_{I'I\Lambda}(R) \ . \end{aligned} \tag{IV.72}$$

We can prove that

$$\langle (I'L')J'\mu'\beta|(IL)J\mu\alpha\rangle = \langle (I'L')J'\mu'\alpha|(IL)J\mu\beta\rangle \ , \tag{IV.73}$$

and

$$\langle (I'L')J'\mu'\beta|V_2|(IL)J\mu\alpha\rangle = \langle (I'L')J'\mu'\alpha|V_1|(IL)J\mu\beta\rangle \ , \tag{IV.74}$$

from (IV.69) and (IV.72) by switching primed and unprimed variables and substituting $x(|\vec{r}-\vec{R}|)$ for $x(r)$. (IV.69) can be rewritten by expressing the spherical harmonics through associated Legendre functions of the first kind,

$$\left|Y_{LM}(\theta,0)\right| = \left[\frac{2L+1}{4\pi}\frac{(L-|M|)!}{(L+|M|)!}\right]^{\frac{1}{2}} P_L^{|M|}(\cos\theta) \ , \tag{IV.75}$$

the sign of Y_{LM} is $(-)^M$, if M is positive, and + otherwise. Since either $\bar{m}_l$ or $-\bar{m}_l$ is non-positive, there will be exactly one factor $(-)^{\bar{m}_l}$ from the two Y's, hence (IV.69) is equivalent to:

$$\begin{aligned} & I^{(x)}_{I'I\Lambda}(R) \\ & = \frac{1}{4\pi}\left[(2l+1)(2l'+1)\right]^{\frac{1}{2}} \sum_{\bar{m}_l=-l}^{l} \begin{pmatrix} l & l' & \Lambda \\ \bar{m}_l & -\bar{m}_l & 0 \end{pmatrix} \left[\frac{(l-|\bar{m}_l|)!}{(l+|\bar{m}_l|)!}\frac{(l'-|\bar{m}_l|)!}{(l'+|\bar{m}_l|)!}\right]^{\frac{1}{2}} \\ & \int_0^\infty r^2\,dr \int_{-1}^{1} d(\cos\bar{\theta}_r)\psi_{I'}(r)x(r)\psi_I(|\vec{r}-\vec{R}|)P_l^{|\bar{m}_l|}(\cos\bar{\theta}_r)P_{l'}^{|\bar{m}_l|}(\cos\bar{\theta}_{r-R}) \ . \end{aligned} \tag{IV.76}$$

Thus, $I^{(x)}_{I'I\Lambda}(R)$ is proportional to a sum over $\bar{m}_l$ of the Wigner 3-j symbol times a function that depends on the absolute value of $\bar{m}_l$ only; by the symmetry property of the 3-j symbol, i.e., $\begin{pmatrix} l & l' & \Lambda \\ \bar{m}_l & -\bar{m}_l & 0 \end{pmatrix} = (-)^{l+l'+\Lambda}\begin{pmatrix} l & l' & \Lambda \\ -\bar{m}_l & \bar{m}_l & 0 \end{pmatrix}$, the sum reduces to the summand for $\Lambda = 0$ plus, in the case that $l+l'+\Lambda$ is even, twice the sum from 1 to l:

$$\begin{aligned} \sum_{\bar{m}_l=-l}^{l} \begin{pmatrix} l & l' & \Lambda \\ \bar{m}_l & -\bar{m}_l & 0 \end{pmatrix} K(|\bar{m}_l|) &= \begin{pmatrix} l & l' & \Lambda \\ 0 & 0 & 0 \end{pmatrix} K(0) \\ &+ 2\delta_{l+l'+\Lambda,even} \sum_{\bar{m}_l=1}^{l} \begin{pmatrix} l & l' & \Lambda \\ \bar{m}_l & -\bar{m}_l & 0 \end{pmatrix} K(\bar{m}_l) \ . \end{aligned} \tag{IV.77}$$

(IV.77) also proves parity conservation, when applied to (IV.76), by showing that I vanishes, if $l + l' + \Lambda$ is odd. The recoil corrections would allow non-normal parity transfer with $l + l' + \Lambda$ odd. Most interesting from our point of view is the consequence of (IV.76) and (IV.77) that $I^{(x)}_{I'I\Lambda}(R) = I^{(x)}_{II'\Lambda}(R)$, if $x(r)$ is transformed to $x(|\vec{r} - \vec{R}|)$ under the integral sign. (IV.73) and (IV.74) follow, because the 3-j and 6-j symbols in (IV.72) and hence the whole expression on the right hand side are invariant under an exchange of primed and unprimed variables.

IV.7 Even and odd states

There is an additonal symmetry in the problem, of which we have not taken advantage yet: the indistinguishability of the two ^{16}O cores. The best method of using this is to change the basis from left and right states $|\alpha\rangle$ and $|\beta\rangle$ to the even and odd linear combinations

$$|''+''\rangle = \frac{1}{\sqrt{2}}(|\alpha\rangle + |\beta\rangle) \tag{IV.78}$$

and

$$|''-''\rangle = \frac{1}{\sqrt{2}}(|\alpha\rangle - |\beta\rangle) \quad . \tag{IV.79}$$

The quotation marks on the + and - shall indicate that this is not our final definition of the $|+\rangle$ and $|-\rangle$ states. In this section and unless stated otherwise, we will omit the indices of angular momenta, it is always to be understood that bra states carry indices $I'M'_I$ and ket states carry indices IM_I. Later on, we treat the effects of the basis change on the complete state, we will use an accumulative label A' or A to denote its angular momentum quantum numbers.

We want the even and odd states to decouple, i.e., we want

$$\langle''+''|X|''-''\rangle = \langle''-''|X|''+''\rangle = 0 \qquad , \tag{IV.80}$$

for our four choices of X. If this is achieved, the number of channels that are coupled to each other is cut in half. This will make the numerical computations much easier, because the computing time grows much faster than linearly with the number of coupled channels. Necessary and sufficient for (IV.80) to hold is that

$$\langle\alpha|X|\beta\rangle = \langle\beta|X|\alpha\rangle \tag{IV.81}$$

and

$$\langle\alpha|X|\alpha\rangle = \langle\beta|X|\beta\rangle \tag{IV.82}$$

However, as it stands now, (IV.81) and (IV.82) are fulfilled neither for X equalling V_1 or V_2 nor for X equalling ∇^2 or $\vec{\nabla}$. This inequality can be remedied for V_1 and V_2 by considering the complete neutron operator $U = V_1 + V_2 + T_n$ instead of V_1 and V_2 separately, (IV.81) and (IV.82) certainly hold for $X = U$. To restore (IV.81) and (IV.82) for the derivative operators we need to return from the representation of the previous section, where the single particle wave functions of α states have argument $\vec{r}$ and those of β states argument $\vec{r} - \vec{R}$, to a more symmetric representation (cf. Section IV.5), where left states (let us call them $|\tilde{\alpha}\rangle$) take argument $\vec{r} + \vec{R}/2$ and right states ($|\tilde{\beta}\rangle$) $\vec{r} - \vec{R}/2$. Clearly, this change of the origin has no effect on the matrix elements of 1 and U,

$$\langle\tilde{\alpha}|\tilde{\beta}\rangle = \langle\alpha|\beta\rangle \qquad , \tag{IV.83}$$

and

$$\langle\tilde{\alpha}|U|\tilde{\beta}\rangle = \langle\alpha|U|\beta\rangle \quad . \tag{IV.84}$$

However, because not only $\tilde{\beta}$, but also $\tilde{\alpha}$ states depend explicitly on $\vec{R}$, the corresponding equations to (IV.83) and (IV.84) for the gradient and the Laplacian do not hold.

To derive the correct relations between derivative formfactors of left/right and even/odd states, we can safely ignore the neutron spin, because the operators are spin-independent, and write

$$\begin{aligned} |\tilde{\alpha}\rangle &= \psi_2(\vec{r}+\vec{R}/2) \quad , \\ |\tilde{\beta}\rangle &= \psi_2(\vec{r}-\vec{R}/2) \quad , \\ \langle\tilde{\alpha}| &= \psi_1^*(\vec{r}+\vec{R}/2) \quad , \\ \langle\tilde{\beta}| &= \psi_1^*(\vec{r}-\vec{R}/2) \quad . \end{aligned} \tag{IV.85}$$

Then, for the transfer

$$\begin{aligned} &\langle\tilde{\alpha}|\big(\vec{\nabla}|\tilde{\beta}\rangle\big) = \int d^3\vec{r}\psi_1^*(\vec{r}+\vec{R}/2)\big[\vec{\nabla}\psi_2(\vec{r}-\vec{R}/2)\big] \\ &= \int d^3\vec{r}\big[\vec{\nabla}\psi_1^*(\vec{r}+\vec{R}/2)\big]\psi_2(\vec{r}-\vec{R}/2) = \big(\langle\tilde{\alpha}|\vec{\nabla}\big)|\tilde{\beta}\rangle = {}^1\!/_2\vec{\nabla}\big(\langle\tilde{\alpha}|\tilde{\beta}\rangle\big) = {}^1\!/_2\big(\langle\alpha|\vec{\nabla}|\beta\rangle\big) \ , \end{aligned} \tag{IV.86}$$

similarly

$$\begin{aligned} &\langle\tilde{\alpha}|\big(\nabla^2|\tilde{\beta}\rangle\big) = \int d^3\vec{r}\psi_1^*(\vec{r}+\vec{R}/2)\big[\nabla^2\psi_2(\vec{r}-\vec{R}/2)\big] \\ &= \int d^3\vec{r}\big[\vec{\nabla}\psi_1^*(\vec{r}+\vec{R}/2)\big]\cdot\big[\vec{\nabla}\psi_2(\vec{r}-\vec{R}/2)\big] = \int d^3\vec{r}\big[\nabla^2\psi_1^*(\vec{r}+\vec{R}/2)\big]\psi_2(\vec{r}-\vec{R}/2) \\ &= \big(\langle\tilde{\alpha}|\nabla^2\big)|\tilde{\beta}\rangle = {}^1\!/_4\nabla^2\big(\langle\tilde{\alpha}|\tilde{\beta}\rangle\big) = {}^1\!/_4\big(\langle\alpha|\nabla^2|\beta\rangle\big) \ , \end{aligned} \tag{IV.87}$$

are found by applying the definition of the states, integration by parts, and use of the relation $\vec{\nabla}_{\vec{R}} = -\frac{1}{2}\vec{\nabla}_{\vec{r}-\vec{R}/2} = \frac{1}{2}\vec{\nabla}_{\vec{r}+\vec{R}/2}$. We find for the inelastic formfactors

in the same way

$$\begin{aligned}\langle\tilde{\alpha}|\big(\vec{\nabla}|\tilde{\alpha}\rangle\big) &= \int d^3\vec{r}\psi_1^*(\vec{r}+\vec{R}/2)\big[\vec{\nabla}\psi_2(\vec{r}+\vec{R}/2)\big] \\ &= -\int d^3\vec{r}\psi_1^*(\vec{r}-\vec{R}/2)\big[\vec{\nabla}\psi_2(\vec{r}-\vec{R}/2)\big] \\ &= -\langle\tilde{\beta}|\big(\vec{\nabla}|\tilde{\beta}\rangle\big) = -1/2\langle\beta|\big(\vec{\nabla}|\beta\rangle\big) = 0\ .\end{aligned} \tag{IV.88}$$

and

$$\begin{aligned}\langle\tilde{\alpha}|\big(\nabla^2|\tilde{\alpha}\rangle\big) &= \int d^3\vec{r}\psi_1^*(\vec{r}+\vec{R}/2)\big[\nabla^2\psi_2(\vec{r}+\vec{R}/2)\big] \\ &= \int d^3\vec{r}\psi_1^*(\vec{r}-\vec{R}/2)\big[\nabla^2\psi_2(\vec{r}-\vec{R}/2)\big] = 1/4\langle\tilde{\beta}|\big(\nabla^2|\tilde{\beta}\rangle\big) \\ &= 1/4\int d^3\vec{r}\psi_1^*(\vec{r})\big[\nabla^2\psi_2(\vec{r}-\vec{R})\big] = 1/4\langle\beta|\big(\nabla^2|\beta\rangle\big)\ .\end{aligned} \tag{IV.89}$$

The relations $\langle\tilde{\alpha}|\vec{\nabla}|\tilde{\beta}\rangle = \langle\tilde{\beta}\vec{\nabla}|\tilde{\alpha}\rangle$, $\langle\tilde{\alpha}\big(|\vec{\nabla}|\tilde{\alpha}\rangle\big) = \big(\langle\tilde{\alpha}\vec{\nabla}\big)|\tilde{\alpha}\rangle$ and analogously for the Laplacian follow trivially, too.

Thus, (IV.81) and(IV.82) are proven for $X = 1,U,\nabla^2$, or $\vec{\nabla}$ for $\tilde{\alpha}$ and $\tilde{\beta}$ states; moreover, (IV.86)-(IV.89) allow us to express the matrix elements in the new basis through those in the old basis as presented in Section IV.6.

The above relations also hold for the complete states $|(IL)J\mu\gamma\rangle$ for $X = 1$ and $X + U$ by linearity; e.g., from (IV.83), i.e., $\langle I'M_I'\tilde{\alpha}|IM_I\tilde{\beta}\rangle = \langle I'M_I'\alpha|IM_I\beta\rangle$, follows immediately $\langle(I'L')J'\mu'\tilde{\alpha}|(IL)J\mu\tilde{\beta}\rangle = \langle(I'L')J'\mu'\alpha|(IL)J\mu\beta\rangle$. The same is true for the radial derivative, $X = \frac{\partial}{\partial R}$, because this operator does not affect the spherical harmonics in (IV.35). However, $X = \nabla^2$ requires some more work. We use a cumulative index A to abbreviate the set $\{ILJ\mu\}$ and analogously A' for

$\{I'L'J'\mu'\}$. $\langle A'\tilde{\alpha}|\nabla^2|A\tilde{\beta}\rangle$ is a sum over terms that contain

$$\begin{aligned}
&\int d\Omega_R Y^*_{L'M'_L}(\Omega_R)\Big[Y_{LM}(\Omega_R)\langle I'M'_I\tilde{\alpha}|\nabla^2|IM_I\tilde{\beta}\rangle + \langle I'M'_I\tilde{\alpha}|IM_I\tilde{\beta}\rangle\,\nabla^2 Y_{LM_L}(\Omega_R)\\
&\qquad + 2\left(\vec{\nabla}Y_{LM_L}(\Omega_R)\right)\cdot\langle I'M'_I\tilde{\alpha}|\vec{\nabla}|IM_I\tilde{\beta}\rangle\Big]\\
&= \int d\Omega_R Y^*_{L'M'_L}(\Omega_R)\Big[Y_{LM}(\Omega_R)\,{}^1\!/_4\langle I'M'_I\alpha|\nabla^2|IM_I\beta\rangle\\
&\qquad + \langle I'M'_I\alpha|IM_I\beta\rangle\,\nabla^2 Y_{LM_L}(\Omega_R) + \left(\vec{\nabla}Y_{LM_L}(\Omega_R)\right)\cdot\langle I'M'_I\alpha|\vec{\nabla}|IM_I\beta\rangle\Big]\ .
\end{aligned} \tag{IV.90}$$

(The equality follows from (IV.86) and (IV.87).) The first two amplitudes on the right hand side are calculated in Section IV.6, the third we get from expanding the integrals over $d\Omega_R$ in the known $\langle A'\alpha|\nabla^2|A\beta\rangle$ (cf. (IV.38)), in the same way as we have done here, the result is the same as (IV.90) except that no factor ${}^1\!/_4$ appears in front of the amplitude involving the Laplacian, and the factor 2 remains in front of the amplitude with the gradient. We can extend by linearity from the integrals over $d\Omega_R$ to the full matrix elements and find:

$$\begin{aligned}
\langle A'\tilde{\alpha}|\nabla^2|A\tilde{\beta}\rangle = \frac{1}{4}\Big[\frac{1}{R}\frac{\partial^2}{\partial R^2}R\langle A'\alpha|A\beta\rangle + \frac{1}{R^2}\langle A'\alpha|D|A\beta\rangle\Big]\\
- \frac{L(L+1)+L'(L'+1)}{2R^2}\langle A'\alpha|A\beta\rangle\ .
\end{aligned} \tag{IV.91}$$

The amplitude with $\tilde{\alpha}$ and $\tilde{\beta}$ reversed can be calculated in the same manner, and indeed

$$\langle A'\tilde{\beta}|\nabla^2|A\tilde{\alpha}\rangle = \langle A'\tilde{\alpha}|\nabla^2|A\tilde{\beta}\rangle \qquad . \tag{IV.92}$$

The derivation of the inelastic formfactors is simpler, because in the expansion that corresponds to (IV.90) $\langle I'M'_I\tilde{\gamma}|\vec{\nabla}|IM_I\tilde{\gamma}\rangle$ is zero by parity, so that the result is simply:

$$\langle A'\tilde{\alpha}|\nabla^2|A\tilde{\alpha}\rangle = \langle A'\tilde{\beta}|\nabla^2|A\tilde{\beta}\rangle = \Big[{}^1\!/_4 T_I - \frac{L(L+1)}{R^2}\Big]\delta_{JJ'}\delta_{II'}\delta_{LL'}\delta_{\mu\mu'}\ . \tag{IV.93}$$

In the following, we summarize the matrix elements between complete states in the new representation

$$\begin{aligned} |A+\rangle &= \frac{1}{\sqrt{2}}\left(|A\tilde{\alpha}\rangle + |A\tilde{\beta}\rangle\right) \\ |A-\rangle &= \frac{1}{\sqrt{2}}\left(|A\tilde{\alpha}\rangle - |A\tilde{\beta}\rangle\right) , \end{aligned} \tag{IV.94}$$

The following relations can be derived rather trivially from the definitions (IV.94), the expressions of the matrix elements with the tilde through those without, and the results for these matrix elements in the old representation that were derived in Section IV.6. We define a label p to stand for either + or - in the ket state, and a corresponding label p' for the bra state, $(-)^p$ or $(-)^{p'}$ is the eigenvalue of the parity operator, i.e., $(-)^p = 1$, if $p = +$, and $(-)^p = -1$, if $p = -$. Then,

$$\begin{aligned} &\langle (I'L')J'\mu'p'|X|(IL)J\mu p\rangle \\ &= \delta_{pp'}\Big(\langle (I'L')J'\mu'\tilde{\alpha}|X|(IL)J\mu\tilde{\alpha}\rangle + (-)^p\langle (I'L')J'\mu'\tilde{\beta}|X|(IL)J\mu\tilde{\beta}\rangle\Big) . \end{aligned} \tag{IV.95}$$

Thus,

$$(i) \qquad \hat{R}\cdot\langle A'p'|\vec{\nabla}|Ap\rangle = {}^1\!/_2(-)^p\delta_{pp'}\frac{\partial}{\partial R}\langle A'\alpha|A\beta\rangle ,$$

(ii)

$$\begin{aligned} &\langle A'p'|\nabla^2|Ap\rangle \\ &= \delta_{pp'}\Big[-\frac{L(L+1)}{R^2}\left(\delta_{JJ'}\delta_{\mu\mu'}\delta_{II'}\delta_{LL'} + (-)^p\langle A'\alpha|A\beta\rangle\right) + {}^1\!/_4\delta_{JJ'}\delta_{\mu\mu'}\delta_{II'}\delta_{LL'}\,T_I \\ &+ {}^1\!/_4(-)^p\Big(\frac{\partial^2}{\partial R^2}\langle A'\alpha|A\beta\rangle + \frac{2}{R}\frac{\partial}{\partial R}\langle A'\alpha|A\beta\rangle - \frac{1}{R^2}\langle A'\alpha|D|A\beta\rangle\Big)\Big] , \end{aligned}$$

$$(iii) \qquad \langle A'p'|Ap\rangle = \delta_{pp'}\left[\delta_{JJ'}\delta_{\mu\mu'}\delta_{II'}\delta_{LL'} + (-)^p\langle A'\alpha|A\beta\rangle\right] ,$$

(iv)

$$\begin{aligned} \langle A'p'|U|Ap\rangle = \delta_{pp'}\big[&\epsilon_I(\delta_{JJ'}\delta_{\mu\mu'}\delta_{II'}\delta_{LL'} + (-)^p\langle A'\alpha|A\beta\rangle) \\ &+ \langle A'\alpha|V_2|A\alpha\rangle + (-)^p\langle A'\alpha|V_1|A\beta\rangle\big] . \end{aligned}$$

T_I is given by (IV.60), $\langle A'\alpha|A\beta\rangle$ by (IV.69) and (IV.71) with $X = 1$, $\langle A'\alpha|V_1|A\beta\rangle$ by the same equations with $X = V_1$, and $\langle A'\alpha|V_2|A\alpha\rangle$ by (IV.51) and (IV.52).

IV.8 The coupled channels equations

We are now able to write out (IV.33) with all formfactors (i)-(iv) inserted. We utilize the even and odd states $|p\rangle$, and again use the cumulative indices A and A' for j and i, respectively. It is possible to combine the term with $2/R\,\frac{\partial}{\partial R}\langle A'\alpha|A\beta\rangle$ in (ii), which is multipied by $\chi_A(R)$ in (IV.33), with the first term that arises, when $\frac{d}{dR}(\chi_A(R)/R)$ is expanded into $\frac{1}{R}\frac{d\chi_A(R)}{dR} - \frac{\chi_A(R)}{R^2}$, this last expression is multiplied by $\frac{\partial}{\partial R}\langle A'\alpha|A\beta\rangle$ in (IV.33). Much more simplification is not possible, and the net result is:

$$\sum_A \Bigg\{ \langle A'p|Ap\rangle \frac{d^2}{dR^2}\chi_A(R) + (-)^p \Big(\frac{\partial}{\partial R}\langle A'\alpha|A\beta\rangle\Big)\frac{d}{dR}\chi_A(R)$$
$$+ \Big[-\frac{L(L+1)+L'(L'+1)}{2R^2}\langle A'p|Ap\rangle + {}^1\!/_4\delta_{AA'}T_I + {}^1\!/_4(-)^p\frac{\partial^2}{\partial R^2}\langle A'\alpha|A\beta\rangle$$
$$- {}^1\!/_2(-)^p\frac{1}{R}\frac{\partial}{\partial R}\langle A'\alpha|A\beta\rangle + {}^1\!/_4(-)^p\frac{1}{R^2}\langle A'\alpha|D|A\beta\rangle - \frac{2m}{\hbar^2}\Big(\langle A'\alpha|V_2|\ A\alpha\rangle$$
$$+ (-)^p\langle A'\alpha|V_1|A\beta\rangle + (V_c(R)+\epsilon_I - E)\langle A'p|Ap\rangle\Big)\Big]\chi_A(R)\Bigg\} = 0\ . \qquad \text{(IV.96)}$$

(IV.96) is a set of coupled equations, A' labels the equation number. (IV.96) is valid for p even and odd, but the two parities do not couple to each other. The two terms containing derivatives of $\chi_A(R)$ can be brought into a form that is reminiscent of a *Sturm-Liouville equation*: $\frac{\partial}{\partial R}(\langle A'p|Ap\rangle\frac{d\chi_A}{dR})$. (IV.96) can be abbreviated to

$$\sum_A \big[(f_{AA'}\chi'_A)' + g_{AA'}\chi_A\big] = 0 \qquad , \qquad \text{(IV.97)}$$

where the $'$ denotes differentiation with respect to R. Since f and g are both real

and symmetric, unitarity follows from the difference of the two derived equations

$$\begin{aligned} \sum_{A,A'} \left[\chi^*_{A'}(f_{AA'}\chi'_A)' + g_{AA'}\chi^*_{A'}\chi_A\right] &= 0 \quad , \\ \sum_{A,A'} \left[\chi_A(f_{AA'}\chi^{*\prime}_{A'})' + g_{AA'}\chi_A\chi^*_{A'}\right] &= 0 \quad ; \end{aligned} \tag{IV.98}$$

this difference is

$$\begin{aligned} 0 &= \sum_{A,A'} \left[\chi^*_{A'}(f'_{AA'}\chi'_A + f_{AA'}\chi''_A) - \chi_A(f'_{AA'}\chi^{*\prime}_{A'} + f_{AA'}\chi^{*\prime\prime}_{A'})\right] \\ &= \frac{d}{dR}\sum_{A,A'} f_{AA'}\left(\chi^*_{A'}\chi'_A - \chi^{*\prime}_{A'}\chi_A\right) , \end{aligned} \tag{IV.99}$$

proportional to the derivative of the flux.

As a final note we mention that all matrix elements of the complete states are functions of R only, we have used the notation of the partial derivative in (IV.96) and above for convenience in the transition from the equations of Section IV.6; and also all formfactors are independent of the spin projection μ (provided that bra and ket state have the same spin projection, otherwise the formfactors are zero).

IV.9 Renormalization of energies

The experimental energy E_x, i.e., the kinetic energy that target and projectile (in the center-of-momentum frame) have when they are far apart long before the collision, determines the asymptotic wave number k of the incoming channel i (precisely: I_i, L_i,J_i, μ_i, γ_i):

$$k = \sqrt{\frac{2m}{\hbar^2}E_x} \quad . \tag{IV.100}$$

For large distances R, the equations (IV.96) decouple into

$$\frac{d^2}{dR^2}\chi_A(R) + \left[{}^1\!/_4 T_A + \frac{2m}{\hbar^2}(E - \epsilon_A)\right]\chi_A(R) = 0 \, , \tag{IV.101}$$

so that the channel A has asymptotic wave number

$$k_A^{(\infty)} = \left[{}^1\!/_4 T_A + \frac{2m}{\hbar^2}(E - \epsilon_A) \right]^{\frac{1}{2}} \quad , \tag{IV.102}$$

(this wave number is the same for all channels A with the same spin I, we will use the notation k_I for $k_A^{(\infty)}$, if A includes I, later on, but this must be clearly distinguished from the local wave number $k_A(R)$). From (IV.100) and (IV.101) we find

$$E_x = E - \epsilon_i + \frac{\hbar^2}{8m} T_i \quad , \tag{IV.103}$$

and

$$k_A^{(\infty)} = \left[{}^1\!/_4 (T_A - T_i) + \frac{2m}{\hbar^2}\left(E - (\epsilon_A - \epsilon_i)\right) \right]^{\frac{1}{2}} \quad . \tag{IV.104}$$

But now the definition of the Q-value becomes ambiguous, on the one hand it is the (negative) excitation energy in ^{17}O, i.e.

$$\bar{Q}_A = \epsilon_i - \epsilon_A \quad , \tag{IV.105}$$

on the other hand it is the difference in experimental collision energy for different channels,

$$Q_A = \frac{\hbar^2}{2m}\left[(k_A^{(\infty)})^2 - k^2 \right] \quad . \tag{IV.106}$$

From (IV.104) it follows that $Q_A \neq \bar{Q}_A$, if $T_A \neq T_i$. The reason for this discrepancy lies in the neglect of recoil corrections. We choose to make (IV.106) the physical Q-value in order to give the right asymptotic behavior to the wave functions and thus treat the dynamical effects of the Q-values correctly.

IV.10 IWBC

The incoming wave boundary condition cannot be formulated as unambiguously in the multi-channel case as in the one-channel case. In order to preserve linearity of the boundary condition of each channel individually, we keep only the diagonal contributions to the local wave number. Then,

$$\frac{d}{dR}\Big(\langle Ap|Ap\rangle \frac{d\chi_A}{dR}\Big) + k_A^2(R)\chi_A(R) = 0 \qquad . \tag{IV.107}$$

$k_A^2(R)$ includes all the diagonal contributions from (IV.96). As a further approximation we neglect $\frac{d}{dR}\langle Ap|Ap\rangle$ and choose as boundary condition that near the boundary R_0

$$\chi_A(R) = \frac{N}{\sqrt{\kappa_A(R)}} \exp\Big(-i\int_{R_0}^{R} \kappa_A(\bar{R})d\bar{R}\Big) \qquad , \tag{IV.108}$$

where N is an arbitrary normalization constant (so that we really stipulate only the logarithmic derivative of χ_A at R_0), and

$$\kappa_A(R) = \frac{k_A(R)}{\sqrt{\langle Ap|Ap\rangle_R}} \qquad . \tag{IV.109}$$

IV.11 Cross sections

We assume that the initial configuration before the collision is an α state, i.e., in Fig.13 the ^{17}O impinges from the left onto the ^{16}O that comes from the right. Then the boundary condition for large R stipulates that asymptotically the wave function consists of (1) a Coulomb function (i.e., a plane wave modified by the infinite-range Coulomb potential) in an α state with spin $I = I_{in}$ and spin projection μ along the direction $\hat{z}$ of the wave vector of the Coulomb wave function (μ is also the spin

projection of the total angular momentum J, because the Coulomb wave function does not carry an angular momentum component in the direction of its motion), and (2) of an outgoing spherical wave in all other channels.

Thus, the wave function can be written as

$$|\Phi_\mu(\vec{R})\rangle = \frac{\sqrt{\pi}}{kR}\sum_{J,L}\sqrt{2L+1}\,i^{L+1}\langle L0I_{in}\mu|J\mu\rangle\sum_{\gamma,L',I'}\chi^{J\gamma}_{L(L'I')}(R)\,|(I'L')J\mu\gamma\rangle\ , \tag{IV.110}$$

where asymptotically for large R

$$\chi^{J\gamma}_{L(L'I')}(R) \sim u^{(-)}_L(k_{I'}R)\delta_{I'I_{in}}\delta_{LL'}\delta_{\gamma\alpha} - S^{J\gamma}_{L(L'I')}e^{2i\sigma_{L'}}u^{(+)}_{L'}(k_{I'}R)\ . \tag{IV.111}$$

We use the same notation as in Chapter III, $u^{(+)}_L$ and $u^{(-)}_L$ are the spherical Coulomb functions, and σ_L is the Coulomb phase shift. Chapter III's S^J_L becomes here a $S^{J\gamma}_{L(L'I')}$, L' and I' are the labels of the actual channel, to which the coefficient S belongs, while L denotes the orbital angular momentum of the incoming channel in the set of equations, from which S is determined (the incoming spin is always I_{in}, so an extra index is superfluous, similarly, γ is the partition of the actual channel, whereas an index for the partition of the incoming channel, i.e. α, is superfluous, too). J and μ are constants of motion of (IV.96). Then the construction on the right hand side of (IV.110) produces exactly the required asymptotic form for Φ_μ. The radial wave functions χ do not carry an index μ, because the formfactors in (IV.96) are independent of μ as shown in Section IV.6.

When the incoming flux is 1, the fusion flux of one set of channels for given J

and L is

$$F_L^J = \frac{-i}{2k} \sum_{L',I',\gamma'} \sum_{L'',I'',\gamma''} \Big\{ \langle (I'L')J\mu\gamma' | (I''L'')J\mu\gamma'' \rangle \times \Big[\chi^{J\gamma''}_{L(L''I'')} \frac{d}{dR} \big(\chi^{J\gamma'}_{L(L'I')}\big)^* - \big(\chi^{J\gamma'}_{L(L'I')}\big)^* \frac{d}{dR} \chi^{J\gamma''}_{L(L''I'')} \Big] \Big\} . \tag{IV.112}$$

The complete fusion cross section is obtained from multiplying by the appropriate coefficients from (IV.110). Also, besides a double summation as in (IV.112), there will be a sum over J and L and additionally one over, say $\tilde{J}$, $\tilde{L}$; this comes from expanding $|\Phi_\mu\rangle$ once as a ket and once as a bra state and calculating the expectation value of the flux operator between these. However, because the $|(IL)J\mu\gamma\rangle$ do not mix for different J, the double sum over J and $\tilde{J}$ collapses to one sum. Also, as we will see, if we average over incoming spin projection μ, the Clebsch-Gordan coefficient in (IV.110) and its counterpart from the complex conjugate give a Kronecker-δ in L and $\tilde{L}$ under the sum over μ, i.e.

$$\sum_\mu \langle L0I_{in}\mu | J\mu \rangle \langle \tilde{L}0I_{in}\mu | J\mu \rangle = \frac{2J+1}{2L+1} \delta_{L\tilde{L}} . \tag{IV.113}$$

Therefore, different L's in (IV.110) do not mix either. When all the coefficients are sorted out, the complete (unpolarized) fusion flux becomes:

$$\sigma_{fus} = \frac{\pi}{k^2} \frac{1}{2I_{in}+1} \sum_{J,L} (2J+1) F_L^J \quad . \tag{IV.114}$$

Because solving the coupled channels equations is easier in the even/odd than in the left/right basis, we will express cross sections in this representation. (IV.110) becomes

$$|\Phi_\mu(\vec{R})\rangle = \frac{1}{kR} \sqrt{\frac{\pi}{2}} \sum_{J,L} \sqrt{2L+1}\, i^{L+1} \langle L0I_{in}\mu | J\mu \rangle \sum_{p,L',I'} \chi^{Jp}_{L(L'I')}(R)\, |(I'L')J\mu p\rangle , \tag{IV.115}$$

by the definition

$$\chi^{Jp}_{L(L'I')}(R) = \chi^{J\alpha}_{L(L'I')}(R) + (-)^p \chi^{J\beta}_{L(L'I')}(R) \ , \tag{IV.116}$$

and the boundary condition for large R becomes:

$$\chi^{Jp}_{L(L'I')}(R) \sim u^{(-)}_L(k_{I'}R)\delta_{I'I_{in}}\delta_{LL'} - S^{Jp}_{L(L'I')} e^{2i\sigma_{L'}} u^{(+)}_{L'}(k_{I'}R) \ . \tag{IV.117}$$

Hence,

$$S^{Jp}_{L(L'I')} = S^{J\alpha}_{L(L'I')} + (-)^p S^{J\beta}_{L(L'I')} \tag{IV.118}$$

In (IV.117), unlike in (IV.111), there is no Kronecker-δ symbol for the partitions, so that the boundary condition for the ingoing flux is the same for even and odd states. Because of the additional factor $\sqrt{1/2}$ in (IV.115), there will be a new factor $1/2$, when F^J_L is expressed by $\chi^{Jp}_{L(L'I')}$:

$$F^J_L = \frac{-i}{4k} \sum_{L',I',p} \sum_{L'',I'',p} \Big\{ \langle (I'L')J\mu p | (I''L'')J\mu p \rangle \times \Big[\chi^{Jp}_{L(L''I'')} \frac{d}{dR} \big(\chi^{Jp}_{L(L'I')}\big)^* - \big(\chi^{Jp}_{L(L'I')}\big)^* \frac{d}{dR} \chi^{Jp}_{L(L''I'')} \Big] \Big\} \ . \tag{IV.119}$$

Now, also p is a constant of the motion. In the formalism of this section, no use has been made of the conservation of parity of the radial motion (i.e., L's of different parity do not couple). An insertion of this constraint into the notation would just make the expressions longer. The equations as stated are perfectly correct, the radial wave functions $\chi^{Jp}_{L(L'I')}$ and thus the coefficients $S^{Jp}_{L(L'I')}$ are simply identical to zero if L and L' have different parity.

The elastic and inelastic cross section follow from the asymptotic form of the wave function $|\Phi_\mu\rangle$ for large R. We have to extend the formalism of Chapter III to

the multi-channel case to extract a scattering amplitude $f(\theta,\varphi)$ from the scattering state. An additional complication arises from the different application of the Pauli principle: An elastic (inelastic) scattering into a solid angle given by θ and φ is in principle undistiguishable from a transfer reaction into the ground state (excited state) at angles $(\pi-\theta)$ and $(\pi+\varphi)$. Therefore, the amplitudes for these processes have to be added coherently. Hence, for the inelastic cross section from spin I_{in} into spin I' and spin z-component from μ into μ':

$$\frac{d\sigma}{d\Omega}(I_{in}\to I',\mu\to\mu') = \left|f^{\alpha}_{I',\mu'}(\theta,\varphi)+f^{\beta}_{I',\mu'}(\pi-\theta,\pi+\varphi)\right|^2 . \qquad \text{(IV.120)}$$

$f^{\alpha}_{I'\mu'}$ and $f^{\beta}_{I'\mu'}$ are the scattering amplitudes extracted from the α and β components with appropriate spin labels of $|\Phi_\mu\rangle$ and we dropped the index R on θ and φ. In the formalism of Messiah[29] for matching the asymptotic wave function to in- and outgoing spherical Coulomb function, the amplitude f_C of the pure Coulomb scattering solution must be added to the elastic amplitude:

$$\frac{d\sigma}{d\Omega}(I_{in}\to I_{in},\mu\to\mu') = \left|f^{\alpha}_{I',\mu'}(\theta,\varphi)+f^{\beta}_{I',\mu'}(\pi-\theta,\pi+\varphi)+\delta_{\mu\mu'}f_C(\theta,\varphi)\right|^2 . \qquad \text{(IV.121)}$$

Why f_C is added only to the elastic channel with $\mu'=\mu$, can be explained both formally and physically: Formally, by choosing the form (IV.110) with asymptote (IV.111) for $|\Phi_\mu\rangle$, a Coulomb scattering wave function has been subtracted in the incoming channel, therefore the corresponding amplitude has to be added back on in (IV.121) in that channel only and not at all in (IV.120). Physically, if there were no nuclear potential, the Rutherford scattering alone could not produce inelastic excitation, transfer, or spin flip, therefore, the cross section would be the Coulomb cross section in the incoming channel and zero everywhere else.

(IV.110) becomes asymptotically (cf. (IV.111)):

$$|\Phi_\mu(\vec{R})\rangle \sim \frac{\sqrt{\pi}}{kR}\sum_{J,L}\sqrt{2L+1}\,i^{L+1}\langle L0I_{in}\mu|J\mu\rangle$$
$$\sum_{\gamma,L',I'}\left[u_L^{(-)}(k_{I_{in}}R)\delta_{LL'}\delta_{\gamma\alpha}\delta_{I'I_{in}} - S^{J\gamma}_{L(L'I')}e^{2i\sigma_{L'}}u_{L'}^{(+)}(k_{I'}R)\right] \qquad \text{(IV.122)}$$
$$\sum_{\mu'}\langle L'(\mu'-\mu)I'\mu'|J\mu\rangle|I'\mu'\gamma\rangle Y_{L'(\mu-\mu')}\ ,$$

when the definition (IV.34) of $|(I'L')J'\mu\gamma\rangle$ is applied. The parity transformation property of the spherical harmonics is

$$Y_{lm}(\pi-\theta,\varphi+\pi) = (-)^l Y_{lm}(\theta,\varphi) \qquad . \qquad \text{(IV.123)}$$

The scattering amplitudes $f^\alpha_{I'\mu'}$ and $f^\beta_{I'\mu'}$ can now be had from (IV.122), we find for the sum

$$f^\alpha_{I'\mu'}(\theta,\varphi) + f^\beta_{I'\mu'}(\pi-\theta,\pi+\varphi) = \frac{\sqrt{\pi}}{ik}\sum_{J,L}\sqrt{2L+1}\,\langle L0I_{in}\mu|J\mu\rangle$$
$$\sum_{L'}\left(S^{J\alpha}_{L(L'I')} + (-)^{L'}S^{J\beta}_{L(L'I')} - \delta_{LL'}\delta_{I'I_{in}}\right)e^{2i\sigma_{L'}}\langle L'(\mu-\mu')I'\mu'|J\mu\rangle Y_{L'(\mu-\mu')}(\theta,\varphi). \qquad \text{(IV.124)}$$

The sum or difference of the S's is just the even or odd coefficient $S^{Jp}_{L(L'I')}$, even if L' is even, odd otherwise. We will denote this quantity as $S^{Jp(L')}_{L(L'I')}$.

An unpolarized cross section from spin I_{in} to $I' \neq I_{in}$ is the average over incoming spin projections μ and sum over μ' of the cross section (IV.121):

$$\frac{d\sigma}{d\Omega} = \frac{1}{2I_{in}+1}\sum_{\mu\mu'}\left|f^\alpha_{I',\mu'}(\theta,\varphi) + f^\beta_{I',\mu'}(\pi-\theta,\pi+\varphi)\right|^2 . \qquad \text{(IV.125)}$$

(IV.125) is evaluated from (IV.124) by expanding the product of two spherical harmonics as the sum over spherical harmonics, and after somewhat lengthy algebra

of the angular momenta coupling matrix elements, the result is:

$$\frac{d\sigma}{d\Omega}(I') = \frac{1}{2I_{in}+1}\frac{1}{4k^2}\sum_{J,L}\sum_{\tilde{J},\tilde{L}}(2J+1)(2\tilde{J}+1)\sqrt{(2L+1)(2\tilde{L}+1)}$$
$$\sum_{L',\tilde{L}'}\left[S^{\tilde{J}p(\tilde{L}')}_{\tilde{L}(\tilde{L}'\tilde{I}')}\right]^* S^{Jp(L')}_{L(L'I')}e^{2i(\sigma_{L'}-\sigma_{\tilde{L}'})}\sqrt{(2L'+1)(2\tilde{L}'+1)}$$
$$\sum_{\Lambda}(2\Lambda+1)\begin{pmatrix}\tilde{L}' & L' & \Lambda\\ 0 & 0 & 0\end{pmatrix}\begin{pmatrix}\tilde{L} & L & \Lambda\\ 0 & 0 & 0\end{pmatrix}\begin{Bmatrix}L' & \tilde{L}' & \Lambda\\ \tilde{J} & J & I'\end{Bmatrix}\begin{Bmatrix}L & \tilde{L} & \Lambda\\ \tilde{J} & J & I_{in}\end{Bmatrix}P_\Lambda(\cos\theta)\ . \tag{IV.126}$$

$\frac{d\sigma}{d\Omega}$ depends only on θ and not φ, because for the unpolarized cross section no azimuthal direction is singled out. (IV.126) can be integrated over $d\Omega$ to form the total inelastic cross section with ^{17}O spin I':

$$\begin{aligned}\sigma(I') &= \int d\Omega\frac{d\sigma}{d\Omega}(I')\\ &= \frac{1}{2I_{in}+1}\frac{\pi}{k^2}\sum_{J,L,L'}(2J+1)\left|S^{Jp(L')}_{L(L'I')}\right|^2\ .\end{aligned} \tag{IV.127}$$

The unpolarized elastic angular distribution is (from (IV.120)):

$$\begin{aligned}\frac{d\sigma}{d\Omega}(e) &= \frac{1}{2I_{in}+1}\sum_{\mu}\Big(\sum_{\mu'}|f^N_{\mu'}|^2+|f_C|^2+2\Re\left[(f^N_\mu)^* f_C\right]\Big)\\ &= |f_C|^2+\frac{1}{2I_{in}+1}\Big(\sum_{\mu\mu'}|f^N_{\mu'}|^2+2\Re\Big[\Big(\sum_\mu f^N_\mu\Big)^* f_C\Big]\Big)\ ,\end{aligned} \tag{IV.128}$$

where the nuclear scattering amplitude $f^N_{\mu'}$ is given by the sum of direct elastic and ground state transfer amplitude with appropriate argument:

$$f^N_{\mu'}(\theta,\varphi) = f^{\alpha}_{I_{in},\mu'}(\theta,\varphi)+f^{\beta}_{I_{in},\mu'}(\pi-\theta,\pi+\varphi)\ . \tag{IV.129}$$

The Coulomb scattering amplitude f_C is given by (cf. (III.13)):

$$f_C(\theta) = -\frac{\eta}{2k}\frac{\exp(-i\eta\ln(\sin^2\theta/2)+2i\sigma_0)}{\sin^2(\theta/2)}\ . \tag{IV.130}$$

The first summand in (IV.128) is the same as (IV.126) with $I' = I_{in}$ and the Coulomb wave subtracted, the second is just the Rutherford cross section, and the third can be had from (IV.124) via:

$$\sum_{\mu}\left(f^{\alpha}_{I_{in},\mu}(\theta,\varphi) + f^{\beta}_{I_{in},\mu}(\pi-\theta,\pi+\varphi)\right) = \frac{\sqrt{\pi}}{ik}\sum_{J,L,\mu}\sqrt{2L+1}\langle L0I_{in}\mu|J\mu\rangle$$
$$\sum_{L'}\left(S^{Jp(L')}_{L(L'I_{in})} - \delta_{LL'}\right)e^{2i\sigma_{L'}}\langle L'0I_{in}\mu|J\mu\rangle Y_{L'0}(\theta,0)\ . \tag{IV.131}$$

The sum over μ of the two Clebsch-Gordan coefficients equals $\delta_{LL'}(2J+1)/(2L+1)$, and if the spherical harmonic is rewritten as a Legendre polynomial and the sum over L' performed, (IV.131) becomes

$$\sum_{\mu}\left(f^{\alpha}_{I_{in},\mu}(\theta,\varphi) + f^{\beta}_{I_{in},\mu}(\pi-\theta,\pi+\varphi)\right)$$
$$= \frac{1}{2ik}\sum_{J,L}(2J+1)\left(S^{Jp(L)}_{L(LI_{in})} - 1\right)e^{2i\sigma_L}P_L(\cos\theta)\ . \tag{IV.132}$$

The total elastic cross section (the integral over $d\Omega$ of (IV.132)) does not exist because of the infinite range of the Coulomb force.

IV.12 ^{17}O levels, potential, and wave function

The energy level scheme of ^{17}O that was described in Section III.1 is unattainable from just a central potential without spin-orbit coupling (because the $1s$ and $1p$ states will always lie lower in energy than the $1d$ state), but this is exactly what is needed for the formalism of the previous sections. A solution to this dilemma is to create a spectrum with $1d$ and $2s$ level at the physical energies of ^{17}O and to ignore the lower $1s$ and $1p$ state (they have much lower energy now). We ignore the high-lying $^1/_2^-$ and $^5/_2^-$ states of the ^{17}O spectrum because of their high Q-value

and their opposite parity to the ground state, we expect very little cross section in these channels compared with the $^1/_2{}^+$ channel in the ^{17}O-^{16}O subbarrier reaction.

Our potential is the sum of a Woods-Saxon and a Gaussian potential:

$$v(r) = -\frac{V_0}{1 + \exp\left(\frac{r-r_0}{a}\right)} + V_1 \exp\left(-\frac{r^2}{r_1^2}\right) \quad , \tag{IV.133}$$

with parameters $V_0 = 60.827$ MeV, $r_0 = 3.034$ fm, $a = 0.66$ fm, $V_1 = 27.3$ MeV, and $r_1 = 1.0$ fm. $v(r)$ is plotted in Fig.14. The two energy levels certainly do not fix all five parameters V_0, V_1, a, r_0, r_1, but we want the diffuseness a and radius r_0 of our Woods-Saxon potential to be as similar as possible to that of the Copenhagen group.[36] However, their potential includes a spin-orbit part, so that we have to add a Gaussian to reproduce the energy levels. Thus, a and r_0 were taken from the Copenhagen potential, r_1 was fixed at 1 fm, and V_0 and V_1 were varied. With these parameters, we find the eigenstates of the Hamiltonian at -4.147 MeV for $l = 2$ (the $d_{5/2}$ ground state) and -3.276 MeV for $l = 0$ (the $s_{1/2}$ excited state). It is the large r behavior of the ^{16}O-n bound state wave functions that determines the formfactors, because the integrands of (IV.51) and (IV.76) peak for large r and $|\vec{r}-\vec{R}|$ if the two nuclei are not too close (and R does not become smaller than the IWBC radius). Therefore, the formfactors are insensitive to the exact shape of $v(r)$ for small r as long as the eigenenergies and the tails of the wave functions are correct.

Numerically, the eigenvalue problem of the bound state radial wave function of a particle in a given nuclear plus centrifugal (with angular momentum $l\hbar$) potential is solved by an iterative method. The eigenvalue, i.e., the bound state energy, is guessed, a solution that is regular at the origin integrated outwards to some matching radius r_M, and then a solution is integrated inwards from some large

radius outside the range of the nuclear potential to r_M. The boundary condition for the inwards solution is that it behaves as the exponentially decaying Hankel function of order l, i.e.,

$$\psi_I(r) \sim N_I h^{(1)}_{l(I)}(i\kappa_I r) \quad , \tag{IV.134}$$

where

$$\kappa_I = \sqrt{\frac{2m|\epsilon_I|}{\hbar^2}} \tag{IV.135}$$

and N_I, the *asymptotic coefficient*, is some normalization constant. This Hankel function is a solution to the Schrödinger equation with the centrifugal potential only (there is no Coulomb potential, because the neutron does not carry electric charge). The ingoing and outgoing wave functionc match logarithmic derivatives at r_M if an eigenvalue was used for the energy in the Hamiltonian and in the boundary condition for large r; thus, a zero in the difference of the logarithmic derivatives must be found as a function of trial energy by some standard numerical method such as a half-point algorithm. The integration cannot be integrated outwards to large distances or inwards to small distances, because of an exponential rise of numerical accuracy errors due to the inadvertent small admixture of the unwanted other solution of the second order differential equation.

The potential parameters are found by simple trial and error. When the potential and its eigenfunctions are found, the two-dimensional integrals $\mathcal{I}^{(1)}_{I',I,\Lambda}(R)$, $\mathcal{I}^{(v)}_{I',I,\Lambda}(R)$, and $\mathcal{J}_{I',I,\Lambda}(R)$ can be computed by numerical integration. The integral over the angle is performed with the Simpson algorithm, the infinite integration over dr proves to be much more accurate by a simple summing up of the integrand at a

few hundred mesh points (there is good convergence due to the exponential decay of the wave functions) than by a Gaussian integration at tens of points. There are six sets of labels $\{I', I, \Lambda\}$ for which $I^{(v)}$ has to be calculated, namely $\{1/2, 1/2, 0\}$, $\{1/2, 5/2, 2\}$, $\{5/2, 1/2, 2\}$, $\{5/2, 5/2, 0\}$, $\{5/2, 5/2, 2\}$, and $\{5/2, 5/2, 4\}$. For $I^{(1)}$ and J there are only five sets, because $\{5/2, 1/2, 2\}$ and $\{1/2, 5/2, 2\}$ give the same result. The symmetry property (IV.23) provides an additional constraint on the integrals:

$$I^{(v)}_{1/2,5/2,2} - I^{(v)}_{5/2,1/2,2} = (\epsilon_{1/2} - \epsilon_{5/2}) J_{1/2,5/2,2} \ , \qquad \text{(IV.136)}$$

this is used as a numerical check.

The sixteen integrals are needed as functions of R from about 5 fm to about 25 fm, with small step size, about 0.01 fm. Calculating these sixteen integrals for that many points would require hundreds of hours of CPU time on a VAX 750. Luckily, the integrals vary slowly over the small step size and fall off exponentially for large R. Therefore, we calculate the integrals at R from 5.5 fm to 13.5 fm with a step size of 0.1 fm and at $R = 19.5$ fm. An exponential function is fit to the values at 13.5 fm and 19.5 fm and this exponential function is taken as the integral for all R larger than 13.5 fm. Quadratic extrapolation is used to refine the mesh to a step size of 0.01 fm. (IV.136) is imposed exactly, because any violation of it would destroy unitarity in the coupled channels equations, and the unitarity condition is used as a check of numerical accuracy in the integration of these equations. The integrals J, $I^{(1)}$, and $I^{(v)}$ are plotted in Figs.15-17.

In summary, we estimate the numerical error in the calculation of the formfactors to a few percent within our model and for given potential, the error is thus less than that resulting from the neglect of recoil. Energies and formfactors are consis-

tent in such a way that, when they are inserted into the discretized coupled channels equations, make them a practically exactly Hermitian finite difference system, and all flux non-conservation will stem from numerical inaccuracy in the integration of these equations.

IV.13 Numerical solution of the coupled channels equations

Whereas the adiabatic system of equations

$$\chi_i''(R) + k_i^2(R)\chi_i(R) = \sum_{j \neq i} u_{ij}(R)\chi_j(R) \qquad \text{(IV.137)}$$

can be solved rather efficiently for most systems, the numerical integration of the non-adiabatic equations (IV.96) is rather cumbersome. For systems with not too large coupling terms $u_{ij}(R)$ and a non-trivial number of channels (say: more than one or two), (IV.137) is best solved in a Born series:[37] As a first step, the elastic channel is integrated with the wave function in all other channels set to zero; then, in each subsequent steo, the wave function in some channel I is integrated by using the solutions so far obtained for the other channels, i is chosen by cyclically going through all channels. The set of wave functions converges for small enough u_{ij} (sometimes at least in an asymptotic way), but often a Padé resumming accelerates the convergence. The integration of a wave function χ_i can be done very efficiently with the Numerov algorithm.[33] This efficiency stems from the asymptotic shrinking of the local error in the integration with the sixth power of the step size. Unfortunately, in this algorithm, calculation of χ_i at a mesh point requires knowledge of the value of the right hand side of (IV.137), and hence of all other channel wave

functions, at this point. This is the reason for the somewhat awkward sequential calculation of the channels.

The functions χ_i that we are after correspond to continuum (scattering) states, the numerically stable direction of integration is outwards. Thus, the IWBC is easily incorporated by choosing an arbitrary value for χ_i at the IWBC radius and fixing χ_i at the next mesh point so that the (discretized two-point) logarithmic derivative of χ_i is $-ik_i$, where k_i can be taken at the IWBC radius, at the next mesh point, or - most accurately - at the half-point between these two possibilities. The other boundary condition, namely that χ_i at large distances goes asymptotically as $u^{(+)}(k_iR)\delta_{ie} + A_iu^{(-)}(k_iR)$, where e denotes the ingoing (elastic) channel, is incorporated as follows: In step one, the calculated elastic wave function χ_e is matched to $u^{(-)}$ and $u^{(+)}$ at large R, then χ_e is scaled so that it has coefficient of $u^{(+)}$ equal to 1. In subsequent steps, χ_i is calculated twice, with different starting value (at the IWBC radius). Since the coefficient of $u^{(+)}$ is a linear function of the starting value, these two solutions determine the starting value that produces the appropriate coefficient (i.e., 1 for $i = e$, and 0 otherwise). The χ_i is then once more integrated, this time with the correct starting value.

Despite this triple integration of each step in the algorithm and possibly a large number of steps before convergence (maybe ten steps per channel), this method is in most cases much more efficient than conceptually easier methods that require matrix inversion at each mesh point or that do not have as good convergence properties in the local integration error as the Numerov algorithm.

However, the non-adiabatic equations (IV.96) cannot be integrated by the Nu-

merov algorithm because of the occurrence of a first-order derivative in them. We adopt a simpler three-point finite difference formula for the second-order derivative and a two-point formula for the first-order derivative, namely $(\chi_i^{n+1} - 2\chi_i^n + \chi_i^{n-1})/h^2$ and $(\chi_i^{n+1} - \chi_i^{n-1})/(2h)$, respectively, where the upper index on the wave function denotes the mesh point and h is the step size. The local error of this discretization approaches zero as the fourth power of the step size. In practice, this difference of fourth and sixth power behavior makes a considerable change in the acceptable step size in our system (the simpler formula requires a step size of the order one tenth that of the Numerov algorithm for comparable accuracy).

Whereas in the Numerov algorithm knowledge of the inhomogeneous term (and thus of all other wave functions) at mesh points number $n-1$, n, and $n+1$ is necessary for the computation of the wave function at mesh point with number $n+1$, the inhomogeneous term is only needed at the n-th point for the simpler algorithm. Therefore, the sequential Born series is no longer advantageous over a direct integration, where at each mesh point all channels are calculated simultaneously.

The boundary conditions for large R are imposed by choosing the right linear combination of a complete set of solutions (each of which consists of one wave function in each channel). Determination of this linear combination involves (numerically costly) matrix inversion, but only at one point.

Before integration, the equations are brought into the discretized form

$$\chi_i^{n+1} = \sum_j \left(F_{ij}^n \chi_j^n + G_{ij}^n \chi_j^{n-1}\right) \quad . \tag{IV.138}$$

It does take matrix inversion at each point to transform (IV.96) into (IV.138), but the matrix inversion is independent of the value of the energy, and thus needs to

be performed only once for the wave function determinaton at different energies. Also, the number of channels involved in each integration is only four (or even 2 or 3 for $J = 1/2$ and $J + 3/2$, respectively), namely the $s_{1/2}$ channel with some $L = L_0$, and $d_{5/2}$ channels with $L = L_0 - 2$, $L = L_0$, and $L = L_0 + 2$. Matrix inversion of a 4×4 matrix is not too CPU time consuming, but this method would become unacceptable for a large number of channels.

We use a step size of 0.01 fm and integrate from $r_0 = 5.5$ fm to between $r_1 = 22$ fm and $r_1 = 24$ fm, the highest total angular momentum taken into account varies from $J = 16\,1/2$ to $J = 18\,1/2$, depending on the energy. The convergence in angular momentum is good for the fusion cross section, but for the inelastic cross section at the highest energies a somewhat larger J would have improved the precision. The IWBC, however, allows only a certain orbital angular momentum L, because otherwise the centrifugal potential will fill in the attractive pocket of the nuclear plus Coulomb potential, and instead of incoming and outgoing wave the exponentially increasing and decreasing waves become the eigenfunctions of the Hamiltonian.

Unitarity is achieved to better than 1% in all channels, and the error in the sum of fluxes is always much smaller than the fusion flux. This is not true if the equations are integrated without the non-adiabatic terms, in that case the total unitarity can be violated up to 1% in the cases we tested, but the error can be larger than the fusion flux by more than an order of magnitude.

IV.14 Results and comparison with experiment

The results of the calculation together with the available experimental data are plotted in Figs.18 to 21.

Fig.18 shows the measured fusion cross section from Thomas *et al.* together with our results for $^{17}O+^{16}O$, for comparison, the calculated curve for $^{16}O+^{16}O$ is also presented. The *s*-wave barrier height is at about 10 MeV. Above this energy, the data are well reproduced, in this region, the channel coupling is largely irrelevant for the fusion process, and the ^{17}O-^{16}O cross section is proportional to that for ^{16}O-^{16}O. This trend would hold for all energies in a one-channel calculation. However, the experimental data clearly show the typical subbarrier enhancement. Our calculation reproduces this enhancement down to 8 MeV, i.e., $^4/_5$ the barrier height. Around 9 MeV, our model even overpredicts the data slightly, however, this error is within two (experimental statistical) standard deviations. Also, Thomas *et al.* have shifted down their raw data normalized to their best measurement of beam current so that the data agree with the scaled $^{16}O+^{16}O$ values at above-barrier energies. For the measurements at the lowest energies, i.e., between 6.5 MeV and 8 MeV, theory and experiment deviate and cannot be said to be in quantitative agreement any more. If we accept the experimental data as right, then the channels of our model do not provide enough entry into the compound nucleus. We conjecture that the constraint of inert ^{16}O cores causes the underprediction. In an improved model this constraint could be eased by allowing a certain shell model admixture of particle-hole excitations of the ^{16}O core in the ^{17}O excited state (or perhaps even the ground state). However, it might well be that the Hilbert sub-

space thus spanned is insufficient, too, and that the shape of the two-nucleus system shortly before it reaches the compound nucleus stage must be taken into account in a much more sophisticated way at the lowest energies. It is possible that a correct antisymmetrization between all nucleons or at least all surface nucleons becomes necessary, too. Here, this unusual and very interesting feature of the subbarrier process shows itself clearly: that the more complicated, interior and usually higher energy nuclear structure effects reveal themselves at the lower energies. However, there remains the gratifying result that for quite some region below the barrier, the IWBC model with addition of the obvious channels in simple parametrization proves to be successful, when all implications of the model are taken into account very carefully.

The excitation function of the $^1/_2{}^+$ state in ^{17}O as measured by Thomas *et al.* and calculated here is plotted in Fig.19. The data lie consistently below the theory, from 25% at the lowest to 70% at the highest energies. This is not surprising because of the neglect of spectroscopic factors for ground and excited state. The spectroscopic factor S is a measure for how much a given physical state is made up of a theoretical single-particle state. S is defined operationally for a specific reaction, e.g. S has been measured for ^{17}O by the stripping reaction ^{16}O(d,p)^{17}O. Here S is defined as the measured cross section into the specified state of ^{17}O divided by the DWBA (*distorted wave Born approximation*) prediction using the model wave function of the state. Cooper *et al.*[38] thus find spectroscopic factors of $S_{5/2} = 0.81$ for the $^5/_2{}^+$ ground state and $S_{1/2} = 0.78$ for the $^1/_2{}^+$ excited state at their lowest bombarding energy of $E_d = 25.4$ MeV with a decreasing tendency of S for decreasing

energy. In a pure DWBA calculation, the $^{16}O+^{17}O$ inelastic cross section would be multiplied by the product $S_{5/2}$ times $S_{1/2}$. Gelbke *et al.*[39] measured an inelastic differential cross section for $^{17}O(^{16}O,^{16}O)^{17}O^*$ at $E_{^{17}O} = 22$ MeV, corresponding to 11.3 MeV in the center-of-momentum frame. They can reproduce their data reasonably well, when they scale their DWBA results by $S_{1/2}S_{5/2} = 0.7$. This is also the value by which our calculated total inelastic cross section has to be scaled at that energy to coincide with the measurement by Thomas *et al.*. However, this agreement in the product of spectroscopic factors comes only from an almost coincidentally good agreement in the asymptotic bound state wave function. The inelastic cross section in this energy range depends mainly on the asymptotic large r behavior and not the interior of the single particle bound state wave function in ^{17}O. Indeed, Gelbke *et al.* find a reasonable fit to their data by using only the asymptotic strength N_I and no other information from the radial wave function in their calculation. The N_I are given by the asymptotic behavior of the $\psi_I(R)$ (cf. (IV.134)). The values N_I depend very strongly on the parametrization of the single particle potential and can vary widely for different reasonable potentials with the same bound state spectrum. Gelbke *et al.* cite $N_{5/2} = 0.363$ fm$^{-3/2}$ and $N_{1/2} = 1.133$ fm$^{-3/2}$, whereas our potential gives $N_{5/2} = 0.362$ fm$^{-3/2}$ and $N_{1/2} = 1.172$ fm$^{-3/2}$. To get the same product $S_{1/2}S_{5/2}N_{1/2}N_{5/2} = 0.288$ fm^{-3}, we would need $S_{1/2}S_{5/2} = 0.68$. We have plotted the inelastic angular distribution at $E_{cm} = 11.3$ MeV, we graphed both the unscaled results (no spectroscopic factor) and the results scaled by 0.7 to bring the total inelastic cross section in agreement with the measurement by Thomas *et al.* . It should be stressed that in our exact

formalism (no DWBA), the cross section depends only approximately linearly on the product $S_{1/2}S_{5/2}$. Nevertheless, a reasonably good agreement exists between the data and our numbers, when they are scaled by 0.7.

Similar arguments apply to the elastic differential cross section, but here a failure of fine-tuning of the ground state spectroscopic factor leads to large errors in the ratio of complete to Rutherford cross section, because of the intereference of the nuclear amplitude with the Rutherford amplitude. We present our results without incorporation of a spectroscopic factor in Fig.21 for $E_{cm} = 10.65$ MeV. This energy corresponds to 22 MeV in the lab for ^{16}O(^{17}O,^{17}O)^{16}O, for which measurements were done by Burzynski *et al.*.[40] The dashed curve in Fig.21 is a simple one-channel calculation without transfer or inelastic excitation that uses just the ^{16}O-^{16}O potential. (Plotted is the ratio of the total cross section over the Rutherford cross section.) This curve is in good agreement with an optical potential calculation without transfer by Burzynski *et al.*. However, by fitting their ground state spectroscopic factor and treating the transfer elastic amplitude in DWBA, they achieve a very good fit to their data. Their final curve shows small oscillations about the one-channel curve. Our calculation shows the same oscillations (solid curve in Fig.21), but too pronounced for the large angles. The reason for this is that these oscillations come from the interference of the nuclear with the Rutherford amplitude (cf. (IV.128)), a small scaling error (i.e., a wrong spectroscopic factor) will cause a large error in the cross section ratio, when $|f_C|^2$ is comparable to $\frac{2}{2I_{in}+1}\Re[f_N^* f_C]$. This effect makes this reaction so valuable in the determination of the spectroscopic factor and allows a precision in the extraction

of this factor comparable only to magnetic electron scattering. We do not attempt to fit a spectroscopic factor to achieve a good reproduction of the data a posteriori, as our main goal is the fusion cross section. In the above notation, Burzynski *et al.* use an asymptotic strength $N_{5/2}$ of 0.354 $\mathrm{fm}^{-3/2}$ and find 1.06 for the mean of $S^2_{5/2}$. In order to get the same product $S^2_{5/2}N^2_{5/2}$ (which determines the cross section in DWBA) we would need $S_{5/2} = 1.01$.

IV.15 Coulomb excitation

In the formalism that we developed so far, the single particle excitations in ^{17}O are entirely due to the nuclear and not the Coulomb force, because the neutron does not carry an electric charge, so that the neutron-nucleus potential has no Coulomb component. If the recoil were taken into account, a small Coulomb excitation would result from pushing the ^{16}O core of the ^{17}O nucleus away from the neutron by the ^{16}O-^{16}O electric repulsion. However, it is well known that the recoil effect cannot nearly account for the magnitude of the empirical Coulomb excitation in ^{17}O.

There exists a well-developed semiclassical theory of Coulomb excitations, in which the relative nucleus-nucleus motion is treated classically (Rutherford trajectories) and the probability of excitation is related to the dominant electric or magnetic multipole reduced matrix elements between the ground and the excited state. The reduced matrix element is determined from the experimentally known life-time of the excited state. In the case of ^{17}O, the transition from the $^1/_2{}^+$ excited to the $^5/_2{}^+$ ground state is dominated by the electric transition E2 of multipolarity two.

The total cross section for Coulomb excitation is[41]:

$$\sigma_{E2} = \left(\frac{Z_1 e}{a\hbar v}\right)^2 B(E2)\, f_{E2}(\xi) \quad , \tag{IV.139}$$

where $a = (Z_1 Z_2 e^2)/(Mv^2)$ is half the distance of closest approach of the two nuclei, $\xi = (a|Q|)/(\hbar v)$ is the ratio of the collision time scale to the nuclear excitation time scale, and $B(E2)$ is the usual square of the reduced matrix element divided by $(2I_{in}+1)$, where I_{in} is the spin of the initial state. The $B(E2)$ for the excitation from the ground state is thus $(2I'+1)/(2I_{in}+1)$ times the $B(E2)$ of the deexcitation (which is known from the life-time measurements of ^{17}O), where I' is the spin of the excited state. $f_{E2}(\xi)$ is tabulated in Ref.[41]. (IV.139) is a good approximation for $|Q|/E << 1$ (for our case $|Q| = 0.871$ MeV, and E ranges from 6 to 14 MeV), the Sommerfeld parameter $\eta >> 1$ (here $\eta > 8$), and for the suddenness condition $\xi << 1$ (here $\xi < 0.86$ for $E > 6.5$ MeV). What we call the *sudden* approximation is mostly referred to as the *non-adiabatic* approximation. However, we want to restrict use of the word "non-adiabatic" to the meaning "in general, without invoking the adiabatic approximation". A violation of the suddenness condition will cause an overprediction of the cross section, because there is not enough time during the actual collision for the excitation to happen. The σ_{E2} calculated from (IV.139) are plotted together with the experimental data in Fig.19. Evidently, neglecting the Coulomb excitation in our model is a good approximation for ^{17}O in the energy region of interest.

CHAPTER V

V.1 The two-channel model

In the analysis of the ^{18}O-^{16}O subbarrier scattering, we let ourselves be guided by the experimental findings to construct a suitable model. The data are presented in Fig.5. In comparison to $^{17}O+^{16}O$, at first glance it is striking how small the inelastic cross section is and how little the fusion cross section far below the barrier is enhanced over that for $^{16}O+^{16}O$. However, the relatively small size of the inelastic cross section can be explained by comparing the 1.98 MeV excitation energy of the first excited state in ^{18}O with the corresponding 0.87 MeV for ^{17}O. It is therefore energetically relatively difficult to excite the ^{18}O in a collision of under or little more than 10 MeV. Only the γ ray from the 2^+ to the ground state is observed experimentally. In principle, higher excitations could cascade through the 2^+ state into the ground state, but then a major contribution would be expected from the second excited, the 4^+ state, but no line corresponding to the 4^+ to 2^+ transition is recognizable in the gamma spectra. The smallness of the inelastic cross section in turn explains the small enhancement of the fusion probability, because only the ground state channel of ^{18}O is energetically effectively accessible.

In a semiclassical calculation of the Coulomb excitation (as in Chapter IV), we find that this theory can account for the total experimental inelastic cross section already at $E_{cm} = 10$ MeV and below (cf. Fig.22). The slight overprediction of the calculation should be attributed most likely to a violation of the suddenness

conditon $\xi << 1$. The ratio ξ of the two time scales involved in the problem (cf. Chapter IV) actually crosses the value 1 between 10 and 11 MeV, with $\xi = 2.6$ for $E_{cm} = 6$ MeV. It is clear that any theory without Coulomb excitation must fail to describe the inelastic cross section accurately. The incorporation of the electromagnetic excitation into the coupled channels framework is numerically difficult, but not impossible. However, as our main object under study is the fusion cross section, which is very little affected by the small inelastic excitation, we will not pursue this process here.

Q-value considerations immediately rule out the one-neutron (or, for that matter, the one-proton) transfer process as responsible for the small fusion enhancement. Because of the pairing of the two $s-d$ shell nucleons in ^{18}O, the binding energy in ^{18}O with respect to the ^{16}O+2n threshold is 12.191 MeV, which has to be compared to 8.287 MeV, which is twice the dissociation energy of $^{17}\mathrm{O} \rightarrow {}^{16}\mathrm{O}+\mathrm{n}$.

Therefore, only one channel in addition to the direct elastic remains: the two-neutron transfer into the ground state of ^{18}O. Two-neutron transfer into excited states are excluded by the same energy considerations that apply to the direct inelastic excitations. We will now analytically derive a simple model that incorporates the two-neutron transfer.

We start by writing down the Hamiltonian and wave function just as we did for ^{17}O. In the next section, we will reduce the formfactors to those of ^{17}O in a reasonable approximation, then we will derive the actual equations that have to be solved numerically. In the last section, we will present the results of our numerical computations.

In the center-of-momentum frame, the Hamiltonian can be written as

$$H = T + T_{n_1} + T_{n_2} + V_{1n_1} + V_{2n_1} + V_{1n_2} + V_{2n_2} + V_{n_1n_2} + V_{12} \ , \qquad \text{(V.1)}$$

where the indices "1" and "2" denote the ^{16}O cores and "n_1" and "n_2" the two extra neutrons. Again, we neglect all recoil, so that T is the kinetic energy between the two cores. The neglect of recoil corrections is half as good (or twice as bad) an approximation as it is for ^{17}O+^{16}O, because now the corrections are of order of twice the neutron over the ^{16}O mass (or $1/8$). We can summarize seven of the operators in (V.1) as the two-neutron Hamiltonian U:

$$U = T_{n_1} + T_{n_2} + V_{1n_1} + V_{2n_1} + V_{1n_2} + V_{2n_2} + V_{n_1n_2} \quad . \qquad \text{(V.2)}$$

The two-channel wave function is

$$|\Phi(\vec{r})\rangle = \phi_\alpha(\vec{r})|\alpha\rangle + \phi_\beta(\vec{r})|\beta\rangle \ , \qquad \text{(V.3)}$$

where $|\alpha\rangle$ and $|\beta\rangle$ are the states with ^{18}O on the left and on the right, respectively, and ϕ_α and ϕ_β are the channel wave functions with the core-core separation vector $\vec{r}$ as argument. As the ground state of ^{18}O has zero spin like the ^{16}O ground state, no coupling scheme of spin to orbital angular momentum is needed at this stage (it becomes necessary for the synthesis of the $|\alpha\rangle$ and $|\beta\rangle$ out of single particle states). $|\alpha\rangle$ and $|\beta\rangle$ are eigenstates of the left and right ^{18}O Hamiltonian, so that

$$U|\alpha\rangle = \epsilon|\alpha\rangle + (V_{2n_1} + V_{2n_2})|\alpha\rangle \quad , \qquad \text{(V.4)}$$

and

$$U|\beta\rangle = \epsilon|\beta\rangle + (V_{1n_1} + V_{1n_2})|\beta\rangle \quad , \qquad \text{(V.5)}$$

with ϵ (minus) the separation threshold for ^{18}O$\rightarrow^{16}$O+n+n. We can normalize $|\alpha\rangle$ and $|\beta\rangle$ to unity, but $\langle\alpha|\beta\rangle \neq 0$ because of the different partition. The coupled channels equations in the left/right representation follow from left multiplication of $\langle\alpha|$ on the Schrödinger equation $(H-E)|\Phi(\vec{r})\rangle = 0$:

$$\begin{aligned} 0 =& \langle\alpha|T|\alpha\rangle\phi_\alpha(\vec{r}) + \langle\alpha|T|\beta\rangle\phi_\beta(\vec{r}) \\ &+ (V_{12} - E + \epsilon)\phi_\alpha(\vec{r}) + (V_{12} - E + \epsilon)\langle\alpha|\beta\rangle\phi_\beta(\vec{r}) \\ &+ \langle\alpha|V_{2n_1} + V_{2n_2}|\alpha\rangle\phi_\alpha(\vec{r}) + \langle\alpha|V_{1n_1} + V_{1n_2}|\beta\rangle\phi_\beta(\vec{r}) \ , \end{aligned} \tag{V.6}$$

and the analog for $\langle\beta|$ instead of $\langle\alpha|$. T in (V.6) operates in general on both the kets and the radial wave functions, the restriction of T onto the radial wave functions is the adiabatic approximation, of which we will make no use.

V.2 Formfactors

In order to calculate the formfactors $\langle\alpha|\beta\rangle$, $\langle\alpha|V_{2n_1} + V_{2n_2}|\alpha\rangle$, and $\langle\alpha|V_{1n_1} + V_{1n_2}|\beta\rangle$, we need to choose a form for the potentials and to express the states $|\alpha\rangle$ and $|\beta\rangle$ through single particle wave functions. We use the same neutron-^{16}O potential as in Chapter IV. The Schrödinger equation for the three-body system ^{18}O is solved by perturbation theory in the potential $V_{n_1n_2}$. We treat the perturbation to zeroeth order in the eigenfunctions and first order in the energy (if we did the analysis to higher order, additional integration of formfactors other than the ones done in Chapter IV would become necessary). The two-neutron wave function is thus a linear combination of the product of ^{17}O single particle ground state wave functions, where the coefficients in the linear combination couple the total angular momenta $\vec{j}_1$ and $\vec{j}_2$ of the single particle states (with spin $^5/_2$) to the total angular momentum $\vec{J}$ of the ^{18}O nucleus (with expectation value $\langle\vec{J}\rangle = 0$). Thus, for $\gamma = \alpha$

or β:

$$|\gamma\rangle = \sum_m \langle {}^5\!/_2 m\, {}^5\!/_2 \, -m | 00\rangle \, |m\gamma\rangle \, |-m\gamma\rangle \ . \qquad \text{(V.7)}$$

$|m\gamma\rangle \, |-m\gamma\rangle$ is the direct product of the state of angular momentum $^5\!/_2$ and projection m of the first neutron and $^5\!/_2$, $-m$ for the second neutron. It is perhaps surprising that, as we will show, (V.7) is the correctly antisymmetrized and normalized ^{18}O wave function. Not normalized is the state $2^{-1/2} \sum_m \langle 5/2\, m\, 5/2 \ -m \,|\, 00 \rangle$ $(|m\gamma\rangle \, |-m\gamma\rangle - |-m\gamma\rangle |m\gamma\rangle)$, which would be written in second quantization as $\sum_m \langle 5/2\, m\, 5/2 \ -m \,|\, 00 \rangle \ a^\dagger_m(\gamma) a^\dagger_{-m}(\gamma)|0\rangle$, with $|0\rangle$ the single particle vacuum (here the ^{16}O core plus the other ^{16}O nucleus) and $a^\dagger_n(\gamma)$ the particle creation operator for spin projection n. The antisymmetry property of $|\gamma\rangle$ is inherent in the form (V.7), because $\langle jmj-m|00\rangle$ changes sign under exchange of m and $-m$ for half-integer j.

In first-order perturbation theory, the energy ϵ of the ^{18}O Hamiltonian becomes

$$\langle\alpha|T_{n_1} + T_{n_2} + V_{1n_1} + V_{1n_2} + V_{n_1n_2}|\alpha\rangle = 2\epsilon(^{17}\mathrm{O}) + \langle\alpha|V_{n_1n_2}|\alpha\rangle \ , \qquad \text{(V.8)}$$

where $\epsilon(^{17}\mathrm{O})$ is the eigenenergy of the ^{17}O Hamiltonian. We choose $V_{n_1n_2}$ in such a way that $2\epsilon(^{17}\mathrm{O}) + \langle\alpha|V_{n_1n_2}|\alpha\rangle$ equals ϵ, the experimental ^{18}O eigenenergy. We do not really need to specify $V_{n_1n_2}$ as a function of the inter-neutron distance, because only the matrix element $\langle\alpha|V_{n_1n_2}|\alpha\rangle$ (or the identical $\langle\beta|V_{n_1n_2}|\beta\rangle$) enter into the calculation.

At first, we calculate the "inelastic" formfactor $\langle\alpha|X|\alpha\rangle$, where we let X equal 1 to test the normalization in (V.7) or equal V_{2n_1} or V_{2n_2}. All three operators can be expressed as direct products of a single particle operator on neutron "n_1" and a single particle operator on "n_2", viz. $1 = 1 \otimes 1$, $V_{2n_1} = V_2 \otimes 1$, and $V_{2n_2} = 1 \otimes V_2$,

where V_2 is the potential between the ^{16}O nucleus on the right and a neutron. For an operator of the form $x \otimes 1$, we find from (V.7):

$$\langle \alpha | x \otimes 1 | \alpha \rangle = \sum_{m,n} \langle {}^5\!/_2 m \, {}^5\!/_2 - m | 00 \rangle \langle {}^5\!/_2 n \, {}^5\!/_2 - n | 00 \rangle \langle m\alpha | x | n\alpha \rangle \langle -m\alpha | - n\alpha \rangle \ . \quad \text{(V.9)}$$

$\langle -m\alpha | - n\alpha \rangle$ is the overlap of single particle states with spin projections $-m$ and $-n$, and hence equals δ_{mn}, so that

$$\langle \alpha | x \otimes 1 | \alpha \rangle = \sum_m \Big(\langle {}^5\!/_2 m \, {}^5\!/_2 - m | 00 \rangle \Big)^2 \langle m\alpha | x | m\alpha \rangle \ . \quad \text{(V.10)}$$

The $\langle m\alpha | x | m\alpha \rangle$ were derived in Chapter IV for $x \equiv 1$, they equal unity, and for $x = V$, (cf. (IV.50)),

$$\begin{aligned} \langle m\alpha | V | m\alpha \rangle = & \sqrt{\pi} (-)^{1/2 - m} \sum_{\Lambda, \nu} 30 \sqrt{2\Lambda + 1} \begin{pmatrix} {}^5\!/_2 & {}^5\!/_2 & \Lambda \\ -m & m & 0 \end{pmatrix} \\ & \begin{pmatrix} 2 & 2 & \Lambda \\ 0 & 0 & 0 \end{pmatrix} \begin{Bmatrix} {}^5\!/_2 & {}^5\!/_2 & \Lambda \\ 2 & 2 & {}^1\!/_2 \end{Bmatrix} Y_{\Lambda\nu}(\Omega_r) J_{5/2,5/2,\Lambda}(r), \ , \end{aligned} \quad \text{(V.11)}$$

where $J_{5/2,5/2,\Lambda}(r)$ is given by (IV.51). (V.10) can thus be evaluated, when $x \equiv 1$, the sum over the square of the Clebsch-Gordan coefficients equals unity, and indeed $\langle \alpha | 1 \otimes 1 | \alpha \rangle = 1$. When (V.11) is inserted into (V.10), the sum over the square of the Clebsch-Gordan coefficients and Wigner 3-j symbol that contain m can be performed, the result vanishes for $\Lambda \neq 0$ and the left-over Wigner symbols in (V.11) are easily evaluated for $\Lambda = 0$, the net result is:

$$\langle \alpha | V \otimes 1 | \alpha \rangle = {}^1\!/_2 J_{5/2,5/2,0}(r) \quad . \quad \text{(V.12)}$$

As a check for (V.12), we note that $J_{5/2,5/2,0}(r) = 2$, if instead of the potential function $v(r)$ the unit function is inserted under the integral in (IV.51), so that

again we recover the normalization. The amplitude (V.12) is obviously the same for $1 \otimes V$ instead of $V \otimes 1$, thus

$$\langle \alpha | V_{2n_1} + V_{2n_2} | \alpha \rangle = J_{5/2,5/2,0}(r) \ . \tag{V.13}$$

This formfactor is isotropic, i.e., does not depend on Ω_r, as expected for spin 0 states.

Next, we calculate the transfer amplitude $\langle \alpha | X | \beta \rangle$ for X equalling $1 \otimes 1$, $V_1 \otimes 1$, and $1 \otimes V_2$. For $x \otimes 1$ we find

$$\langle \alpha | x \otimes 1 | \beta \rangle = \sum_{m,n} \langle {}^5\!/\!_2 m \, {}^5\!/\!_2 - m | 00 \rangle \langle {}^5\!/\!_2 n \, {}^5\!/\!_2 - n | 00 \rangle \langle m\alpha | x | n\beta \rangle \langle -m\alpha | -n\beta \rangle \ . \tag{V.14}$$

We extract the single particle matrix elements $\langle m\alpha | x | n\beta \rangle$ from Chapter IV, and perform all the angular momentum algebra, the end result is:

$$\langle \alpha | x \otimes 1 | \beta \rangle = 24\pi^2 \sum_{\Lambda} \sqrt{2\Lambda + 1} \left(\begin{Bmatrix} {}^5\!/\!_2 & {}^5\!/\!_2 & \Lambda \\ 2 & 2 & {}^1\!/\!_2 \end{Bmatrix} \right)^2 I^{(x)}_{5/2,5/2,\Lambda}(r) I^{(1)}_{5/2,5/2,\Lambda}(r) \ . \tag{V.15}$$

(V.15) can be checked by letting $x = 1$ and considering the case of $r = 0$, when α and β states are identical, with $I^{(1)}_{5/2,5/2,\Lambda}(0) = \sqrt{5}/(2\pi)\delta_{\Lambda 0}$, we find indeed that $\langle \alpha | 1 \otimes 1 | \beta \rangle = 1$ for $r = 0$. $\langle \alpha | 1 \otimes V_2 | \beta \rangle = \langle \alpha | V_2 \otimes 1 | \beta \rangle$, so that the total transfer potential formfactor $\langle \alpha | V_{2n_1} + V_{2n_2} | \beta \rangle$ equals twice the expression (V.15) for $x = v$.

V.3 The "coupled" channels equations

In order to use the symmetry of the two identical ^{16}O cores, we construct the even and odd states as in Chapter IV. We have to transform to the ˜representation of section IV.7, so that that the derivative operators that come from the kinetic energy term in the Hamiltonian do not couple even and odd states. The transformation

is much simpler here than for ^{17}O because of the spinlessness of the ^{18}O ground state and the resulting isotropy of the formfactors. Thus, when the Laplacian and gradient are split into radial and angular momentum part, only the radial part will operate on the formfactors.

We define

$$|p\rangle = \frac{1}{\sqrt{2}}\Big(|\tilde{\alpha}\rangle + (-)^p|\tilde{\beta}\rangle\Big) \quad . \tag{V.16}$$

The $|\tilde{\alpha}\rangle$ and $|\tilde{\beta}\rangle$ differ from the $|\alpha\rangle$ and $|\beta\rangle$ by their choice of origin for $\vec{r}$ (cf. Section IV.7). Overlap and potential matrix elements are not affected by the change in the representation, but only the derivative matrix elements are. Therefore,

$$\langle p|p'\rangle = \delta_{pp'}\left[1 + (-)^p 24\pi^2 \sum_{\Lambda} \sqrt{2\Lambda+1}\left(\left\{\begin{array}{ccc} 5/2 & 5/2 & \Lambda \\ 2 & 2 & 1/2 \end{array}\right\} I^{(1)}_{5/2,5/2,\Lambda}(r)\right)^2\right] , \tag{V.17}$$

and

$$\langle p|U|p'\rangle = \delta_{pp'}\Bigg[J_{5/2,5/2,0}(r) + (-)^p 48\pi^2 \sum_{\Lambda} \sqrt{2\Lambda+1}\left(\left\{\begin{array}{ccc} 5/2 & 5/2 & \Lambda \\ 2 & 2 & 1/2 \end{array}\right\}\right)^2 I^{(v)}_{5/2,5/2,\Lambda}(r) I^{(1)}_{5/2,5/2,\Lambda}(r) + \epsilon\langle p|p'\rangle\Bigg] . \tag{V.18}$$

The radial derivatives of the $|p\rangle$ in terms of the $|\alpha\rangle$ and $|\beta\rangle$ are evaluated by the same integration tricks as in section IV.7, the results are

$$\langle p|\frac{\partial}{\partial r}|p'\rangle = 1/2\frac{\partial}{\partial r}\langle p|p'\rangle = \delta_{pp'}(-)^p\, 1/2\frac{\partial}{\partial r}\langle\alpha|\beta\rangle \ , \tag{V.19}$$

and

$$\langle p|\frac{\partial^2}{\partial r^2}|p'\rangle = 1/4\frac{\partial^2}{\partial r^2}\langle p|p'\rangle = \delta_{pp'}(-)^p\, 1/4\frac{\partial^2}{\partial r^2}\langle\alpha|\beta\rangle \ . \tag{V.20}$$

Because of the isotropy of the $|p\rangle$, it is clear that it is easiest to first split the Laplacian into its radial part $\frac{1}{r}\frac{\partial^2}{\partial r^2}r$ and angular part $-\vec{L}^2/(\hbar^2 r^2)$ and then to let

the two parts separately act on the product of the ket state and the wave function. If we expand the channel wave function $\phi_p(\vec{r}) = \phi_\alpha(\vec{r}) + (-)^p\phi_\beta(\vec{r})$ into partial waves,

$$\phi_p(\vec{r}) = \frac{1}{r}\sum_L a_L \chi_L^p(r) P_L(\cos\theta) \ , \tag{V.21}$$

where we used the azimuthal symmetry already, and the a_L are as yet unspecified complex constants, then the Schrödinger equation (V.6) becomes for the even and odd states:

$$\begin{aligned}\langle p|p\rangle \frac{d^2\chi_L^p}{dr^2} + 2\langle p|\frac{\partial}{\partial r}|p\rangle\frac{d\chi_L^p}{dr} + \langle p|\frac{\partial^2}{\partial r^2}|p\rangle\chi_L^p \\ - \frac{L(L+1)}{r^2}\langle p|p\rangle\chi_L^p + \frac{2m}{\hbar^2}\Big[(E-V_{12})\langle p|p\rangle - \langle p|U|p\rangle\Big]\chi_L^p = 0 \ .\end{aligned} \tag{V.22}$$

(V.22) holds for p both even and odd, but the two channels are not coupled. (V.22) is thus a single equation for each L, E, and p and no longer a system of coupled channels equations. The adiabatic approximation has the same equation as (V.22) without the second and third term, and after division by $\langle p|p\rangle$, this is just the usual one-channel partial wave Schrödinger equation.

The non-adiabatic equations conserve the flux

$$F_L = \frac{-i}{2k}\sum_p \langle p|p\rangle\Big[\chi_L^p\frac{d}{dr}(\chi_L^p)^* - (\chi_L^p)^*\frac{d}{dr}(\chi_L^p)\Big] \ , \tag{V.23}$$

expressed in units such that the incoming flux is unity. The adiabatic equations for the two-channel case also conserve a flux-like quantity, namely $\frac{-i}{2k}\sum_p[\chi_L^p\frac{d}{dr}(\chi_L^p)^* - (\chi_L^p)^*\frac{d}{dr}(\chi_L^p)]$.

In order to extract the fusion cross section from the partial wave integrations, we have to specify the a_L in (V.21) to provide the right boundary condition for a

scattering state; since we describe the even and odd states, there is an extra factor $2^{-1/2}$ when compared with the left, i.e. the incoming state, thus:

$$a_L = 2^{-\frac{3}{2}} \frac{1}{k}(2L+1)i^{L+1} \quad . \tag{V.24}$$

The fusion cross section thus becomes

$$\sigma_f = \frac{\pi}{2k^2} \sum_L (2L+1)F_L \quad . \tag{V.25}$$

We use the non-adiabatic "coupled" channels equations and the non-adiabatic form (V.23) for F_L.

V.4 Results

We present our results for the fusion cross section in Fig.23. Obviously, our model does not permit the calculation of inelastic excitations. The behavior for the elastic angular distribution is similar to that for $^{17}O+^{16}O$: For subbarrier energies, the Rutherford scattering dominates completely, and for higher energies the coherent addition of the transfer nuclear amplitude provides small oscillations about the curve of the simple one-channel (direct nuclear plus Coulomb) calculation. In Fig.24, we present an angular distribution at $E_{cm} = 12.7$ MeV together with data from Gelbke *et al.*[42] The agreement of the calculation with the data is even worse than for ^{17}O on ^{16}O, because of the simplicity of our transfer model and the high sensitivity to the exact size of the transfer formfactor.

The fusion cross section shows the right enhancement in the subbarrier region and reproduces the data quite well. However, the above-barrier region, where the fit should be good, causes problems. Surprisingly, the measured cross section for $^{18}O+^{16}O$ does not exceed that of $^{16}O+^{16}O$ and $^{17}O+^{16}O$ at these energies, as one

would expect from simple scaling. Thomas *et al.* state that they normalized their data to the above-barrier region in order to correct for systematic errors in the integration of the beam current and shifted the ^{18}O-^{16}O cross section up. Perhaps, the data should be shifted even more, in order to achieve congruence with the scaled ^{16}O-^{16}O and ^{17}O-^{17}O curves (if this is done systematically, however, the shifted points would agree with our calculation above the barrier, but would deviate from our points below the barrier). The experimental data show a certain "ditch" above the barrier, deviating from a smooth behavior. If this is significant and not just a statistical or experimental aberration, it would be a very interesting feature. Such a ditch would most likely not be produced by a large number of contributing channels, but more likely by the destructive interference of the dominant elastic channel with one single additional channel. Our calculation seems to rule out that the ground state transfer constitutes this extra channel. Also, from the semi-classical calculation, it is clear that Coulomb excitation at this energy does not provide enough strength for this process. The fusion cross section at the highest energies is affected relatively little by the channel coupling, so that the relative differences between ^{16}O, ^{17}O, and ^{18}O in our calculation come mainly from the effect of the additional neutrons on the diagonal potential. The bigger size of the heavier isotopes will push the barrier farther out, where the Coulomb force is weaker and will thus decrease the barrier height. In our model for ^{18}O, we overestimate the increase in nuclear size over ^{16}O, because we use the more loosely bound ^{17}O wave functions instead of the correct ^{18}O wave functions that are more tightly bound. This effect should lead to a slight overestimate of the cross section above the barrier, but not

to such an extent as the discrepancy between our calculation and the data. The ^{18}O diagonal potential, i. e., $V_{12}(r) + J_{5/2,\,5/2,0}(r)$, is plotted in Fig.9 together with the ^{16}O potential V_{12} for comparison.

Another calculation[42] attempts to model the ^{18}O+^{16}O enhancement by a coupled channels calculation that takes the inelastic excitation of the lowest 2^+ state, but no particle transfer into account. The result of the calculation is very similar to ours with good agreement below but overprediction above the barrier. Unfortunately, no results for the total inelastic cross section are presented that would allow comparison with the data and check the chosen strength in the inelastic channel. Also, the model does not take any Coulomb excitation into account; as we have shown, this is highly dubious for the lower energies.

In summary, our model reproduces the subbarrier enhancement down to the lowest energies, but has problems in the above-barrier domain, where the calculation, but not the data are proportional to the ^{16}O-^{16}O and ^{17}O-^{16}O curves. The data do not allow a decision, whether there is an interesting and surprising above-barrier structure in the fusion cross section.

CHAPTER VI

Conclusion

The subbarrier fusion cross sections for $^{17}O+^{16}O$ and $^{18}O+^{16}O$ show relatively little enhancement over that for $^{16}O+^{16}O$ when compared with isotope differences for heavier systems. We were able to reproduce these enhancements except for the very low energy region in the ^{17}O system. We found that it is necessary for internal consistency of the IWBC method in models that include transfer and hence non-orthogonal basis states to avoid the adiabatic approximation; however, the full equations are difficult to integrate numerically. It remains to be seen what the practical limitations in the number of channels are for the non-adiabatic equations, but without further approximations they do not seem to be the best tool for very complicated heavy systems.

As we see it, the lesson from the three studied oxygen systems is that a careful multi-channel calculation can reproduce the subbarrier fusion data to some extent, with the low energy behavior of the ^{17}O-^{16}O and the high energy behavior of the ^{18}O-^{16}O systems as limitations. We do not think that the low energy deviation could be remedied by an improvement in the description of the chosen single particle channels, but that a more complicated scheme that incorporates some kind of core excitation is necessary. The high energy deviation for ^{18}O remains puzzling. The advantage of the consistent incorporation of realistic inelastic and transfer channels allows for the calculation of various differential cross sections. A fine-tuning of

spectroscopic factors is necessary in order to accurately reproduce these features. We have not carefully done this in this work, but we believe that we have demonstrated the feasibility of doing so. The subbarrier reaction might thus become an important spectroscopic tool to check nuclear structure models. Above the barrier, DWBA calculations are adequate for this undertaking and because of their smaller numerical scope preferable, because, for example, for the least-square determination of a spectroscopic factor, a large number of full calculations has to be performed. However, below the barrier, a coupled channels calculation is necessary, because of the higher-order effects and non-linearity of the cross section in the coupling potentials. This way, the spectroscopic tool might be extended to testing in a different energy region. It would be desirable for the theoretician if the experimental fusion studies would include as many measurements of elastic, inelastic, and transfer cross sections as possible, in order that free parameters in the model can be clamped down or inadequacies of the model be singled out.

For the oxygen isotopes, the ^{18}O-^{18}O system is an interesting challenge in order to see how complicated reactions can be treated in a similar fashion to the other oxygen systems. This reaction might provide the bridge to the heavier systems from a computational point of view. For nuclear physics, the ^{17}O-^{17}O system is the most interesting of the remaining oxygen systems because of the positive Q-value of the one-neutron transfer.

REFERENCES

[1] A. O. Caldeira and A. J. Leggett, Ann. Phys. **149**, 374 (1983).

[2] L. C. Vaz *et al.*, in: *Proc. Int. Conf. on Nuclear Physics with Heavy Ions* (ed. P. Braun-Munzinger, Nucl. Sci. Res. Conf. Series **6**, Harwood Academic Publishers, Amsterdam, 1983, p.31). Proceedings, Cambridge, MA, 1984: *Fusion Reactions Below the Coulomb Barrier* (ed. S. Steadman, Lecture Notes in Physics **219**, Springer, 1985).

[3] D. Glas and U. Mosel, Phys. Rev. **C10**, 2620 (1974); Nucl. Phys **A237**, 485 (1975).

[4] P. E. Hodgson, *Nuclear Heavy-Ion Reactions* (Clarendon Press, Oxford, 1978).

[5] G. Gamow, Z. Phys. **51**, 204 (1928).

[6] N. Austern, *Direct Nuclear Reaction Theories* (Wiley-Interscience, New York, 1970).

[7] G. R. Satchler, *Direct Nuclear Reactions* (Oxford University Press, Oxford, 1983).

[8] P. G. Reinhard *et al.*, Phys. Rev. **C30**, 878 (1984).

[9] H. Feshbach, Ann. Phys. **5**, 357 (1958); Ann. Phys. **19**, 287 (1962).

[10] L. C. Vaz and J. M. Alexander, in: *Fusion Reactions Below the Coulomb Barrier* (ed. S. Steadman, Lecture Notes in Physics **219**, Springer, 1985, p. 288).

[11] R. G. Stokstad *et al.*, Phys. Rev. Lett. **41**, 465 (1978); Phys. Rev. **C21**, 2427 (1980).

[12] W. S. Freeman *et al.*, Phys. Rev. Lett. **50**, 1563 (1983).

[13] R. G. Stokstad *et al.*, Z. Phys. **A295**, 269 (1980).

[14] M. Beckerman *et al.*, Phys. Rev. Lett. **45**, 1472 (1980); Phys. Rev. **C23**, 1581 (1981); Phys. Rev. **C25**, 837 (1982).

[15] H. Al-Juwair *et al.*, Phys. Rev. **C30**, 1223 (1984).

[16] A. B. Balantekin, S. E. Koonin, and J. W. Negele, Phys. Rev. **C28**, 1565 (1983).

[17] E. C. Kemble, Phys. Rev. **48**, 549 (1935); D. L. Hill and J. A. Wheeler, Phys. Rev. **89**, 1102 (1953).

[18] H. Esbensen, Nucl. Phys. **A352**, 147 (1981).

[19] C. H. Dasso, S. Landowne, and A. Winther, Nucl. Phys. **A405**, 381 (1983).

[20] A. B. Balantekin and N. Takigawa, Ann. of Phys. **160**, 441 (1985).

[21] H. Spinka and H. Winkler, Nucl. Phys. **A233** 456 (1974).

[22] S.-C. Wu, Ph.D. Thesis, California Institute of Technology (unpublished, 1978); S.-C. Wu and C. A. Barnes, Nucl. Phys. **A422**, 373 (1984).

[23] G. Hulke, C. Rolfs, and H. P. Trautvetter, Z. Phys. **A297**, 161 (1980).

[24] J. Thomas *et al.*, Phys. Rev. **C31**, 1980 (1985).

[25] J. Thomas *et al.*, to be published in Phys. Rev. C (1986).

[26] C. A. Barnes, in: *Fusion Reactions Below the Coulomb Barrier* (ed. S. Steadman, Lecture Notes in Physics **219**, Springer, 1985, p. 70); in: *Essays in Nuclear Astrophysics*, (C. A. Barnes, D. D. Clayton, and D. N. Schramm, eds., Cambridge University Press, Cambridge, 1982, p.193).

[27] S. A. Woosley and T. A. Weaver, in: *Essays in Nuclear Astrophysics*, (C. A. Barnes, D. D. Clayton, and D. N. Schramm, eds., Cambridge University Press,

Cambridge, 1982, p.377).

[28] W. A. Fowler, G. R. Caughlan, and B. A. Zimmerman, Ann. Rev. Astron. Astrophys. **5**, 525 (1967).

[29] A. Messiah, *Quantum Mechanics*, (John Wiley & Sons, New York, 1958).

[30] P. R. Christensen and Z. E. Switkowski, Nucl. Phys. **A280**, 205 (1977).

[31] S. C. Pieper, M. J. Rhoades-Brown, and S. Landowne, Phys. Lett. **162B**, 43 (1985).

[32] D. A. Bromley, J. A. Kuehner, and E. Almqvist, Phys. Rev. **123**, 878 (1961).

[33] S. E. Koonin, *Computational Physics* (Benjamin/Cummings, Menlo Park, CA 1986).

[34] R. A. Broglia *et al.*, Phys. Reports **29**, 291 (1977).

[35] A. R. Edmonds, *Angular Momentum in Quantum Mechanics*, (Princeton University Press, 1957).

[36] G. Pollarolo, R. A. Broglia, and A. Winther, Nucl. Phys. **A406**, 369 (1983).

[37] M. Rhoades-Brown, M. H. Macfarlane, and S. C. Pieper, Phys. Rev. **C21**, 2417 (1980).

[38] M. D. Cooper, W. F. Hornyak, and P. G. Roos, Nucl. Phys. **A218**, 249 (1974).

[39] C. K. Gelbke *et al.*, Nucl. Phys. **A219**, 253 (1974).

[40] S. Burzynski *et al.*, Nucl. Phys. **A399**, 230 (1983).

[41] K. Alder *et al.*, Rev. Mod. Phys. **28**, 432 (1956).

[42] C. K. Gelbke *et al.*, Phys. Rev. Lett. **29**, 1683 (1972).

[43] J. Q. Wu, G. Bertsch, and A. B Balantekin, Oak Ridge National Laboratory preprint (1986).

Figure 1

Typical Coulomb (dashed line), nuclear (dot-dashed line) and total inter-nuclear (solid line) potential as a function of the inter-nuclear distance r. (In arbitrary units.)

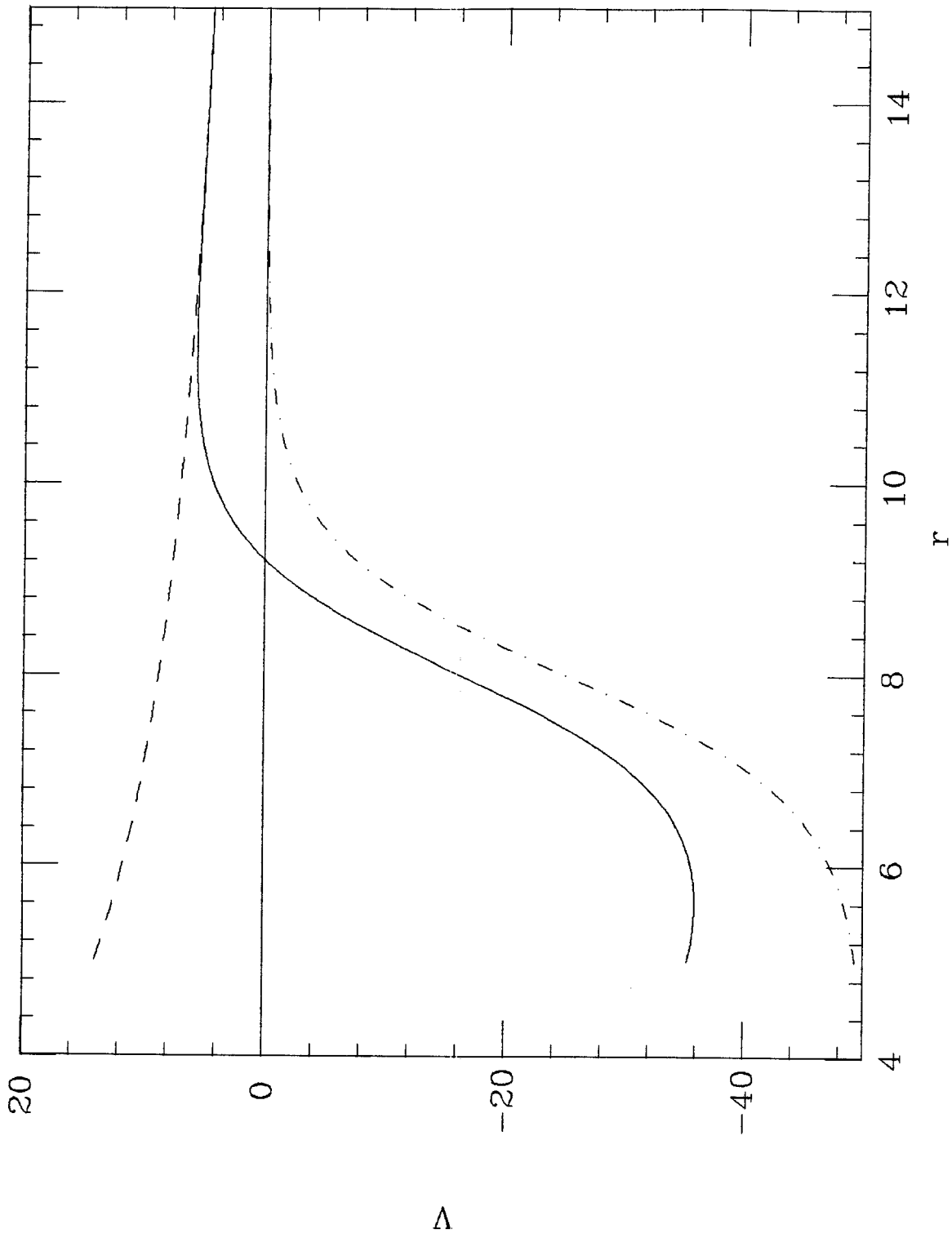
20
0
−20
−40
4
6
8
10
12
14
r
V

Figure 2

Above-barrier fusion cross section for $^{16}O+^{27}Al$ as a function of energy compared with the Glas-Mosel formulas (solid lines). σ_f rises linearly as a function of the inverse energy up to the point where $l_m = l_c$ ((II.4) with a negative V_c) and then falls linearly according to (II.3). Also plotted are some total reaction cross section values. (From Ref.[4].)

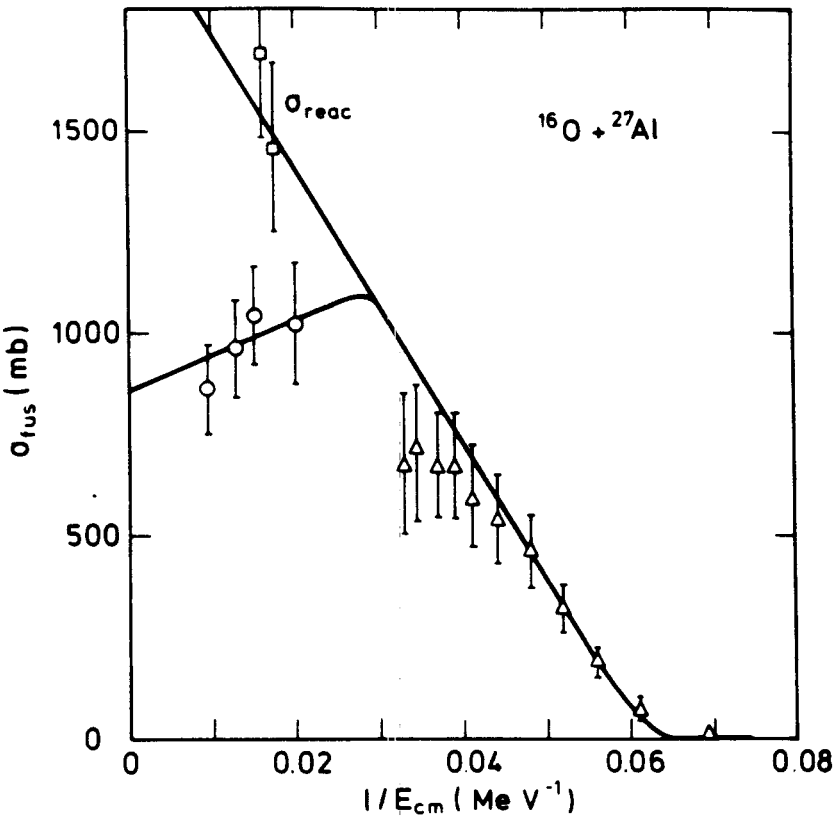
σ_{reac}
$^{16}O + ^{27}Al$
1500
1000
500
0
σ_{fus} (mb)
0
0.02
0.04
0.06
0.08
$1/E_{cm}$ (Me V^{-1})

Figure 3

Measured subbarrier fusion cross section for ^{58}Ni+^{58}Ni compared to the results of a one-dimensional calculation. (From Ref.[14].)

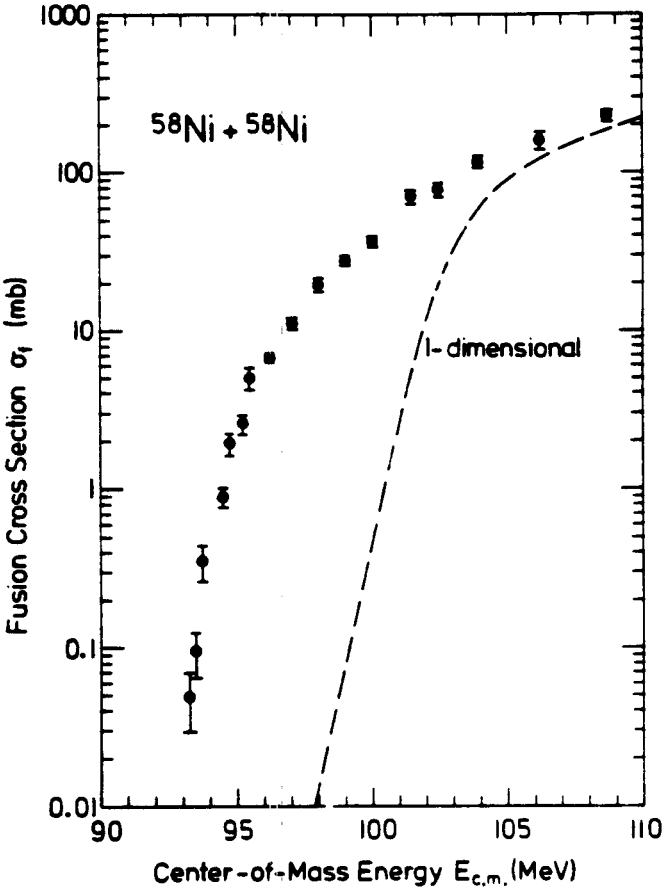
1000
100
10
1
0.1
0.01
90
95
100
105
110
$^{58}Ni + ^{58}Ni$
1-dimensional
Fusion Cross Section σ_f (mb)
Center-of-Mass Energy $E_{c.m.}$ (MeV)

Figure 4

Transmission probabilities in the Dasso, Landowne, Winther model. (a) Uncoupled system, classical (solid line) and quantum mechanical result (dashed line). (b) Same for coupled system. (c) Comparison of (a) (dashed) and (b) (solid). The quantum mechanical curves are schematic and not the result of an actual computation.

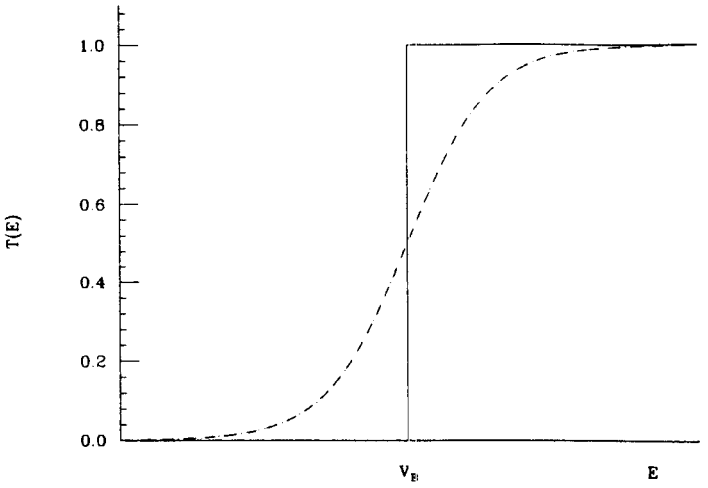
T(E)
1.0
0.8
0.6
0.4
0.2
0.0
V_B
E

(a)

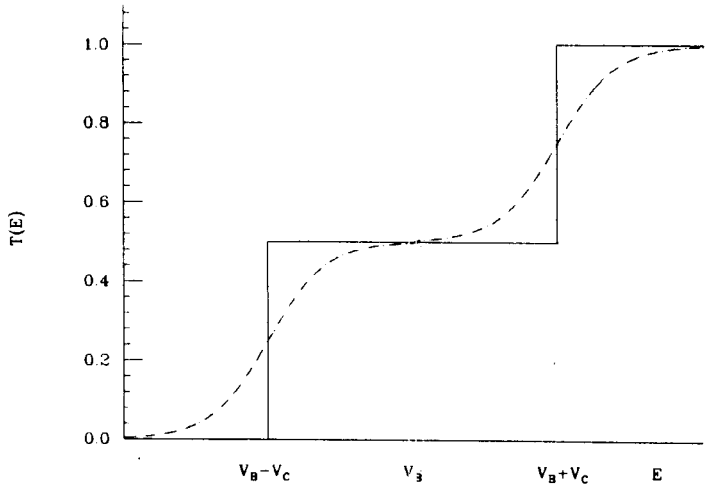
T(E)
1.0
0.8
0.6
0.4
0.2
0.0
V_B-V_C
V_B
V_B+V_C
E

(b)

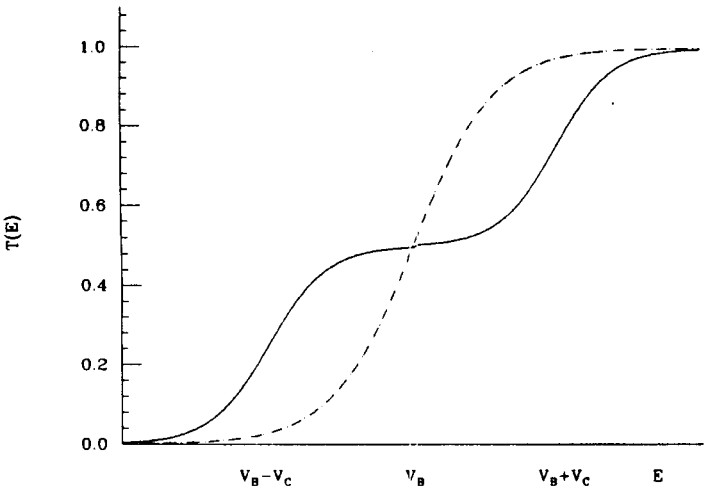
T(E)
1.0
0.8
0.6
0.4
0.2
0.0
V_B-V_C
V_B
V_B+V_C
E

(c)

Figure 5

Energy levels of ^{17}O and ^{18}O with decay thresholds into ^{16}O and neutron(s) as zero energy. Additional bound states and resonances of ^{18}O above the second 0^+ state are omitted. (All energies in MeV.)

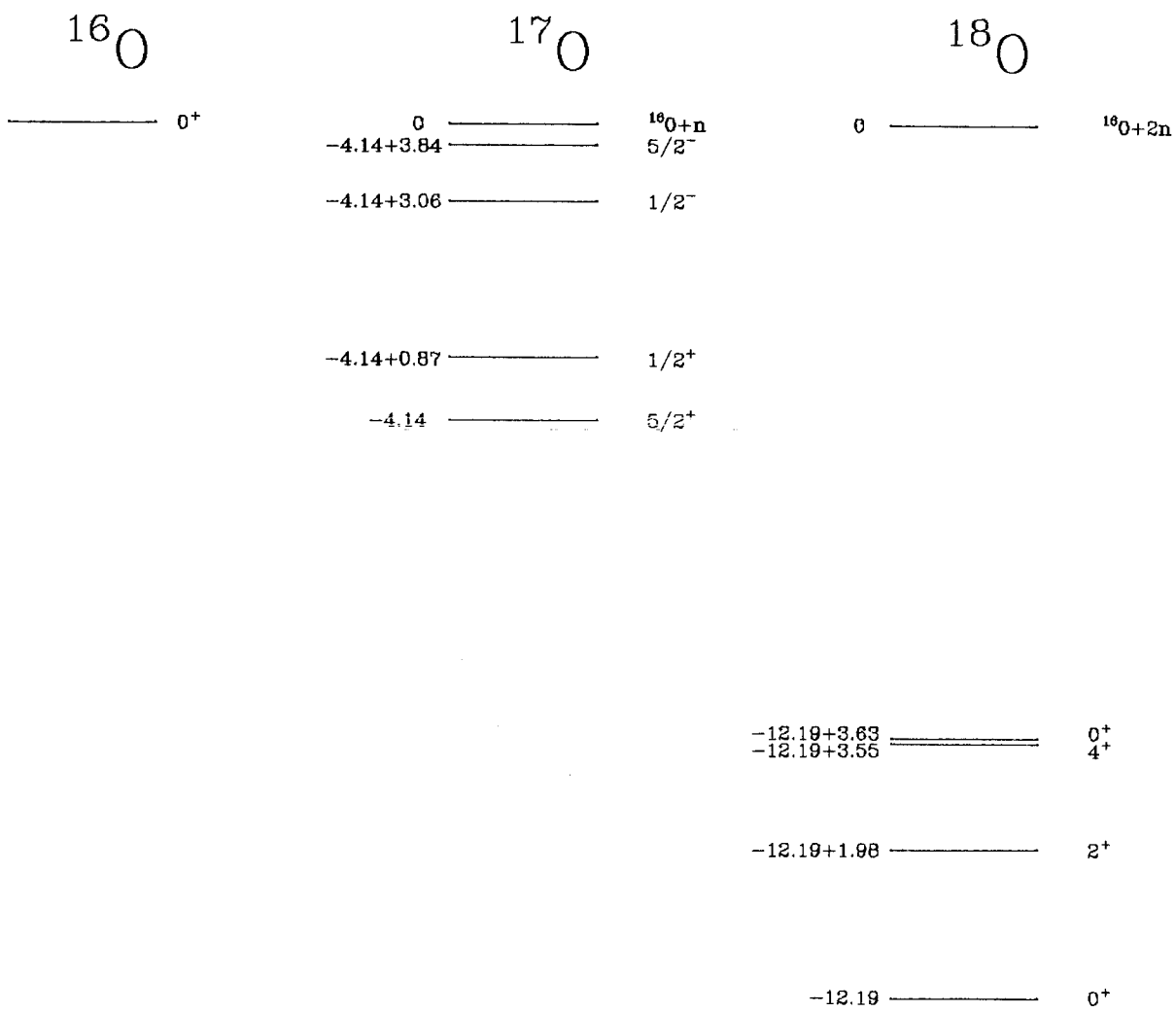
16O
0+
17O
0
16O+n
-4.14+3.84
5/2-
-4.14+3.06
1/2-
-4.14+0.87
1/2+
-4.14
5/2+
18O
0
16O+2n
-12.19+3.63
-12.19+3.55
0+
4+
-12.19+1.98
2+
-12.19
0+

Figure 6

Complete results from Thomas *et al.* for fusion and total inelastic cross sections for the treated oxygen systems. (From Ref. [25].)

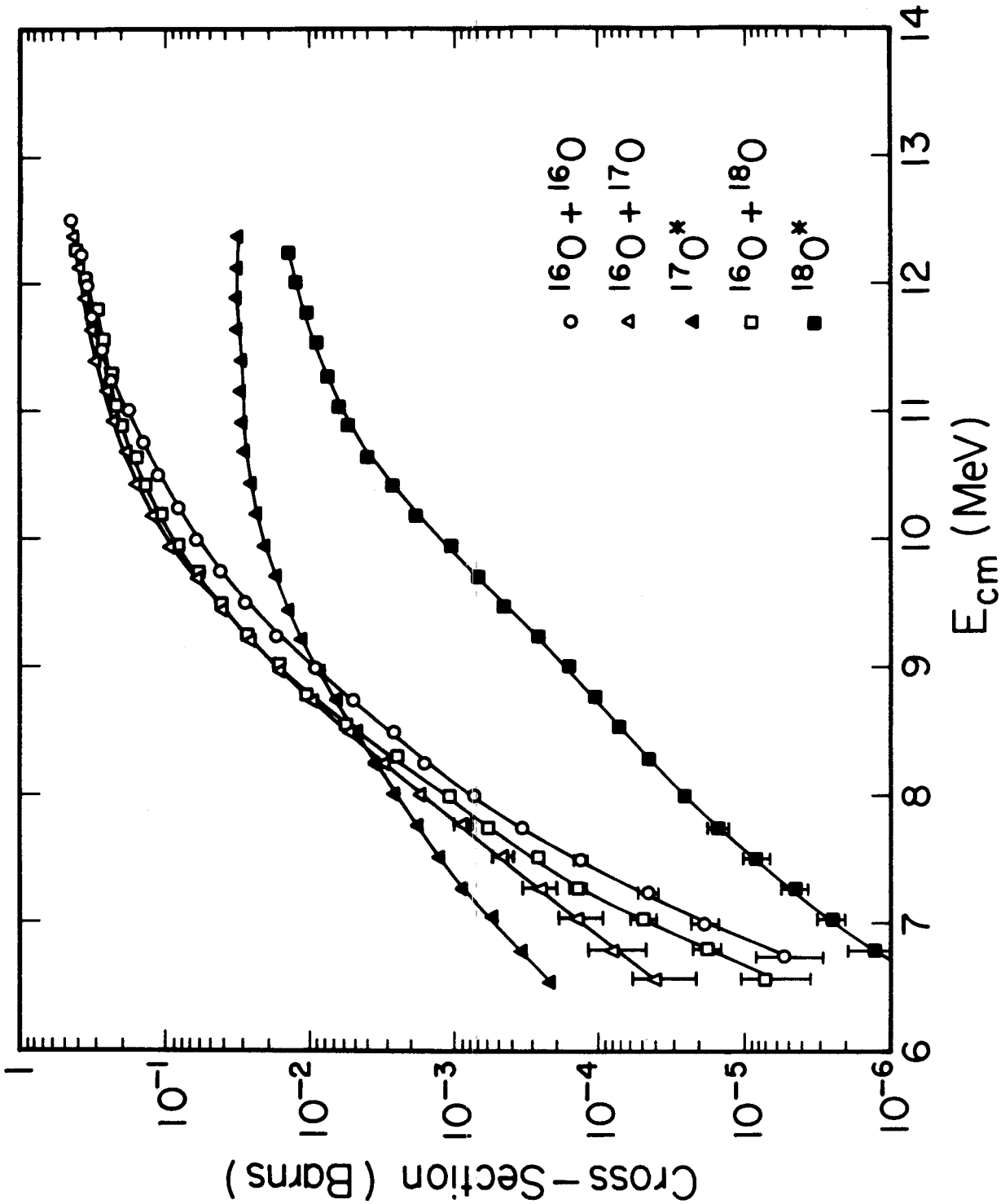
Cross-Section (Barns)
1
10^{-1}
10^{-2}
10^{-3}
10^{-4}
10^{-5}
10^{-6}
6
7
8
9
10
11
12
13
14
E_{cm} (MeV)
$^{16}O + ^{16}O$
$^{16}O + ^{17}O$
$^{17}O^*$
$^{16}O + ^{18}O$
$^{18}O^*$

Figure 7

Effective potential barriers from the BKN inversion of the fusion cross sections measured by Thomas *et al.*. (From Ref.[25].)

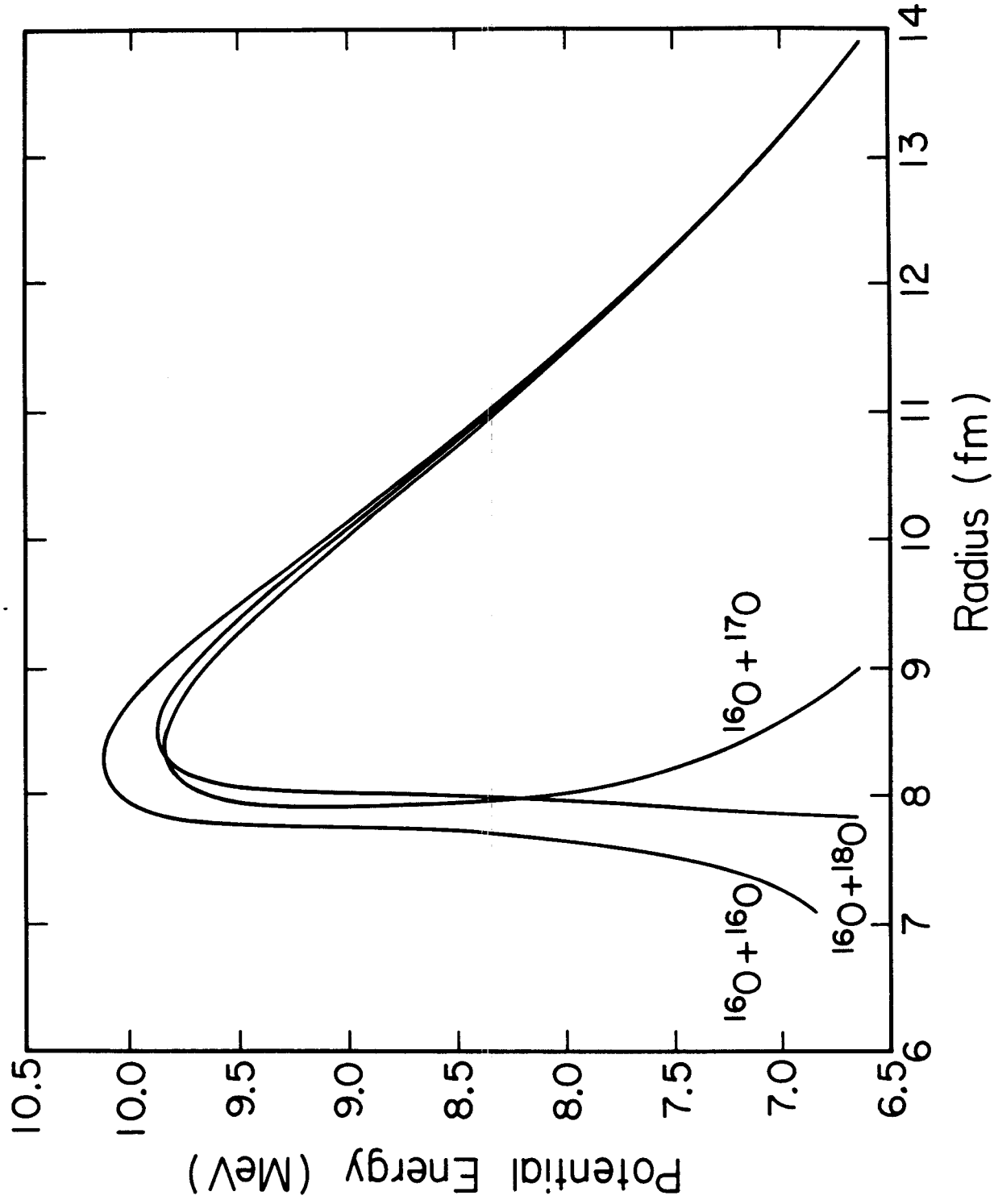
Potential Energy (MeV)
Radius (fm)
10.5
10.0
9.5
9.0
8.5
8.0
7.5
7.0
6.5
6
7
8
9
10
11
12
13
14
$^{16}O+^{16}O$
$^{16}O+^{18}O$
$^{16}O+^{17}O$

Figure 8

Measured astrophysical S-factor from Thomas *et al.* compared to the results of the IWBC calculation with Thomas's potential. The astrophysically important energy region extends down to about 3 MeV.

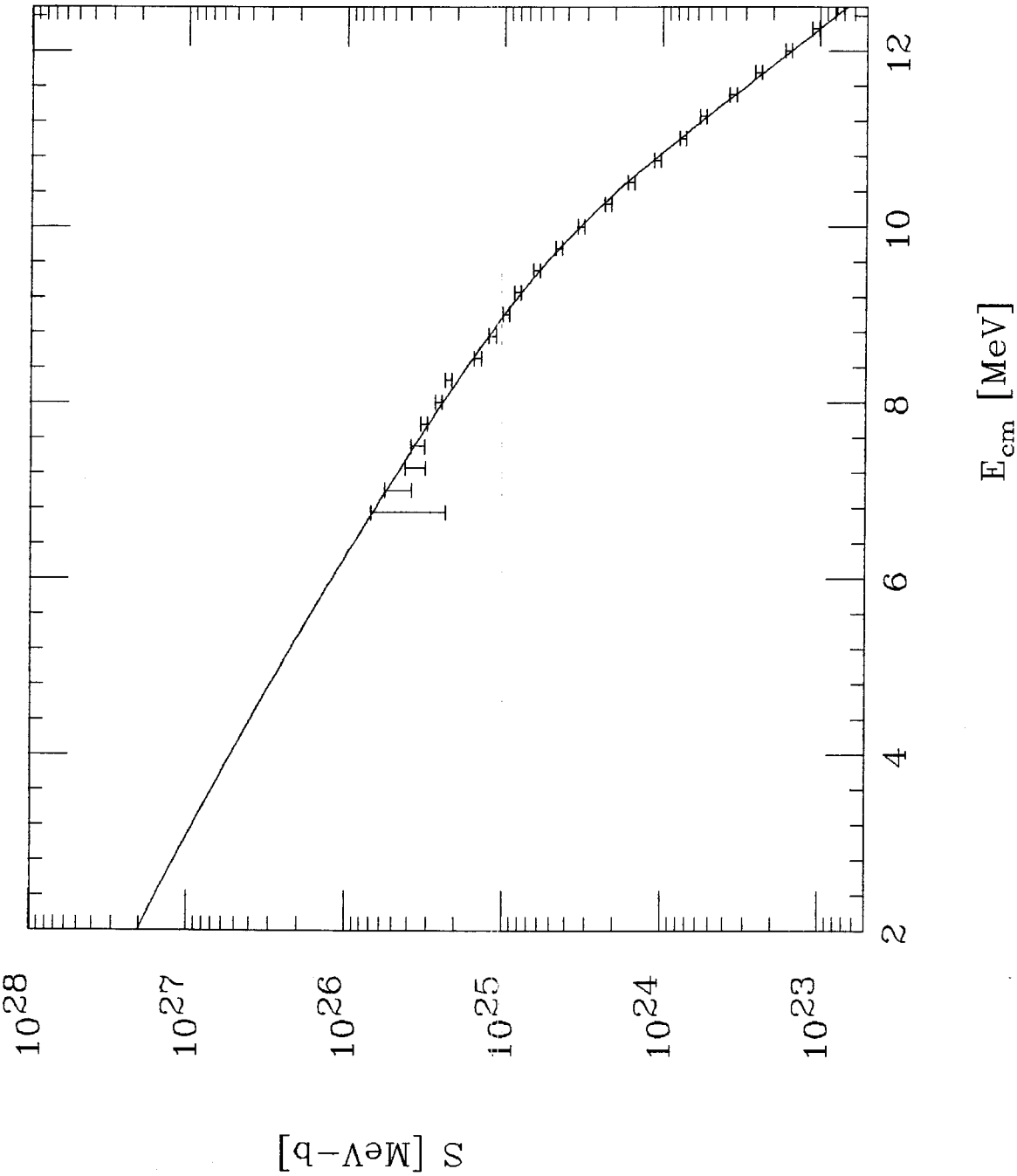
S [MeV-b]
10^{28}
10^{27}
10^{26}
10^{25}
10^{24}
10^{23}
2
4
6
8
10
12
E_{cm} [MeV]

Figure 9

Diagonal potential for $^{18}O+^{16}O$ (solid line) and $^{16}O+^{16}O$ (dashed line) as a function of the inter-nuclear distance r. The diagonal $^{18}O+^{16}O$ potential is that of $^{16}O+^{16}O$ plus the term $J_{5/2,5/2,0}(r)$.

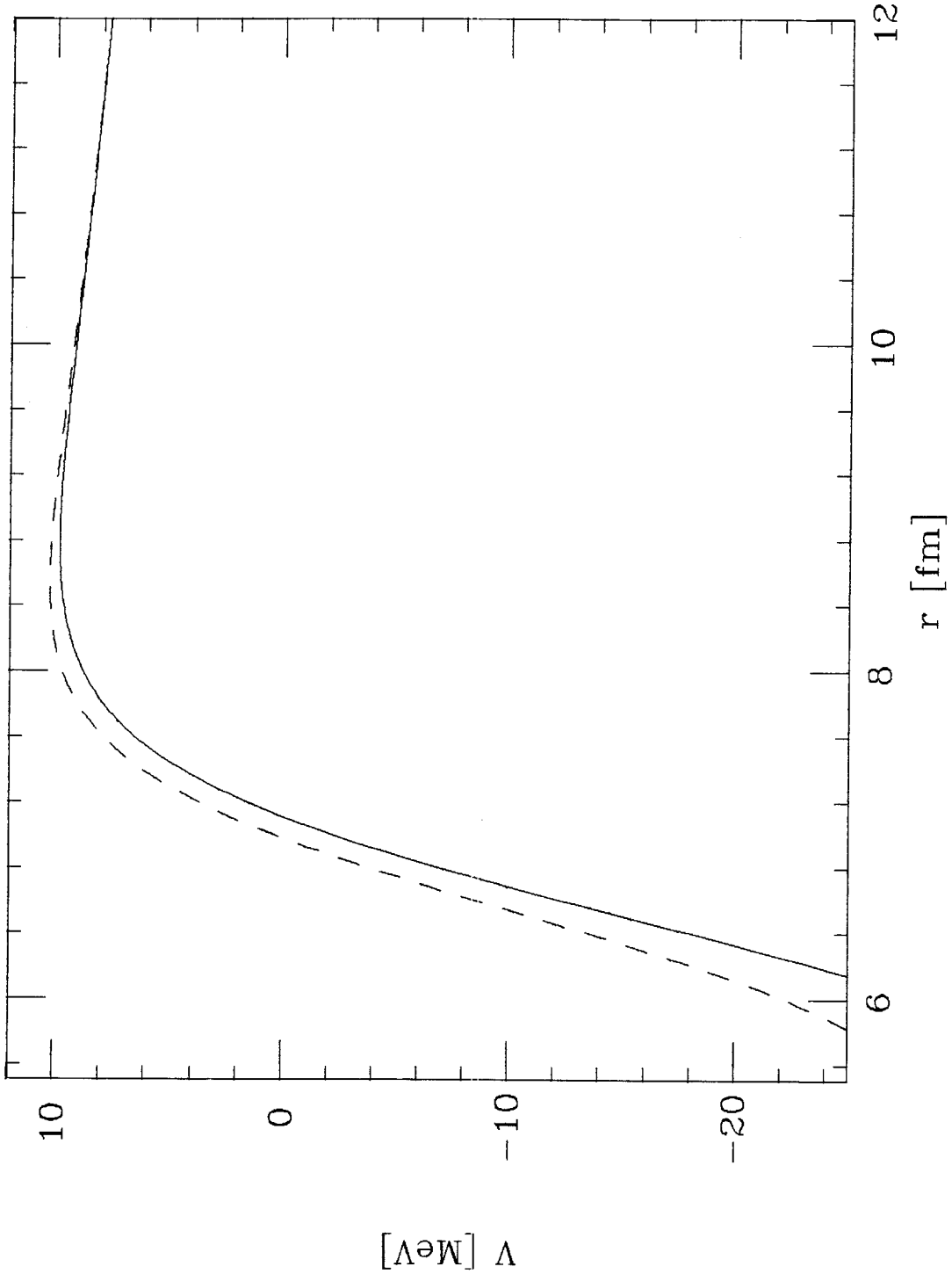
V [MeV]
10
0
−10
−20
6
8
10
12
r [fm]

Figure 10

Calculated fusion cross section for $^{16}O+^{16}O$ and data by Thomas *et al.*.

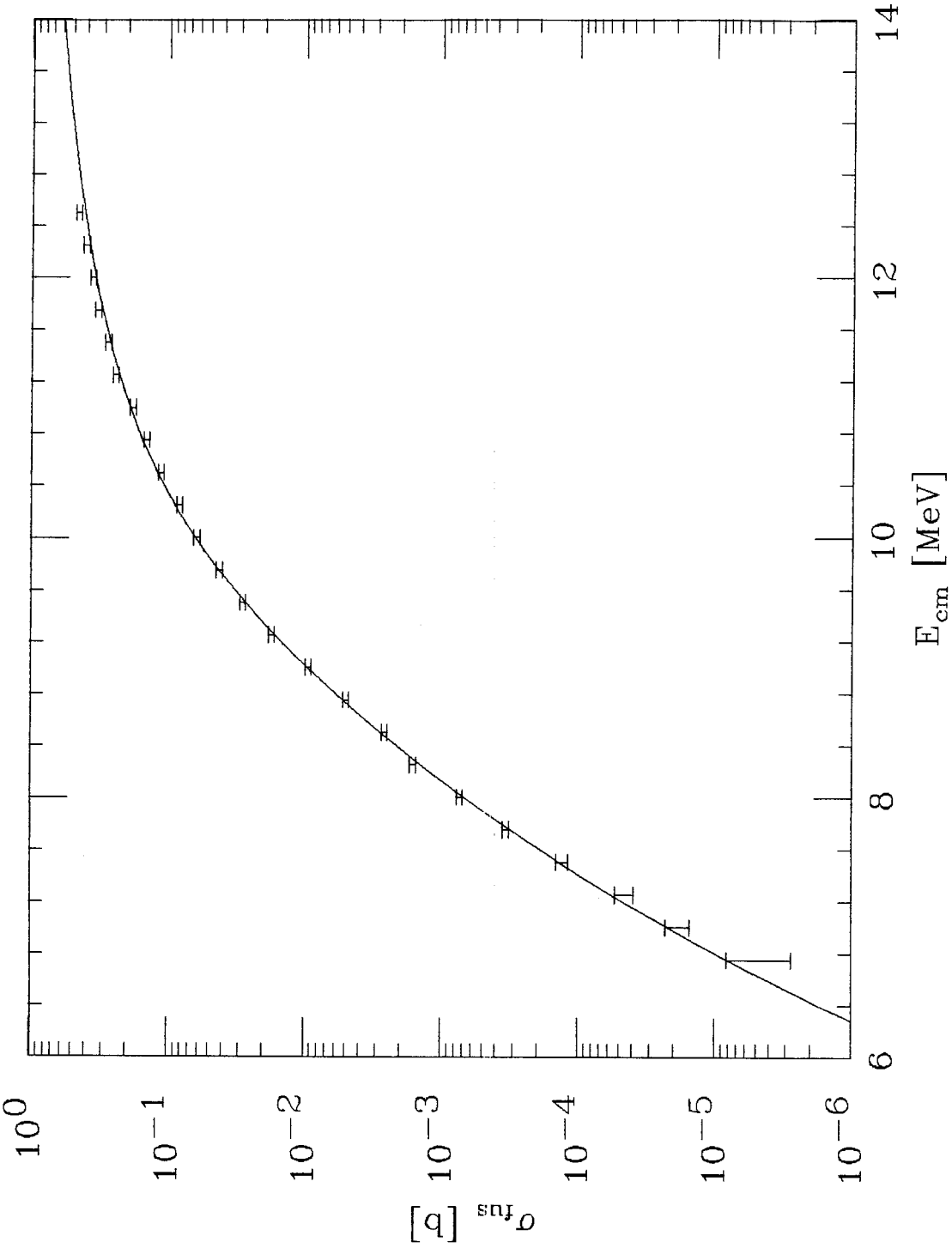
10^0
10^{-1}
10^{-2}
10^{-3}
10^{-4}
10^{-5}
10^{-6}
σ_{fus} [b]
6
8
10
12
14
E_{cm} [MeV]

Figure 11

Calculated elastic differential cross section at 90° for $^{16}O+^{16}O$ and data by Spinka and Winkler. Plotted is the cross section divided by the symmetric Rutherford cross section.

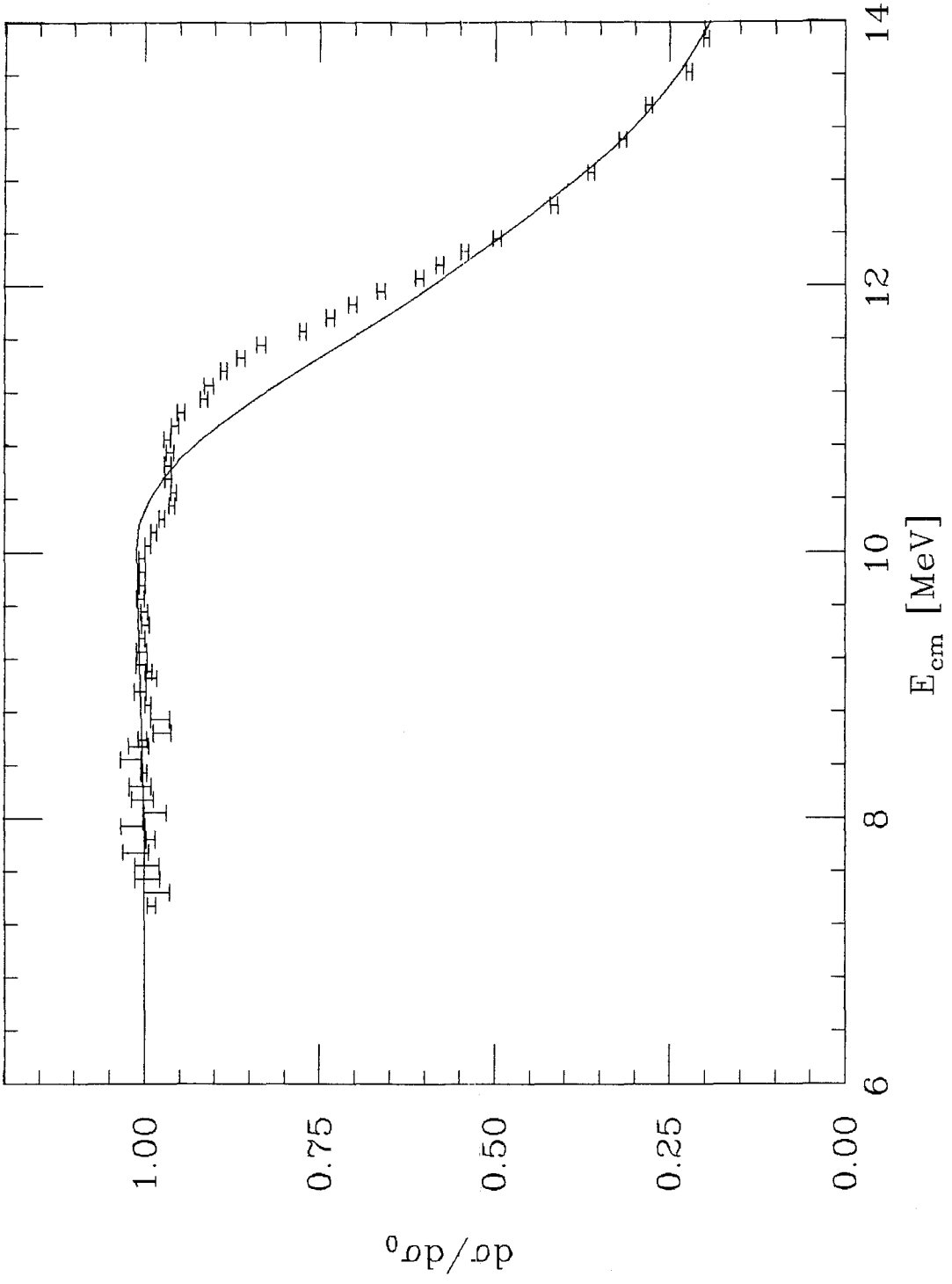
1.00
0.75
0.50
0.25
0.00
dσ/dσ0
6
8
10
12
14
Ecm [MeV]

Figure 12

$^{16}O+^{16}O$ elastic angular distribution at $E_{cm} = 13$ MeV and data from Bromley *et al.*. The data points were read off a plot in Ref. [32], slight deviations from there actual locations are possible.

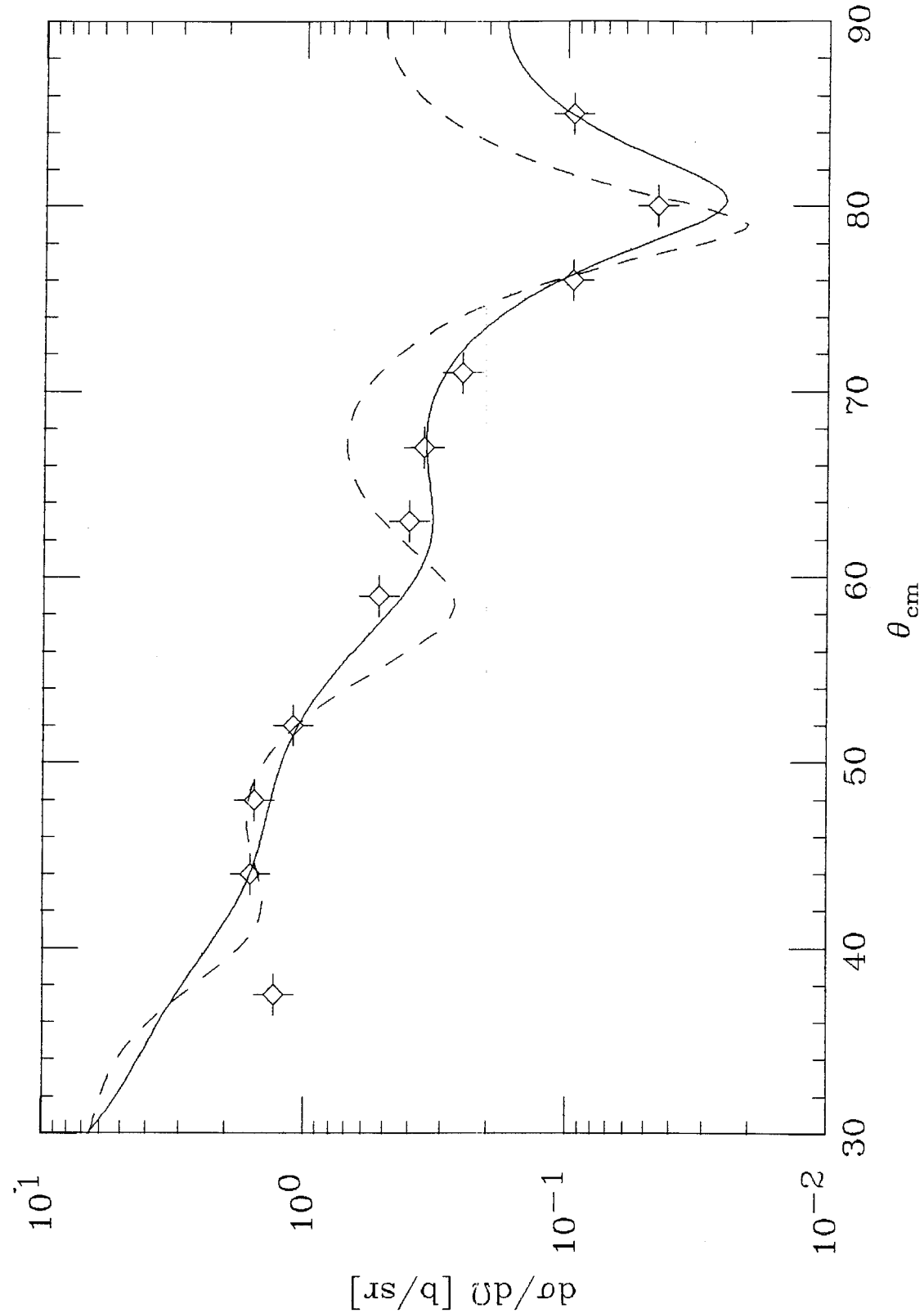
10^1
10^0
10^{-1}
10^{-2}
$d\sigma/d\Omega$ [b/sr]
30
40
50
60
70
80
90
θ_{cm}

Figure 13

Coordinates for the $^{17}O+^{16}O$ model. "1" and "2" refer to the two ^{16}O cores and "n" refers to the extra neutron.

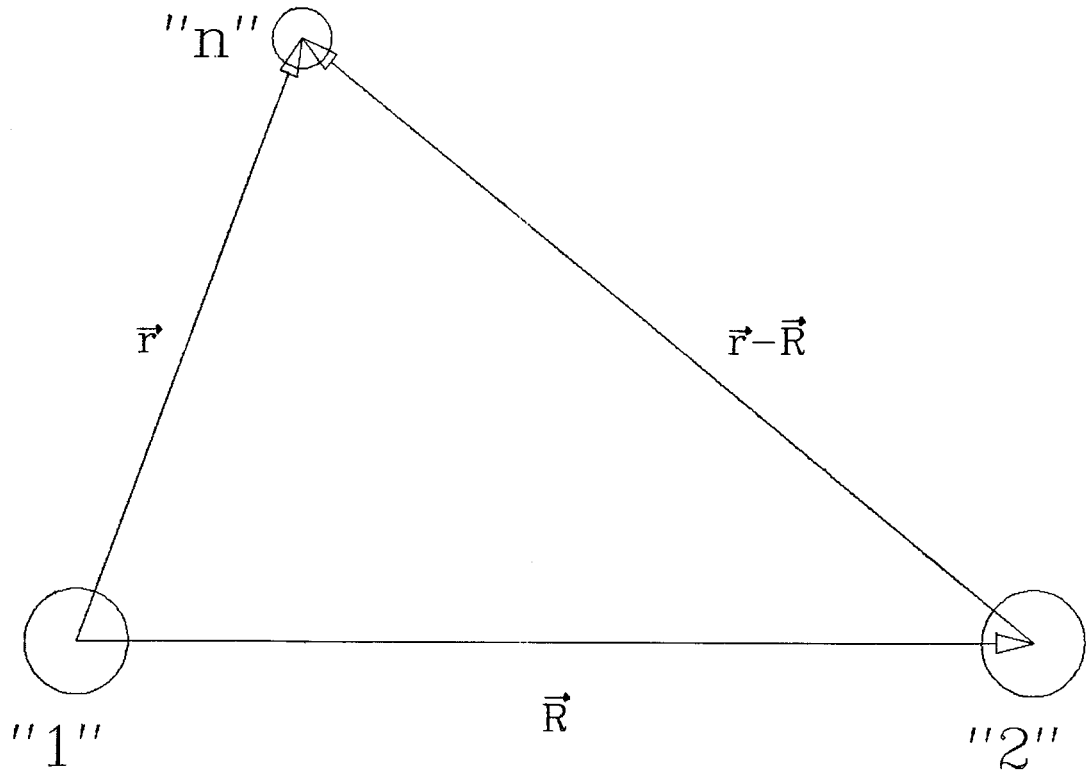
"n"
$\vec{r}$
$\vec{r}-\vec{R}$
"1"
$\vec{R}$
"2"

Figure 14

^{16}O-n potential (and single particle potential in ^{17}O) as a function of the core-neutron separation r.

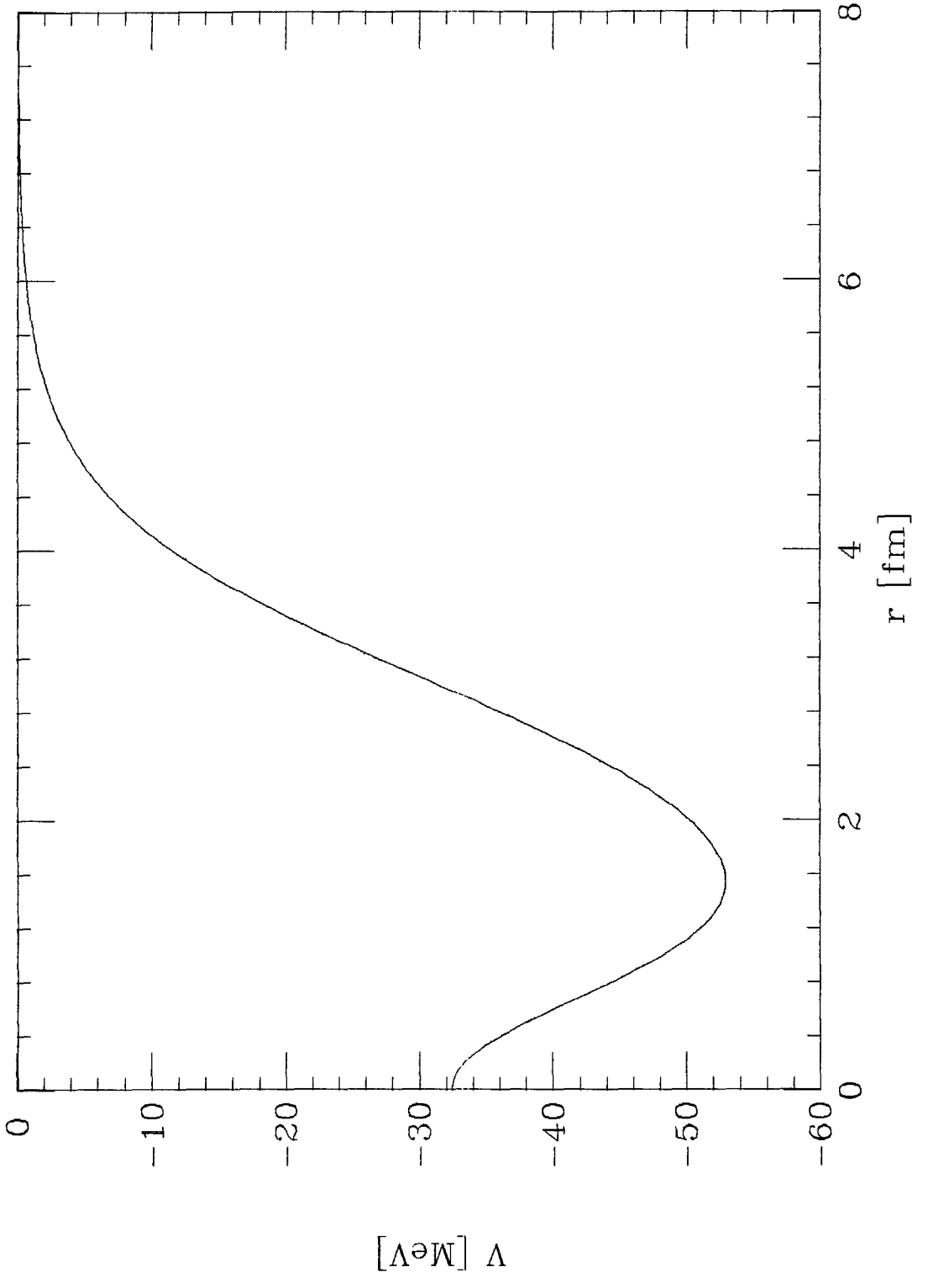
V [MeV]
0
-10
-20
-30
-40
-50
-60
0
2
4
6
8
r [fm]

Figure 15

Integral $J_{a,b,c}(r)$ for the inelastic formfactor of the $^{17}O+^{16}O$ reaction given by (IV.51). The different lines correspond to different index sets: $\{\frac{1}{2},\frac{1}{2},0\}$ solid; $\{\frac{5}{2},\frac{1}{2},2\}$ widely spaced dots; $\{\frac{5}{2},\frac{5}{2},0\}$ dashes; $\{\frac{5}{2},\frac{5}{2},2\}$ dot-dashes; $\{\frac{5}{2},\frac{5}{2},4\}$ narrowly spaced dots. (J in MeV.)

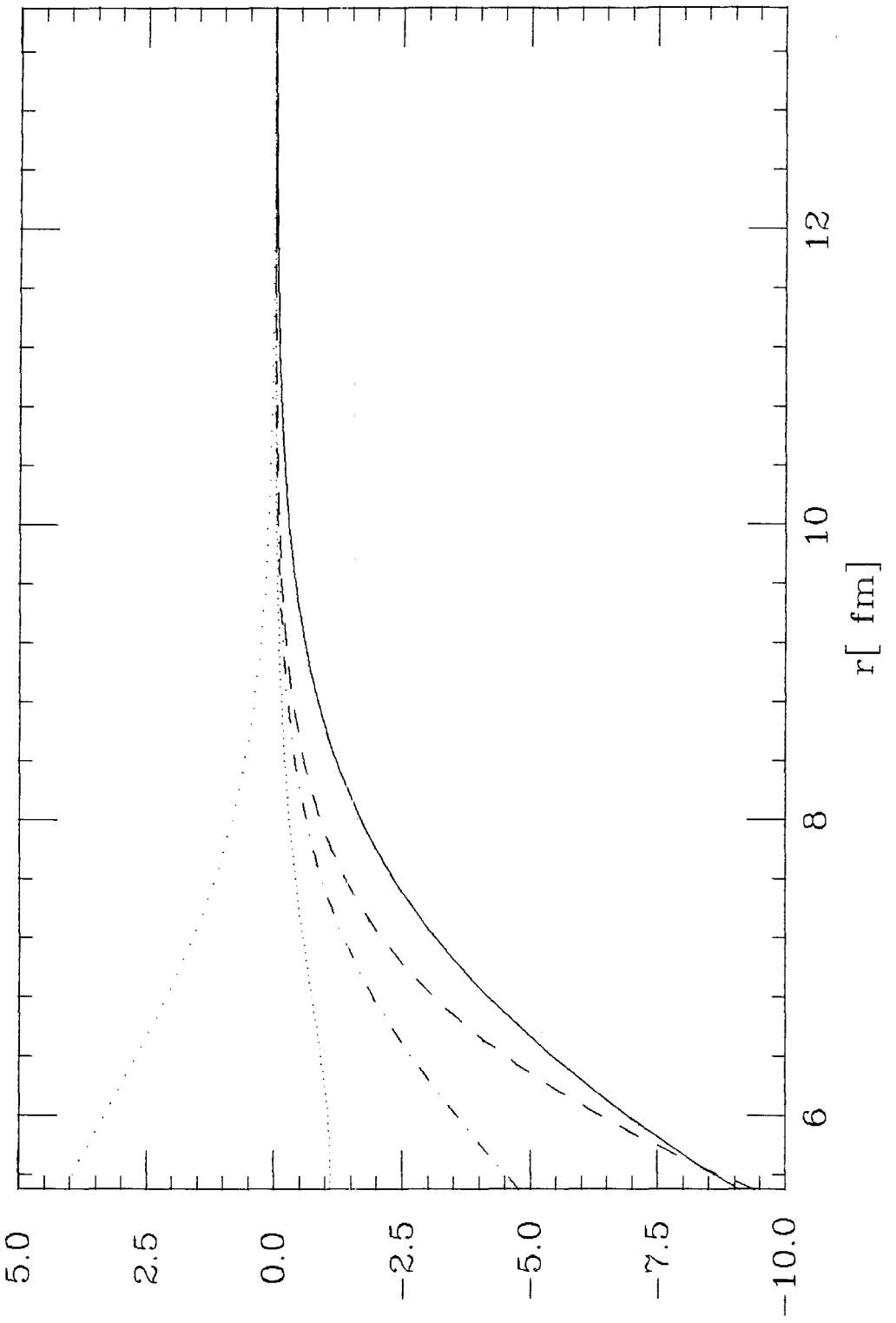
5.0
2.5
0.0
−2.5
−5.0
−7.5
−10.0
6
8
10
12
r[fm]

Figure 16

Integral $\mathcal{I}^{(1)}_{a,b,c}(r)$ for the overlap formfactor of the $^{17}O+^{16}O$ reaction given by (IV.69). The different lines correspond to different index sets: $\{\frac{1}{2},\frac{1}{2},0\}$ solid; $\{\frac{5}{2},\frac{1}{2},2\}$ widely spaced dots; $\{\frac{5}{2},\frac{5}{2},0\}$ dashes; $\{\frac{5}{2},\frac{5}{2},2\}$ dot-dashes; $\{\frac{5}{2},\frac{5}{2},4\}$ narrowly spaced dots. ($\mathcal{I}^{(1)}$ is dimensionless.)

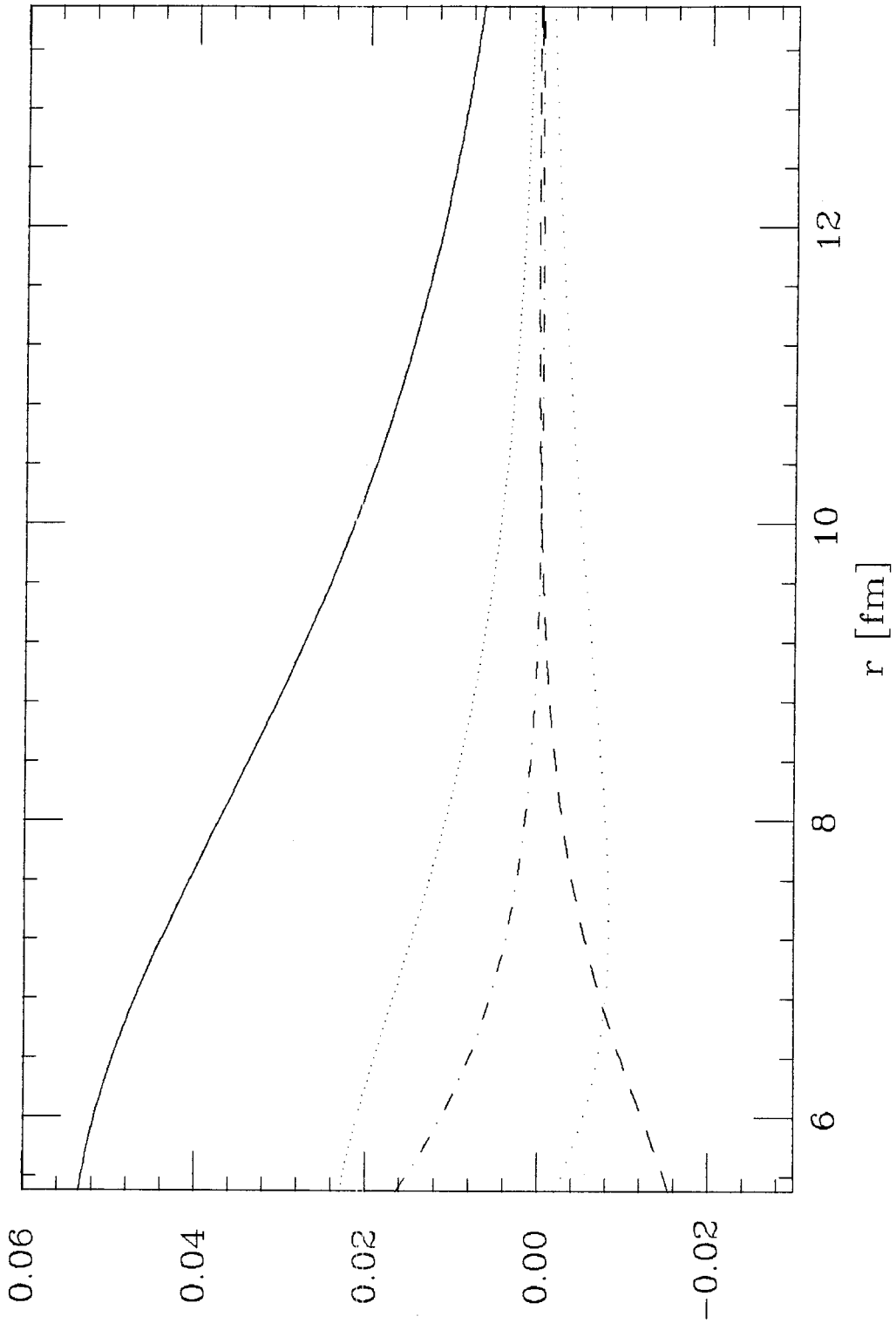
0.06
0.04
0.02
0.00
−0.02
6
8
10
12
r [fm]

Figure 17

Integral $I^{(v)}_{a,b,c}(r)$ for the inelastic formfactor of the $^{17}O+^{16}O$ reaction given by (IV.69). The different lines correspond to different index sets: $\{\frac{1}{2},\frac{1}{2},0\}$ solid (negative values); $\{\frac{5}{2},\frac{1}{2},2\}$ widely spaced dots; $\{\frac{1}{2},\frac{5}{2},2\}$ solid (positive values); $\{\frac{5}{2},\frac{5}{2},0\}$ dashes; $\{\frac{5}{2},\frac{5}{2},2\}$ dot-dashes; $\{\frac{5}{2},\frac{5}{2},4\}$ narrowly spaced dots. ($I^{(v)}$ in MeV.)

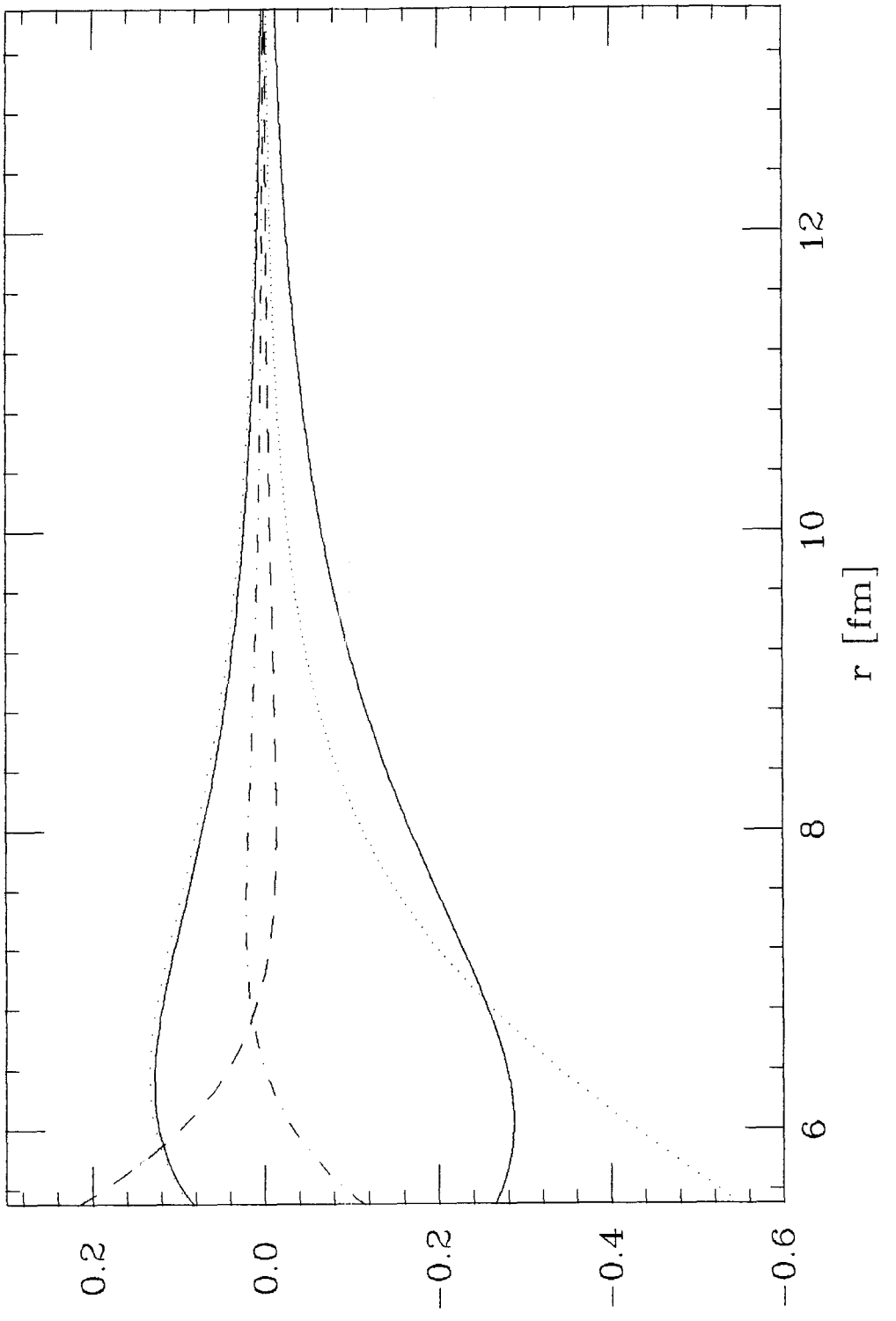
0.2
0.0
−0.2
−0.4
−0.6
6
8
10
12
r [fm]

Figure 18

Calculated fusion cross section for $^{17}O+^{16}O$ as a function of the center-of-mass energy and data by Thomas *et al.* with the same scale as Fig.10 (solid line). The dashed curve is the fusion cross section for $^{16}O+^{16}O$.

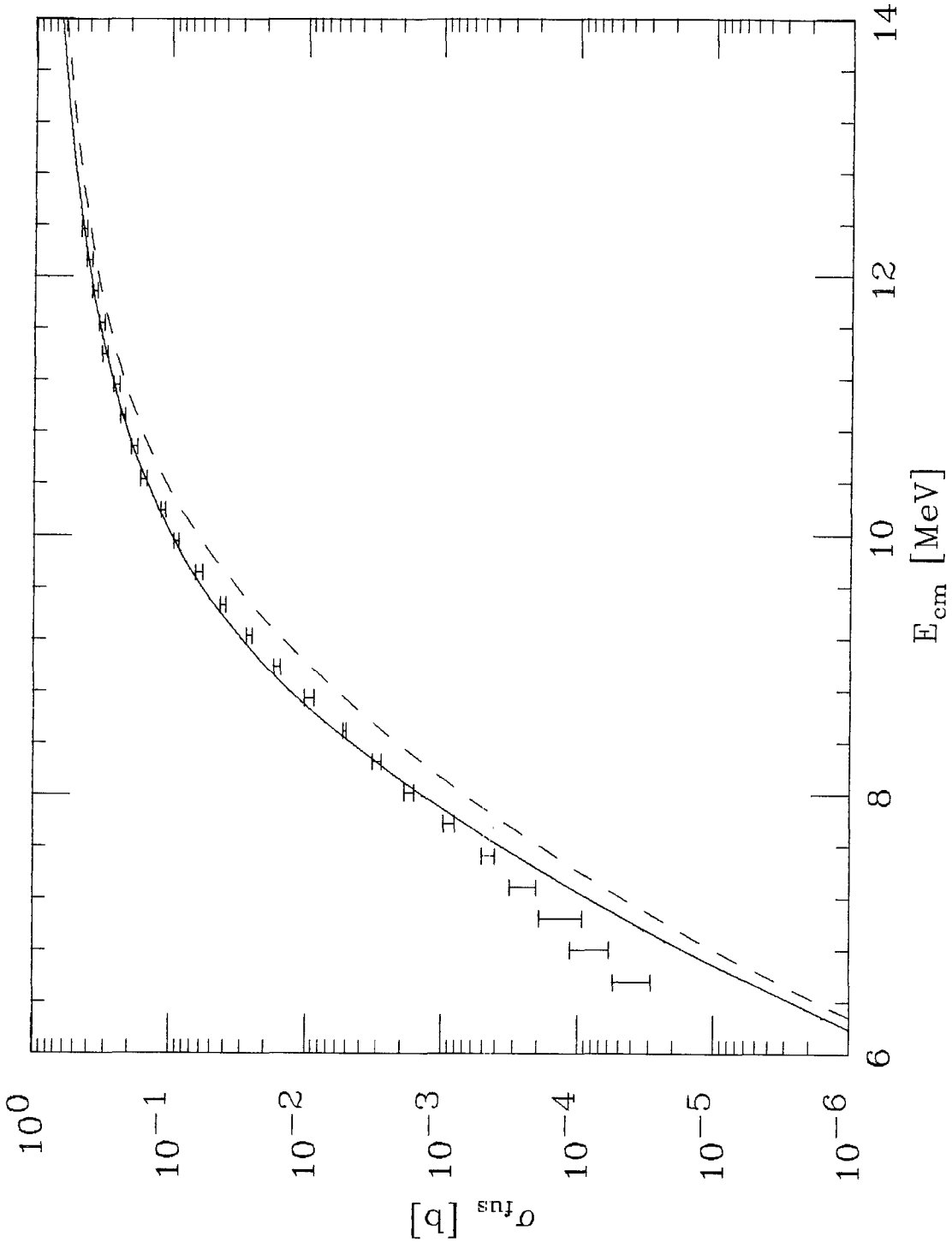
10^0
10^{-1}
10^{-2}
10^{-3}
10^{-4}
10^{-5}
10^{-6}
σ_{fus} [b]
6
8
10
12
14
E_{cm} [MeV]

Figure 19

Total nuclear inelastic cross section for $^{17}O+^{16}O$ (solid line), data by Thomas *et al.*, and semiclassical Coulomb excitation cross section (dashed line) with the same scale as Fig.10.

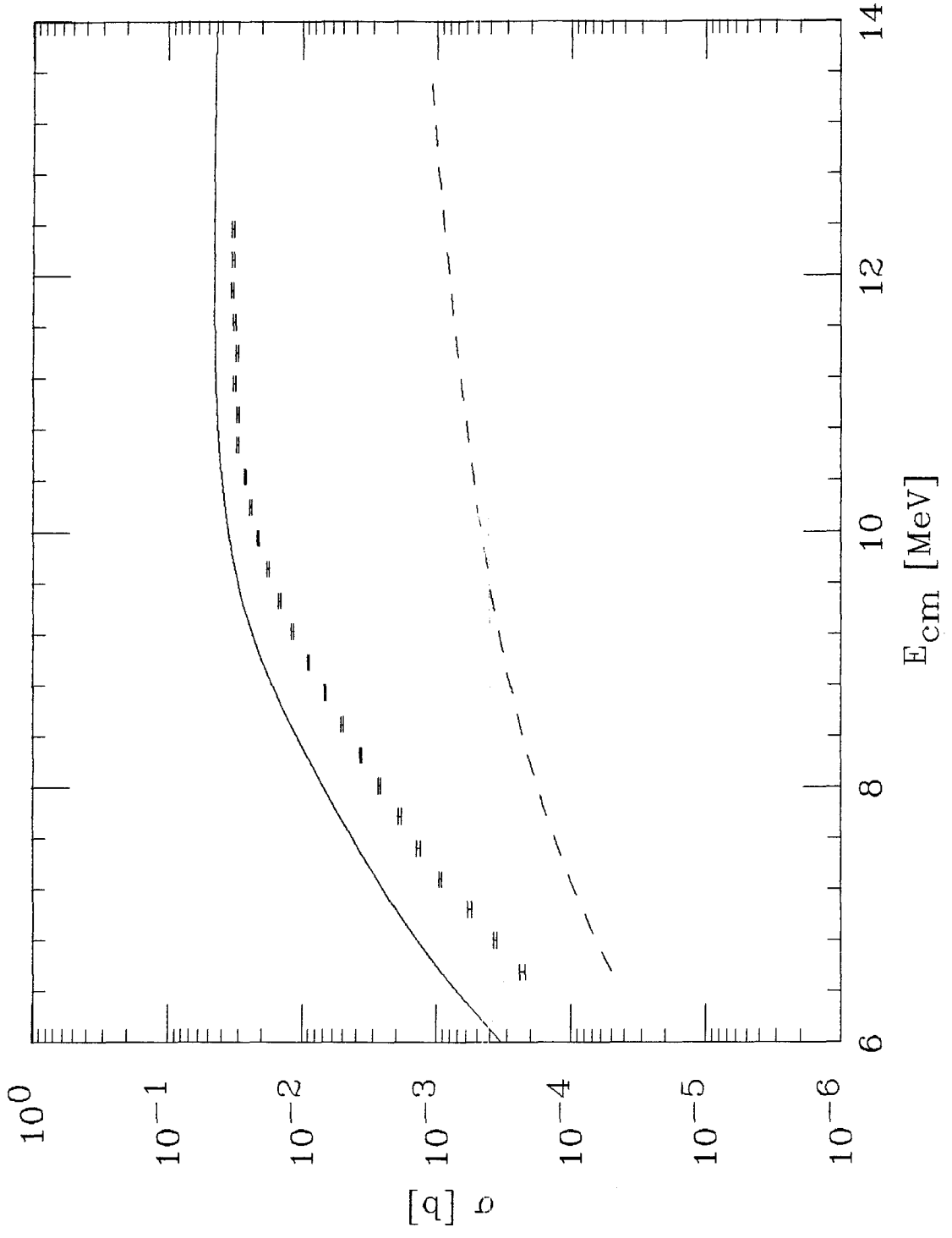
σ [b]
10^0
10^{-1}
10^{-2}
10^{-3}
10^{-4}
10^{-5}
10^{-6}
6
8
10
12
14
E_{cm} [MeV]

Figure 20

Calculated inelastic differential cross section for $^{17}O+^{16}O$ at $E_{cm} = 11.3$ MeV and data by Gelbke *et al.*. The dashed curve is the result of a calculation without spectroscopic factors, the solid curve is scaled by the product $S_{1/2}S_{5/2} = 0.7$. The data points were read off a plot in Ref.[39], slight deviations from there actual locations are possible.

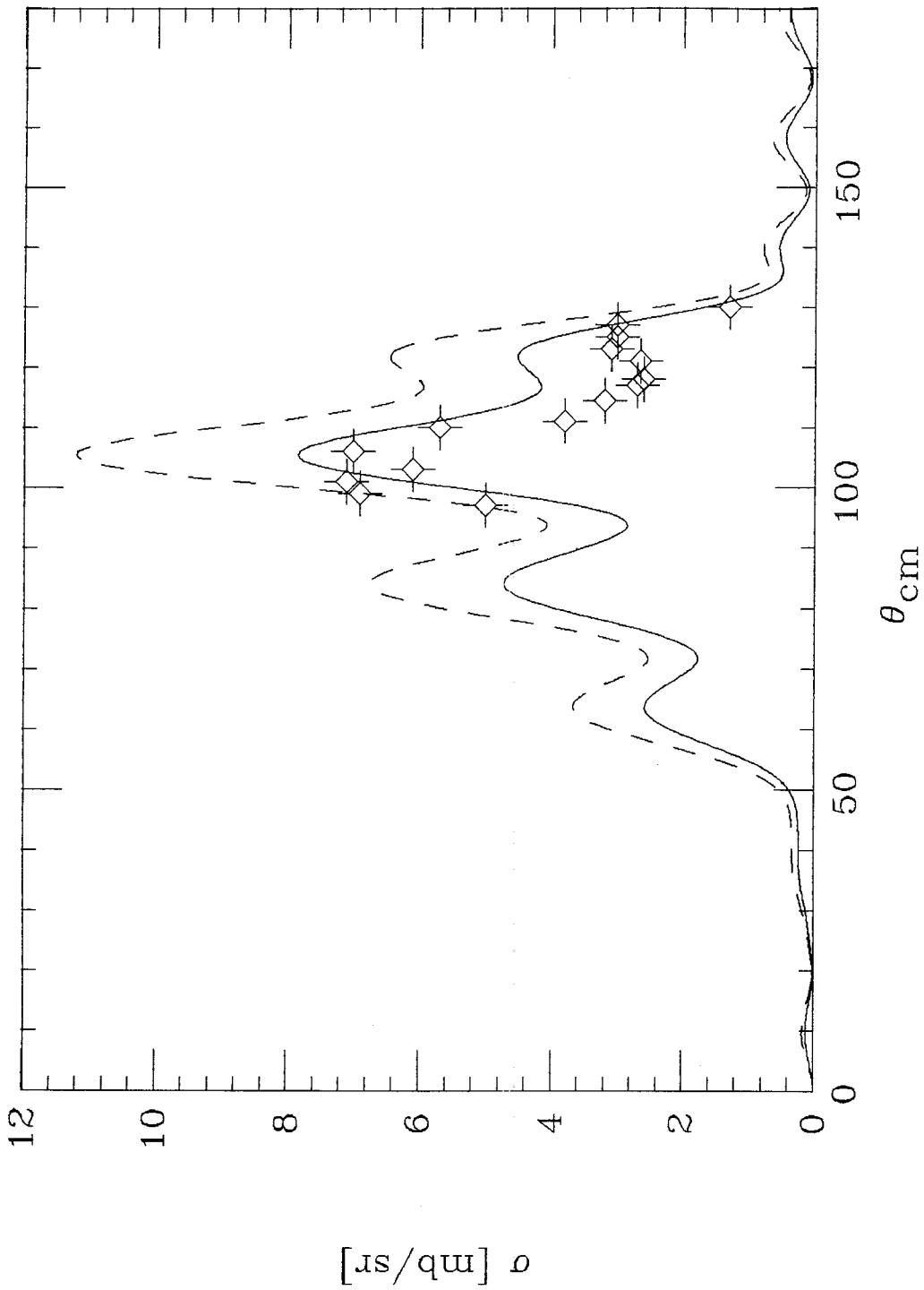
12
10
8
6
4
2
0
0
50
100
150
θ_{cm}
σ [mb/sr]

Figure 21

Calculated elastic differential cross section (solid curve) for $^{17}O+^{16}O$ at E_{cm} = 10.67 MeV and data by Burzynski *et al.*. The data points were read off a plot in Ref.[40], slight deviations from there actual locations are possible. The dashed curve is the result of a one-channel calculation with the $^{16}O+^{16}O$ potential. Plotted are the cross sections divided by the Rutherford cross section.

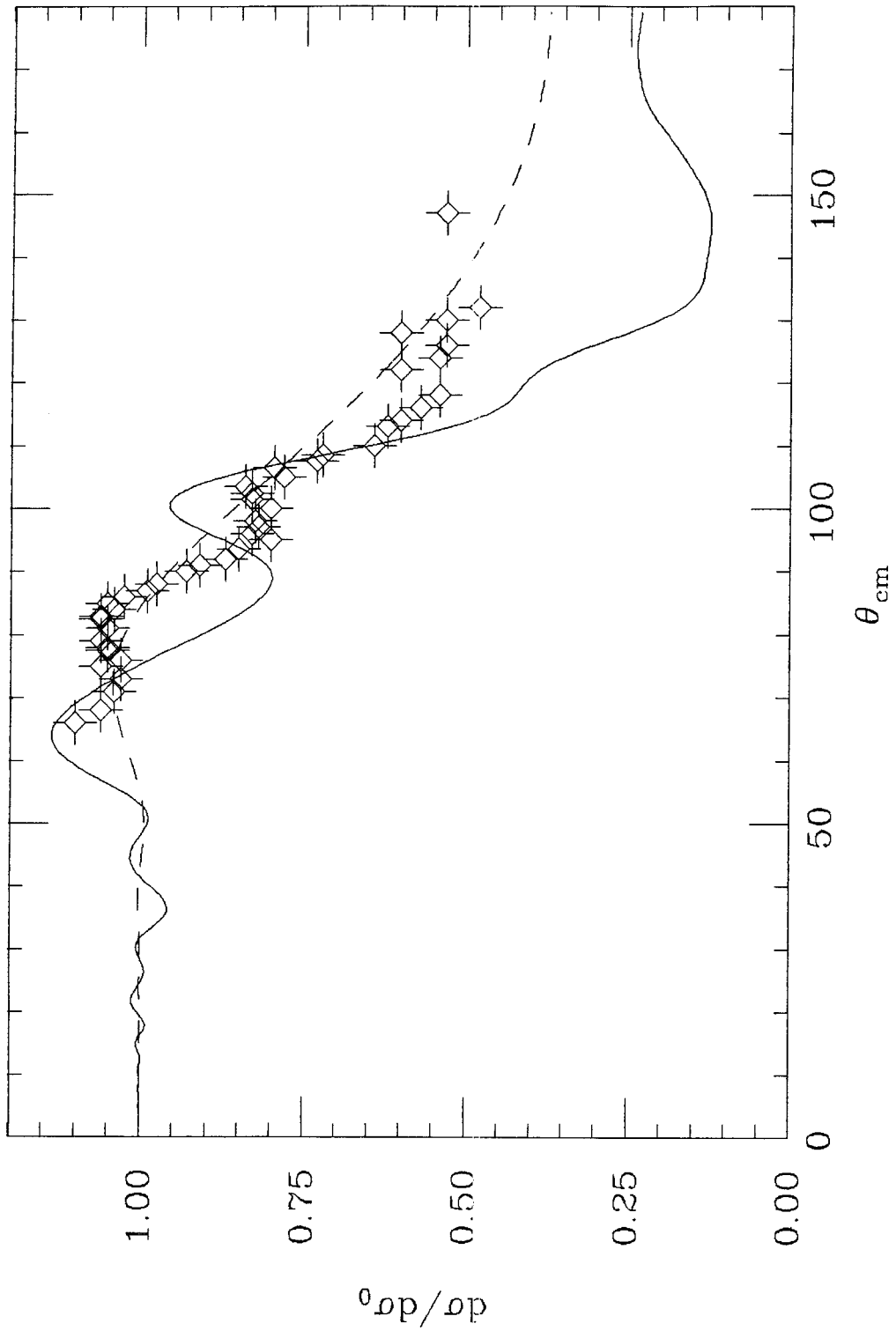
1.00
0.75
0.50
0.25
0.00
0
50
100
150
θ_{cm}
$d\sigma/d\sigma_0$

Figure 22

Semiclassical Coulomb excitation function of the lowest 2^+ state in ^{18}O for the reaction $^{18}O+^{16}O$ and data by Thomas *et al.* with the same scale as Fig.10.

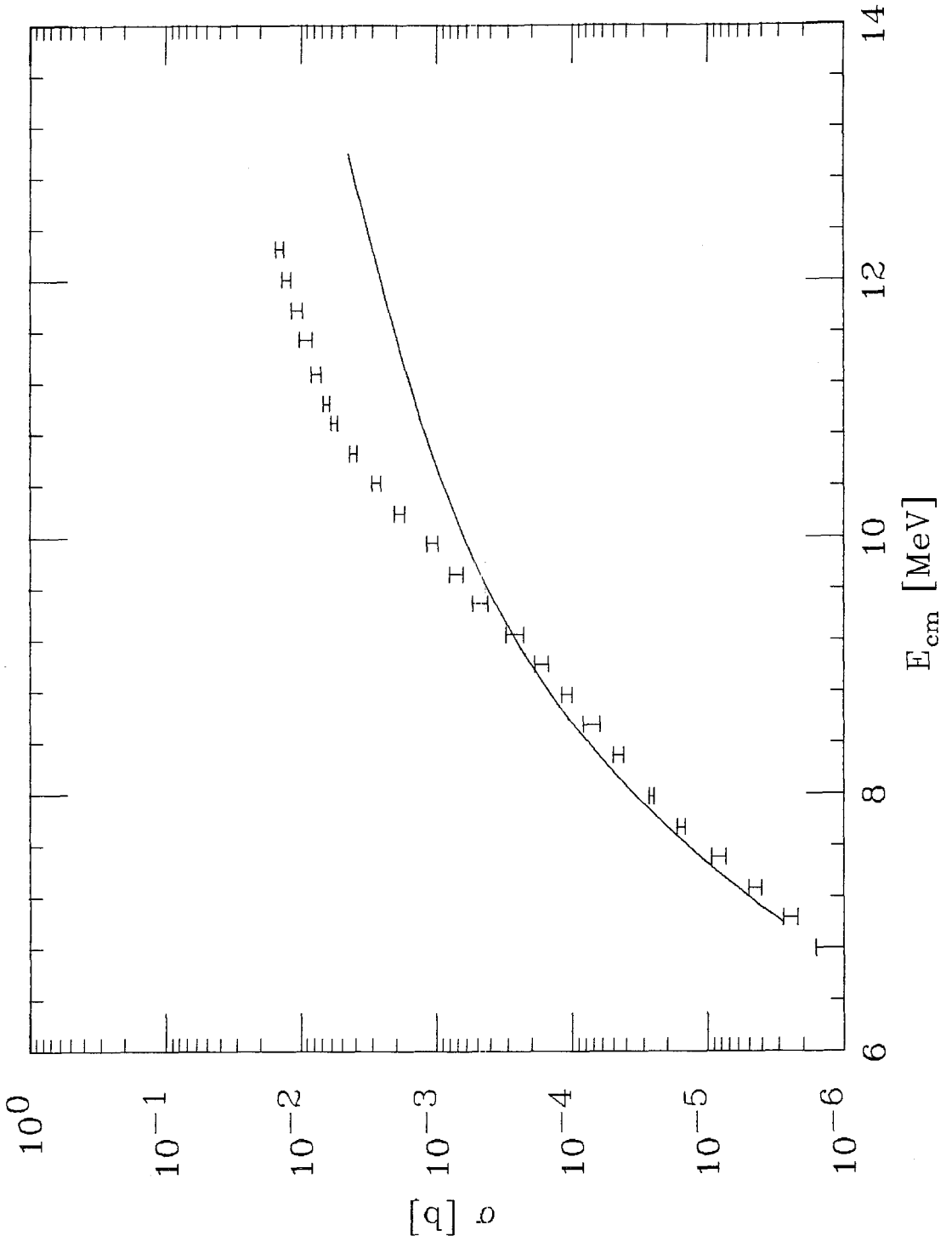
10^0
10^{-1}
10^{-2}
10^{-3}
10^{-4}
10^{-5}
10^{-6}
σ [b]
6
8
10
12
14
E_{cm} [MeV]

Figure 23

Calculated fusion cross section for $^{18}O+^{16}O$ and data by Thomas *et al.* with the same scale as Fig.10. The dashed curve is the fusion cross section for $^{16}O+^{16}O$.

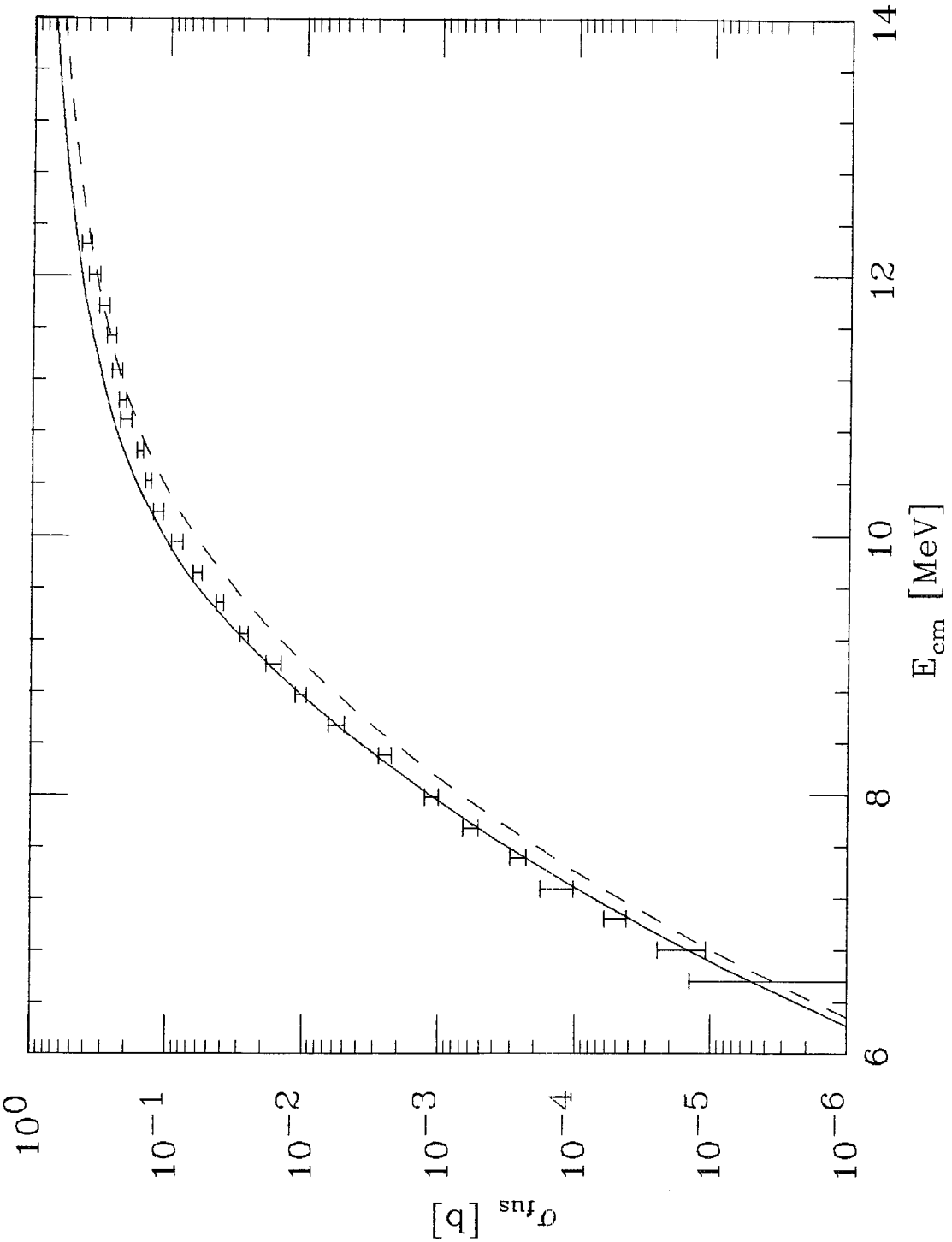
10^0
10^{-1}
10^{-2}
10^{-3}
10^{-4}
10^{-5}
10^{-6}
σ_{fus} [b]
6
8
10
12
14
E_{cm} [MeV]

Figure 24

Calculated elastic differential cross section for $^{18}O+^{16}O$ at $E_{cm} = 12.7$ MeV and data by Gelbke *et al.*. The data points were read off a plot in Ref.[42]; slight deviations from there actual locations are possible. Plotted is the cross section divided by the Rutherford cross section.

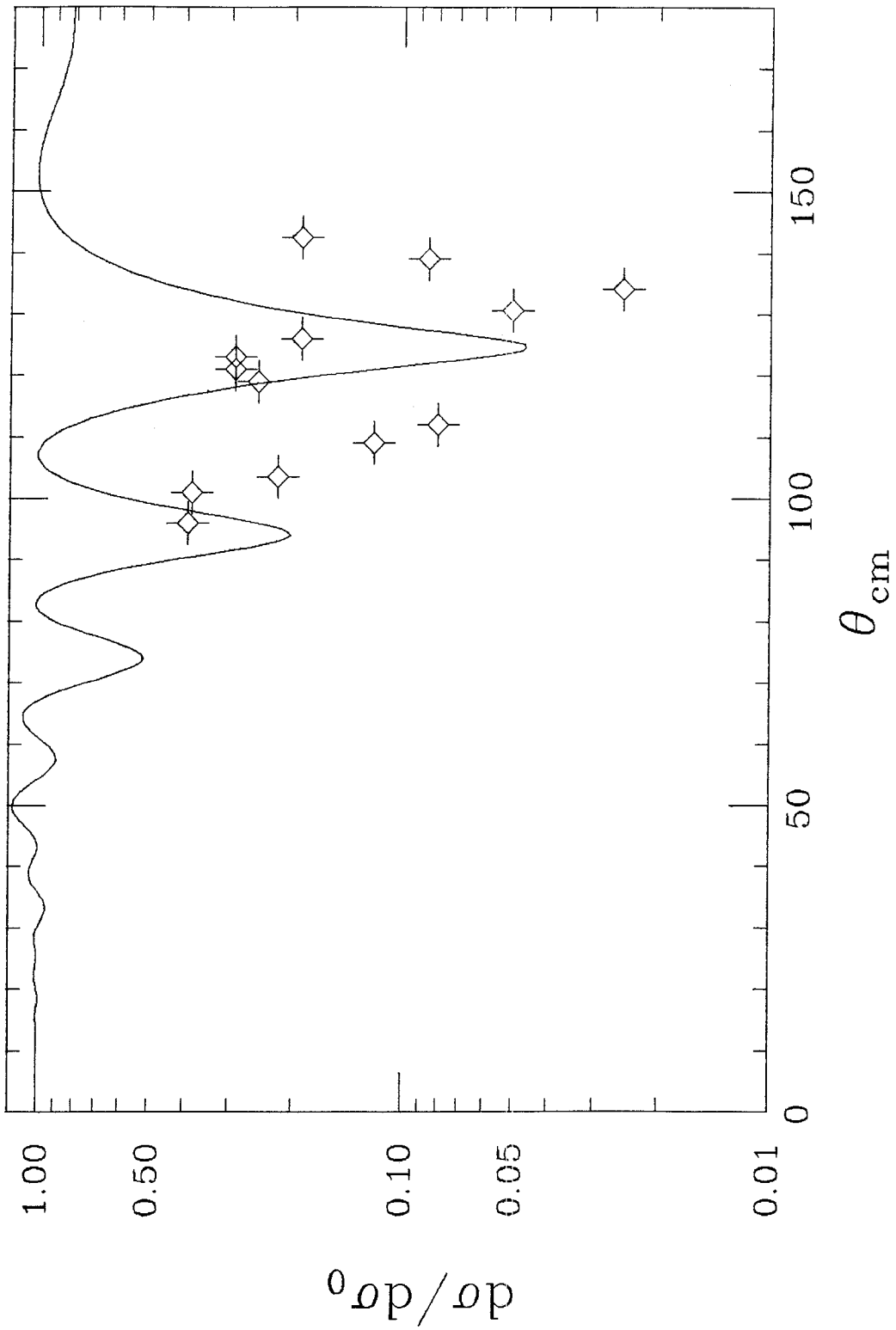
1.00
0.50
0.10
0.05
0.01
0
50
100
150
θ_{cm}
$d\sigma/d\sigma_0$